The Greenland Norwegian Seaway: climatic and cyclic evolution of Late Jurassic-Early Cretaceous sediments

Inaugural-Dissertation
zur Erlangung des Doktorgrades
der Mathematisch-Naturwissenschaftlichen Fakultät
der Universität zu Köln

vorgelegt von
Oliver Swientek
aus Remscheid

Köln 2002

Swientek, Oliver

The Greenland Norwegian Seaway: Climatic and cyclic evolution of Late Jurassic – Early Cretaceous sediments

Dissertation an der Mathematisch-Naturwissenschaftlichen
Fakultät der Universität zu Köln

Berichterstatter: Prof. Dr. Werner Ricken

Prof. Dr. Klaus Krumsiek

Tag der mündlichen Prüfung: 28 Juni 2002

Abstract

Sediments of Late Jurassic-Early Cretaceous age involve very important deposits of petroleum source rocks, oil, gas, coals and non-organic deposits like evaporites, all genetically related to climate. Stable isotope composition of belemnite and bivalve samples (inoceramids and *Buchia*) from Late Jurassic-Early Cretaceous sediments from a transect from Southern Norway to the Barents Sea have been used to estimate paleotemperatures. Internal structures of fossils were studied to estimate the degree of possible diagenetic alteration using SEM-photography, cathodoluminescence, trace element content, stable oxygen-, and carbon isotope composition. SEM investigations have not shown diagenetic alteration whereas cathodoluminescence reveals slight diagenetic alterations in belemnites near the apical line, the rim, and in infilled cracks. Inoceramids and *Buchia* reveal stronger diagenetic influences. Geochemical results also demonstrate good preservation conditions of belemnites in contrast to most bivalve fossils. The estimated temperatures show a relatively warm and increasing trend from the Latest Kimmeridgian to Late Volgian times, with a slightly decrease in the Mid. Volgian. Subsequently followed by a clear shift to cooler temperatures of the Early Berriasian (Ryazanian). From the Mid. Berriasian (Ryazanian) to the Barremian the temperature increase again, with some cooler phases in the Early and Late Valanginian. Estimated temperature gradients from 40°-70° northern latitude are between 0.08-0.18°C/degree latitude with a mean gradient of 0.13°C/degree. In polar regions, these gradients might indicate sub-freezing temperatures in the Early Berriasian (Ryazanian) as well as in the Early and Late Hauterivian. Three types of colour cycles can be distinguished in the investigated sites by means of spectrophotometry. Rhythmic sediments are thought to represent carbonate productivity cycles, redox cycles, or silt dilution cycles. The cycles were described as allogenetic, related to their orbitally driven signature by frequency analyses and evolutionary spectral analyses. Milankovitch patterns are common in every investigated cycle type. The synthesis of stable isotope analyses and frequency analyses documents that anoxia may be controlled by the obliquity, whereas precession and eccentricity controlled the terrestrial factors of sedimentation and nutrient supply as well as fresh water input. The orbital signals are similar in the entire time slice and sites, pointing to one superimposing factor that controls the oceanography. In conclusion, the sedimentology and oceanography of the Greenland Norwegian Seaway at the Jurassic-Cretaceous boundary is best decribed by an estuarine circulation. This circulation resulted from a combination of local tectonics and climatic variations induced by orbital forcing.

Zusammenfassung

Die Sedimente des Späten Jura bis zur Frühen Kreide enthalten sehr bedeutende Mengen Erdöl, Erdgas, Kohlen und nicht organische Rohstoffe, z.B. Evaporite, die in ihrer Entstehung insgesamt auf das Klima bezogen werden können. Zu einer genaueren Charakterisierung dieses Klimas wurden Belemniten und Bivalven (*Inoceramus* und *Buchia*) des Späten Jura und der Frühen Kreide entlang eines Profils von Süd-Norwegen bis in die Barents See untersucht und zur Bestimmung von Paläowassertemperaturen mit Hilfe stabiler Isotopen herangezogen. Um den Grad der Diagenese festzustellen wurden die Fossilien mit dem Raster-Elektonen-Mikroskop, der Kathodenlumineszenz, auf Spurenelemente, sowie auf stabile Sauerstoff- und Kohlenstoffistotopen untersucht. Das Raster-Elektronen-Mikroskop erbrachte keine Hinweise auf eine diagentische Veränderung, wogegen die Kathodenlumineszenz leichte Veränderungen an der Apikal-Linie, dem äußersten Rand des Rostrums und in Rissen der Belemniten aufweist. Inoceramen und Buchien zeigen einen deutlicheren diagenetischen Einfluß. Geochemische Untersuchungen der Spurenelementgehalte zeigen ebenfalls eine, im Gegensatz zu den meisten Bivalven gute Erhaltung der Belemniten. Die ermittelten Temperaturtrends dieser Studie weisen auf relativ warme und steigende Temperaturen vom Späten Kimmeridge bis in das Späte Volgium hin, mit Ausnahme des kühleren Mittleren Volgium. Die nachfolgenden relativ kalten Temperaturen des Frühen Berrias markieren einen deutlichen Schnitt. Abgesehen von kühleren Phasen im Frühen und Späten Hauterive, steigen die Temperaturen ab dem Mittleren Berrias bis zum Barreme erneut an. Die errechneten Temperaturgradienten von 40-70° nördlicher Breite liegen zwischen 0.08-0.18°C/1°N mit einem mittleren Gradienten von 0.13°C/1°N. In polaren Regionen geben die ermittelten Gradienten Anlass zu eisbildenden Bedingungen im Frühen Berrias, sowie im Frühen- und Späten Hauterive. Mit Hilfe eines Spektrophotometers wurden drei Zyklentypen differenziert. Die rhythmisch geschichteten Sedimente wurden als Karbonat-Produktivitäts Zyklen, Redox-Zyklen und Silt-Verdünnungszyklen beschrieben. Die Zyklen sind allogenetischen Ursprungs und beinhalten Milankovitch Hierarchien, wie durch Frequenz-Analysen belegt werden kann. Die Synthese von stabilen Isotopenmessungen und Frequenzanalysen zeigt eine Steuerung der anoxischen Bedingungen durch die Obliquität und ein Steuerung der terrestrischen Sedimentfaktoren, sowie Nähstoff- und Süßwassereintrag durch die Präzession und Exzentrizität. Im wesentlichen wurde das sedimentäre System der Grönland Norwegen See an der Jura-Kreide Grenze durch das Zusammenspiel von lokaler Tektonik und klimatischen Variationen, induziert durch orbitale Steuerung, bestimmt und deutet auf eine ästuarine Zirkulation hin.

Contents

1 Introduction

The aim of this study was to establish a more detailed record of the sedimentation in the Greenland Norwegian Seaway of Late Jurassic to Early Cretaceous age. Special emphasis was taken on the evolution of the sedimentary system and its relation to climate and orbital forcing. This study is part of the German Research Council (DFG) bundle project "Änderungen im Ozean-Atmosphäresystem und seine Einflüsse auf die Evolution der Biosphäre: ausgesuchte Beispiele seit der Atlantiköffnung" (Changes of the ocean-atmosphere-system and its influences on the evolution of the biosphere: selected examples since the opening of the Atlantic). Participants of the project are the Alfred-Wegener-Institute for Polar and Marine Research in Bremerhaven (AWI), the Geomar Research Center in Kiel, the Institute for Chemistry and Biology of the Marine Environment (ICBM) in Oldenburg, the Institute of Geology, Mineralogy, and Geophysics (GMG) at the Ruhr-University Bochum, and the SINTEF Petroleum Research-Trondheim/Norway.

The Late Mesozoic Era (140 Ma to 65 Ma) is generally described as a time of a globally warm and equable climate without polar ice caps. Current literature draws attention to the supposed greenhouse conditions and possible icehouse climates. However, it is still in discussion whether or not there have been intercalated icehouse periods during the Early Cretaceous. In spite of sparse data, many authors give rise to this idea because of aspects as the finding of glendonites in the Valanginian of the Svedrup Basin and an indicative composition of marine flora and fauna (Kemper, 1987), the occurrence of ice-rafted debris in Siberia (Frakes and Francis, 1988), and other aspects (see Price, 1999). Furthermore, some authors propose icehouse conditions in the Early Cretaceous on the basis of stable oxygen isotope temperatures (Ditchfield, 1997; Podlaha et al., 1998; Price et al., 2000) or carbon isotope fluctuations related to greenhouse temperatures (Weissert and Lini, 1991). Numerous complex circulation models have been established, especially for the Kimmeridgian, to explain climatic evolution (Moore, 1992 a, b; Barron, 1994; Valdes, 1992; Valdes, 1995). New oxygen and subordinated carbon isotope paleotemperature data obtained from belemnites, inoceramids, and *Buchia* fragments of Latest Jurassic to Early Cretaceous age on a transect from Southern Norway to the Barents Sea are presented in this study. The preservation of the isotopic content and hence the paleotemperature record can be affected by a number of processes. These are pre-depositional vital effects, non-isotopic equilibrium with ambient seawater, and post-depositional diagenetic processes. To estimate the grade of diagenesis, and hence the plausibility of the calculated temperatures, comparative

geochemical studies beneath the isotope calculations like SEM-Analyses, OES-MS, microprobe, and cathodoluminescence have been undertaken.

In a transect from Southern Norway to the Barents Sea three drill cores from the Upper Jurassic-Lower Cretaceous (Latest Kimmeridgian-Early Barremian) were investigated with a spectrophotometer for cyclic bedding pattern. Rhythmic bedding in the Cretaceous related to Milankovitch cycles are often quoted for sections from tropical to temperate paleo-latitudes (Rawson, 1971; Rawson & Mutterlose, 1983; Nebe & Mutterlose, 1999; Einsele et al., 1991; and de Boer 1994). The aim of this research was to investigate if Milankovitch cycles can even be found in high northern latitudes. Further questions are of what kind they could be and how the sediments are triggered to them. All this can add data to the question of climate of the Early Cretaceous in high northern latitudes, which is far more than just an equable greenhouse climate, as often suggested.

2 Geological setting

2.1 Tectono-sedimentary development

During the Jurassic and Cretaceous three major rift systems separated Pangea into North America, Eurasia, and Gondwana (Moore et al., 1992). The minor Greenland Norwegian Seaway is an appendix of the large Atlantic rifting structure that continues up into the Western Barents Sea. Crustal extension between Norway and Greenland leading to the initial development of the north east Atlantic rift in the Late Devonian, whereas the Barents Sea rift was initiated in the Mid.-Carboniferous (Gudlaugsson, 1998). The Late Permian to Middle Jurassic initial phase of the Pangea break-up was controlled by southward and westward propagation of the Greenland Norwegian Sea and the Tethys rift system, whereas the Late Jurassic to Early Tertiary break-up phase was dominated by the stepwise northward propagation of the central Atlantic (Ziegler, 1990). The rapid opening of the central Atlantic took place in Late Jurassic and Early Cretaceous time and intensified the rifting in the Greenland Norwegian Sea (Ziegler, 1990). In the Early Cenozoic a transform motion between North America-Greenland and Eurasia opened the Greenland Norwegian Sea and the Eurasian Basin of the Arctic (Hay, 1998). A still closed Greenland Norwegian Sea is proposed at Anomaly 25 (55.9 Ma) by Srivastava and Tapscott (Srivastava, 1986). Hay et al. (1999) proposed that the Greenland Iceland Norwegian Sea did not exist during the Cretaceous and that the separation of Greenland and Norway did not occur until Anomaly 26 (57.55 Ma), wether first stretching began about 80 Ma in the Late Cretaceous. Before the opening in the Paleocene there has never been a deep-water connection between the North Atlantic and the Arctic because of the Greenland-Iceland-Scotland Ridge (Hay, 1999). The North Atlantic has been a part of the circum-equatorial Tethys Ocean from its Early Mid.-Jurassic formation until the Late Cretaceous opening of the South Atlantic (Thiede, 1979). The general plate tectonic configuration in the Late Jurassic-Early Cretaceous is described as a large continuous block complex of North America, Greenland, and Eurasia (Fig.1; Mutterlose et al., 2002). This area contained about 80% of a deep Arctic arm of the Pacific, the “South Anyui Ocean Gulf”, that has since been subducted except for some of ophiolitic terranes (Mutterlose et al., 2002).

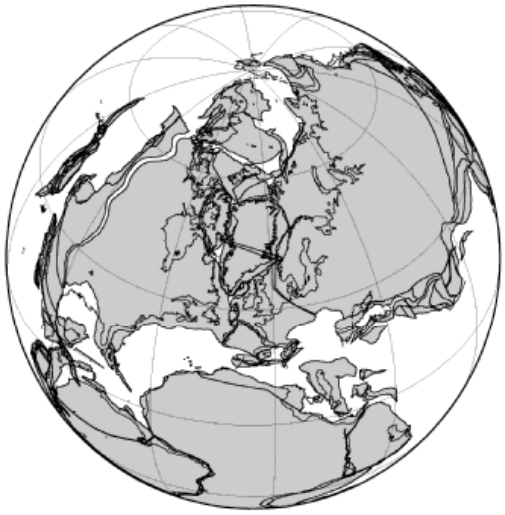

Figure 1 Valanginian-135 Ma reconstruction of plate tectonics (after Mutterlose et al., 2002)

The Norwegian shelf region can be subdivided in three units: the North Sea, the Møre-Lofoten System, and the Barents Sea (Ronnevik, 1975). The basement architecture resulting from the Caledonian, Variscan, and Uralian orogeny represents a fundamental factor for the development of basins and seaways in the Mesozoic. Particularly extensional tectonics controlled the structural, sedimentological, and paleoceanographic setting between the North Sea and the developing Atlantic rift system. This includes the ENE-WSW Hitra Fault Alignment (Møre Trondelag Fault Zone) of Mid. Norway and the Senja-Hornsund Alignment in the Barents Sea. The tectonic development in the study area took place in two phases. First a period characterized by an intense subsidence and rapid sediment accumulation prevailed in the Triassic and the second phase is summarized as the "Late Cimmerian" rift-episode at the Jurassic/Cretaceous boundary (Doré, 1991). The latter one is well known in seismic sequences marked by the Late Cimmerian unconformity. This unconformity represents a widespread change in facies related to a Late Ryazanian transgression (Rawson and Riley, 1982). The Late Jurassic is characterized by a transgressive regime in connection with a widespread rifting. This widespread rifting and fault block rotating was most intense in the Late to Mid.-Jurassic and Early Cretaceous. Strike slip and reverse faulting persisted in the Early Cretaceous on the Barents shelf (Doré, 1991). The triple junction between the Greenland Norwegian Sea, the Faeroe rifts, and the Viking graben became thermally updomed in the Kimmeridgian (Ziegler, 1990). A connection of the Boreal Ocean and the Tethys is proved by faunal assemblages in the Oxfordian and Kimmeridgian (Doré, 1991). A subsequent evolution of structural highs disturbed this connection in Mid.-Volgian times. Black shale deposits like the Spekk Fm. dominated apart from these emergent highs. This

formation is equivalent to the Kimmeridge Clay Fm. of Mid. Norway and the Hekkingen Fm. of the Barents Sea (Swiecicki, 1998). Thick barrier bar- and delta sands around the developing highs complete these formations. The Rogn Fm. sandstone of the Møre-Trondelag area resulted as a barrier-bar complex on the dip-slope of intra-basinal fault blocks (Doré, 1991). The lower Spekk Fm. is part of a first regressive-transgressive cycle of the Mid.-Callovian to Kimmeridgian. The second cycle of Latest Jurassic to Early Cretaceous time is related to significant tectonic activities in the Proto-Atlantic with an intense rifting in Volgian times (Swiecicki, 1998). The top of the Spekk Fm. is limited by the "Near Base Cretaceous" seismic reflector and can be traced over a wide distance in the study area (Rawson and Riley, 1982). This fact is visible in seismic sections by low velocity characteristics (Swiecicki, 1998). The Near Base Cretaceous event marks a major rift episode of Late Ryazanian age (Swiecicki, 1998). It breached the sill that separated the proto-North Atlantic/North Sea rift system from the open waters of Central Atlantic (Knott, 1993). The ongoing tectonic activity of the Early Cretaceous added increasing complexity to the evolving seaway that is characterized by numerous land barriers (Doré, 1991). Volgian to Ryazanian tectonics caused wide ranged regressions and hence isolated basins (Rawson and Riley, 1982). In Berriasian (Ryazanian) times ammonite provincialism was at its most coincident with the development of widespread land barriers (Doré, 1991). These were occasionally exceeded by transgressive events like the Late Berriasian (Ryazanian) transgressive event that can be proved by faunal assemblages. From the Late Ryazanian to the Hauterivian occasionally transgressions are documented (Rawson and Riley, 1982). Marine shales dominated away from the developing deltas, like the Lange Fm. of Mid. Norway and the Knurr- and Kolje Fm. of the Barents Sea (Doré, 1991). From Aptian to the Albian times the seaway was re-established again (Doré, 1991) and revealed first bathyal depth (Gradstein, 1999).

2.2 Late Jurassic-Early Cretaceous Paleoceanography

The study area of the Greenland Norwegian Sea can be defined in the south by the Tethys Ocean at a paleolatitude of 25°N and in the north by the West Siberian Basin connected to the Arctic "South Anyui Gulf" at a paleolatitude of 70-90°N (Mutterlose et al., 2002). Based on Hay et al. (1999) the seaway was 200 to 300 km wide and almost 2000 km long. The southern end is characterized by a small open part of the Atlantic (Mutterlose et al., 2002). The Greenland Norwegian Sea was connected to the Tethyan Region across central Europe via a NE-SW orientated epicontinental sea approximately 500 km in width (Mutterlose et al., 2002). More problematic is the northern end of the seaway. Valanginian to Barremian coal-

bearing non-marine beds of Franz-Josef Land and Severnaya Zemlya are described by Embry (1992) and Sokolov (1990). Ziegler (1988) mentioned a strait between a "Lomonosov High" and Severnaya Zemlya with an unclear connection to the South Anyui Gulf in Berriasian (Ryazanian) to Barremian times. Kazmin and Napatov (1998) proclaim a direct connection from the Greenland Norwegian Sea to the South Anyui Gulf via a strait between Novaya Zemlya and the mainland. Mutterlose et al. (2002) described a distance of about 5000 km for the narrow part of the Greenland Norwegian Sea. The sea might have been influenced also by a more eastern sea along the west side of the Urals that connected the Arctic via Novaya Zemlya and Tethys in Tithonian-Barremian times. The time series of the Latest Jurassic-Earliest Cretaceous (Tithonian-Berriasian (Ryazanian)) is characterized by a distinctive sea-level lowstand that was initiated by low spreading rates (Haq, 1988; Ziegler, 1990; Hardenbol, 1998), whereas in Valanginian and Hauterivian times transgressive conditions prevailed (Rawson and Riley, 1982; Haq, 1988; Ziegler, 1990). However, the landmasses remain stable in the considered area. The seaway was limited in the west by Greenland and in the east by the Fennosarmatia. The Rhenish-Bohemian Massif, the Irish Massif and Rockall Halten Bank mark the south and south-western part of the Greenland Norwegian Seaway (Ziegler, 1990).

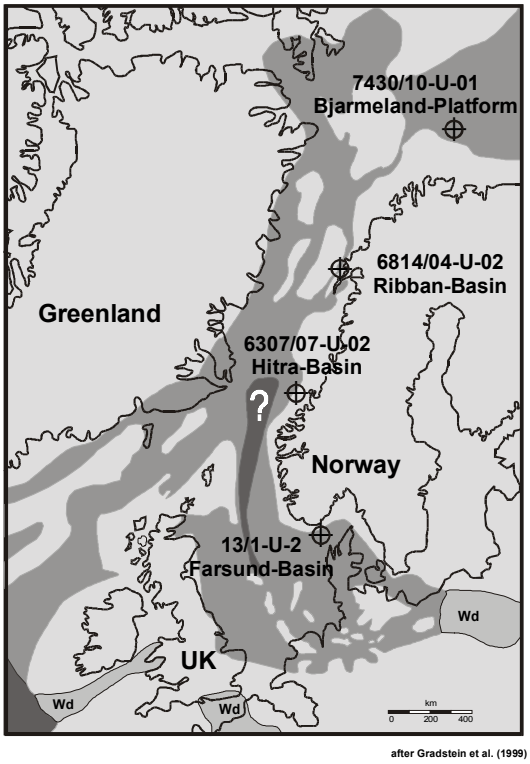

Figure 2 Upper Hauterivian/Barremian paleogeography of the Greenland Norwegian Sea (Wd =Wealden facies; after Gradstein et al., 1999)

2.3 Stratigraphy

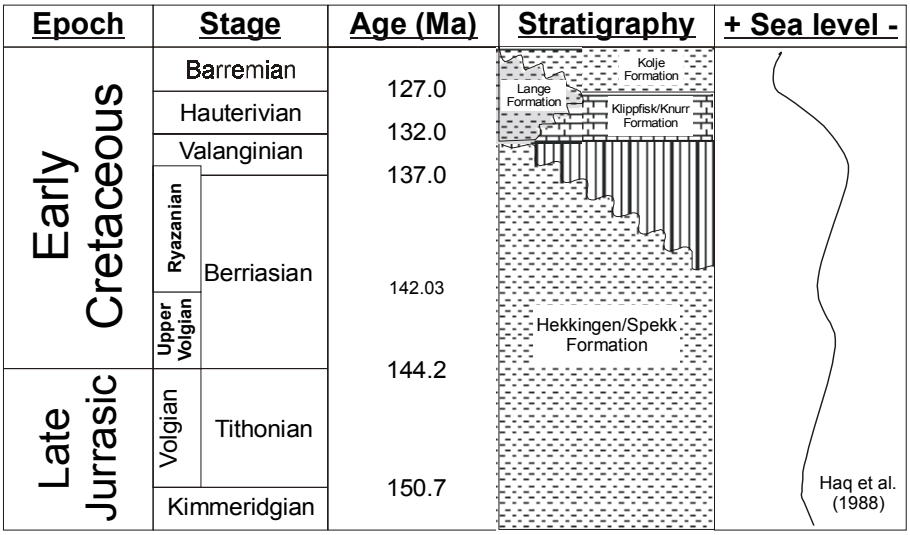

Figure 3 Late Jurassic to Early Cretaceous Stratigraphy of the Greenland Norwegian Seaway and the sea level curve of 3rd order after Haq et al. (1988)

Four cores drilled by the SINTEF Petroleum Research (former IKU) / Trondheim were investigated (Fig.2), forming a transect from south Norway to the Barents Sea. The lithology of these cores is similar and indicates a first genetic connection. All sites were drilled by the SINTEF (former IKU) Petroleum Research in Trondheim /Norway.

2.3.1 Site 7430/10-U-01

Water depth	Core length	Latitude	Longitude
335 m	55.35 m	74°12’47.79’’N	30°14’44.22’’E

Table 1 Key data of core holes; SINTEF Petroleum Research Trondheim/Norway (Bugge et al, 1989)

The northernmost core 7430/10-U-01 of the Bjarmeland platform is restricted by the Nordkapp Basin and the Loppa High in the south, and the Gardabanken High and the Sentralbanken High in the north. The core was drilled in 1987. It covers the Latest Kimmeridgian to Early Barremian. The core reveals condensed sections and some hiatuses. Generally the core can be subdivided in three parts. The Hekkingen Fm. of Latest Kimmeridgian –Berriasian (Ryazanian) age consists of black shales. In the lower part there

are some fine-grained sandstone and siltstone laminae. Seismic reflections at 54 m indicate some beds of glauconitic layers as well as pyrite laminae and concretions. At 47.8 m a mud pebble conglomerate occurs which can also be related to a seismic reflector. To the top the occurrence of brown shales increases and sometimes some greyish layers turn up. At 45 m a sandstone interval appears which contents glauconite. The formation shows a high fossil content of *Buchia, Inoceramus*, and cephalopods. Fish and plant fragments are also described (Bugge, 1988).

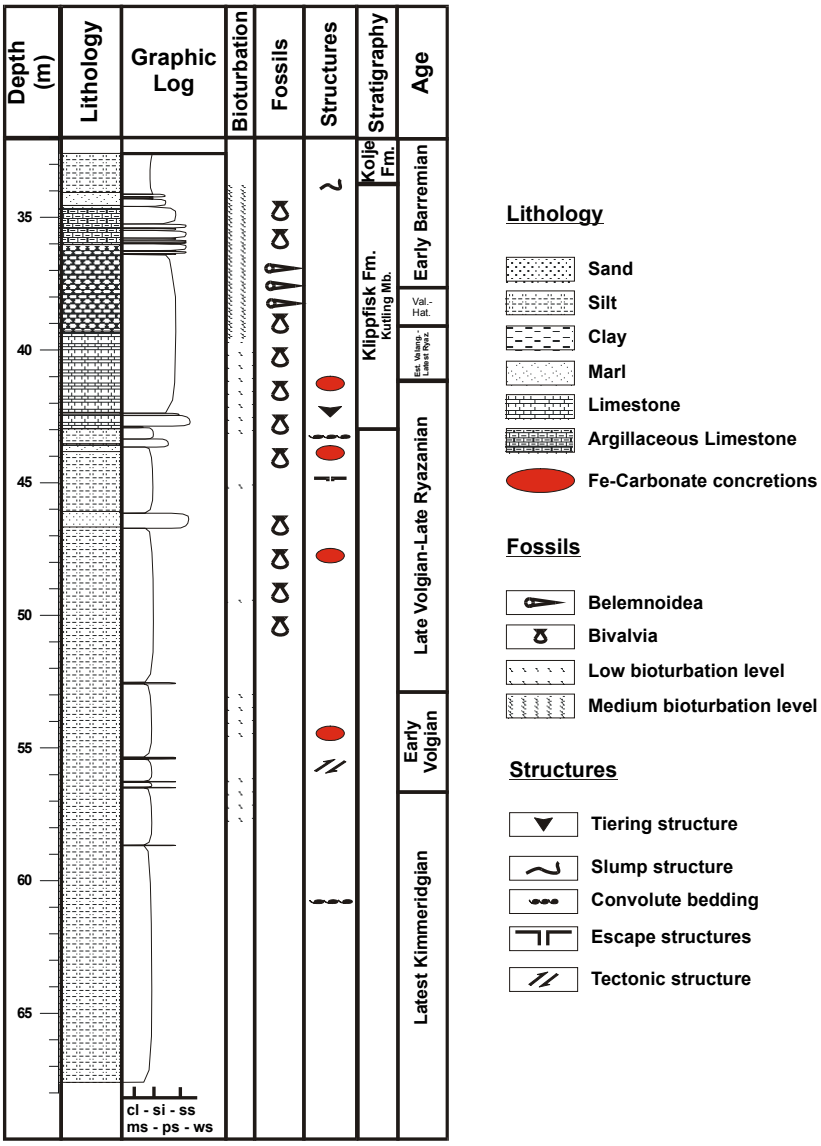

Figure 4 Stratigraphy of site 7430/10-U-01

The gradual transition to the subsequent Klippfisk Fm. (Berriasian (Ryazanian)-Early Barremian), newly introduced for the Western Barents Sea shelf (Smelror, 1998) represents a condensed unit of marls and limestone. The well bioturbated carbonaceous unit consists of a

lower more marly part and an upper part with calcareous shales to clayey wackestone nodules. Burrow filling pyrite, *Buchia*, *Inoceramus,* and belemnites are common. Calcispheres and foraminifera fragments are described (Bugge, 1988). A clear colour shift is recognized at 36 m from the greyish nodular limestone to the reddish brown clayey packstone. Interestingly the darker patches of the formation is related to burrows of the abundant ichnofossils. The formation reveals an abundant *Inoceramus* content and belemnites. The Kolje Fm. of the Early Barremian consists of dark claystones with some dolomitic concretional layers. In the bioturbated unit *Planolites* and *Chondrites* ichnofossils can be observed. The core has a paleolatitude of 59°N (Mutterlose et al. 2002).

2.3.2 Site 6814/04-U-02

Water depth	Core length	Latitude	Longitude
233 m	182.42 m	69°39'45.8''N	14°09'47.1''E

Table 2 Key data of core holes; SINTEF Petroleum Research Trondheim/Norway (Hansen et al, 1991)

Core 6814/04-U-02 was drilled 1991 in the Ribban basin near the Lofoten and bears sediments of Lower Volgian to Lower Barremian. The A unit from Early Volgian up to the Berriasian (Ryazanian) consists of laminated shales with some intercalated carbonate beds of siderite and ankerite. This unit can be correlated to the Hekkingen Formation of the Barents Sea. The fossil content bears wood fragments, cephalopod hooks, and ammonites in the upper section of the lower part. Fe-carbonate beds are characterising the middle part of the A unit as well as some bivalve beds, whereas bioturbation is absent. The upper part of the A unit shows a claystone with increasing silt content, and present ammonites and bivalves. The subsequent gradational B unit contains calcite-cemented siltstones with abundant limestone nodules and beds. A characteristic colour change from grey to a lighter colour and vice versa is documented. Bivalves as *Inoceramus* occur and the whole unit is bioturbated. Woody debris, as well as marine alga and dinoflagellate cysts were described also (Hansen, 1991). The following sharp-based C unit consist of dark pyritic mudstones with carbonate and siltstone beds most likely up to the Lower Barremian. Fe-carbonate beds are common in this unit. The fossil content shows well preserved woody phytoclasts. The Base Cretaceous Reflector is well identified at 39.83 m (Hansen, 1991). This core has a paleolatitude of 54°N (Mutterlose et al. 2002).

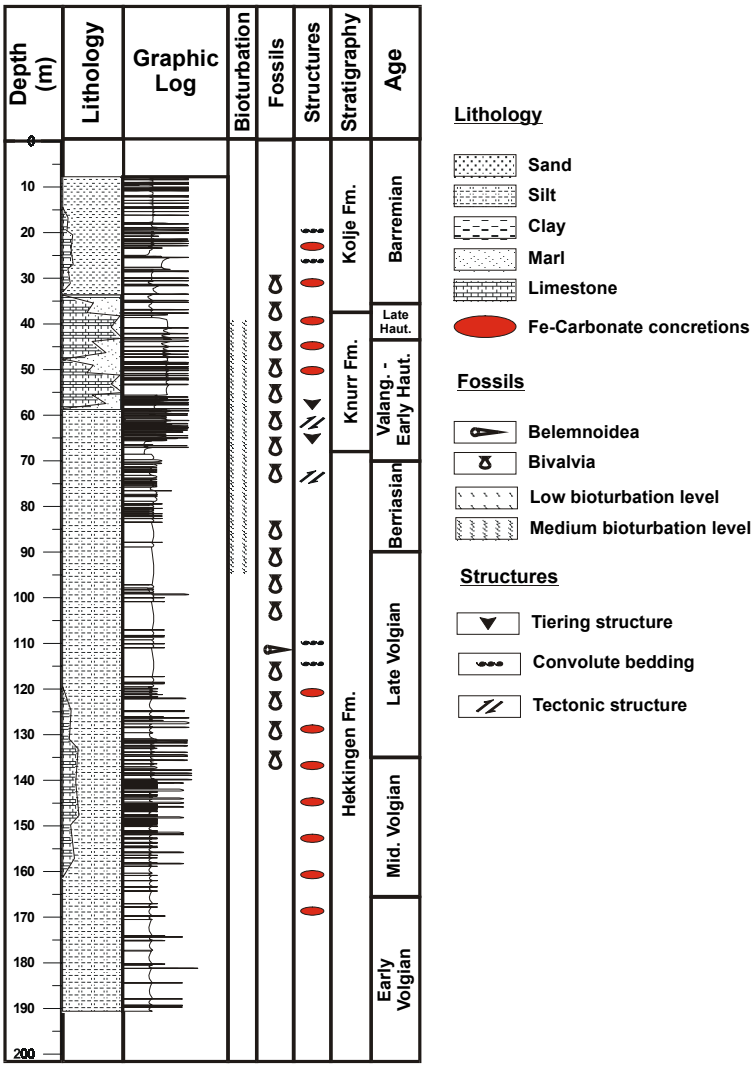

Figure 5 Stratigraphy of site 6814/04-U-02

2.3.3 Site 6307/07-U-02

Water depth	Core length	Latitude	Longitude
290 m	173.91m	63°27’54.35’’N	7°14’44.26’’E

Table 3 Key data of core holes; SINTEF Petroleum Research Trondheim/Norway (Skarbø et al, 1988)

The core 6307/07-U-02 was drilled 1988 off mid Norway in the southern Hitra basin of the Møre -Trondelag area.The investigated section is restricted from the Early Volgian to the Early Valanginian. The shales of the subunit 2 of the Spekk Fm. (104.8 – 36.4 m) include a high amount of silt between 100 to 65 m and sharp silt to finest sand layers below 80 m.

Clastic dykes occur, which are filled with sandy material. The formation shows a high fossil content of fish bones, ammonites, belemnites, and bivalves as well as plant debris. Skarbø et al. (1988) interpret the seismic reflector at 36.4 m between the Spekk and the subsequent Lange Fm. as the Late Kimmerian unconformity.

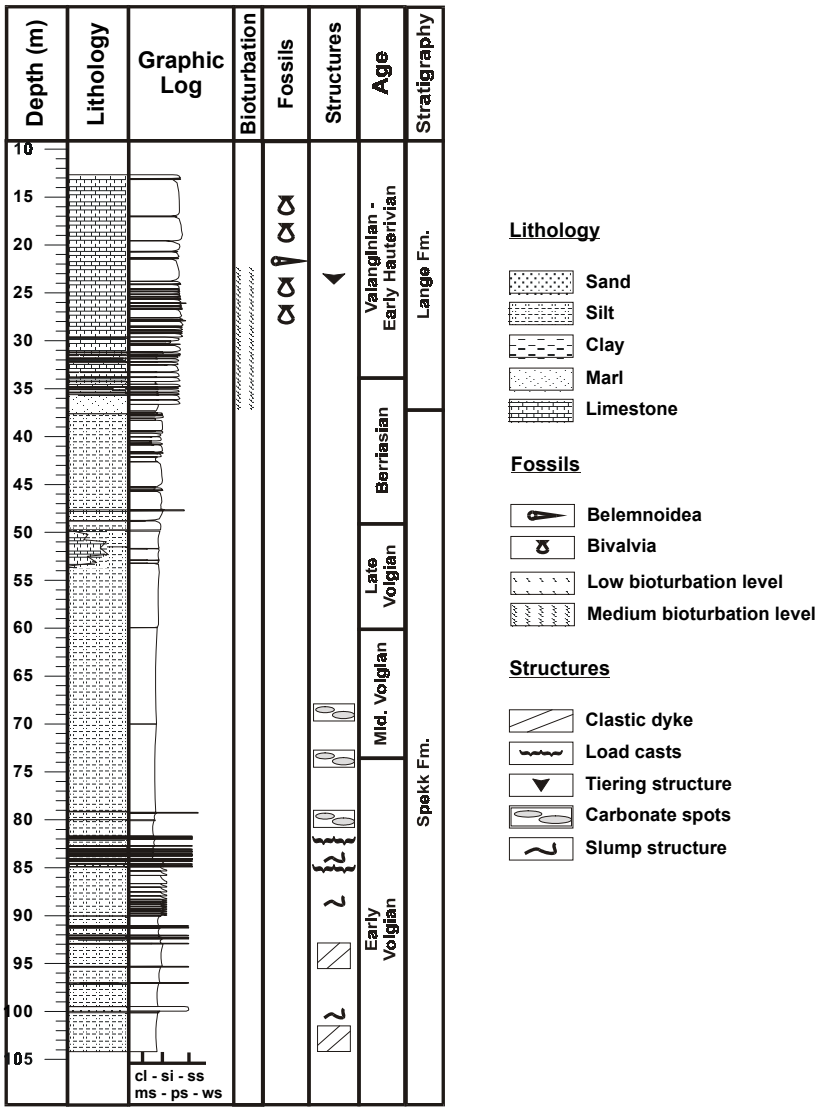

Figure 6 Stratigraphy of site 6307/07-U-02

The carbonate cemented red and grey claystones of the Lange Formation (36.4 – 13.6 m) with a $CaCO_3$ content ranging from 1.1 to 39 % (Mutterlose et al, 2002) can be divided in two parts by their colour. The lower sub unit is of grey claystones whereas the upper unit is red shale. Both units are well bioturbated. The paleolatitude of this core was 48°N (Mutterlose et al. 2002).

2.3.4 Site 13/1-U-2

Water depth	Core length	Latitude	Longitude
505 m	83.9m	57°48'42.78''N	8°12'13.97''E

Table 4 Key data of core holes; SINTEF Petroleum Research Trondheim/Norway (Smelror et al, 1989)

The southernmost Core 13/1-U-2 was drilled 1988 in the Farsund Subbasin/South Norway. The core covers the Early Volgian to Berriasian (Ryazanian) and consists of the Børglum Member of the Bream Formation with shales interrupted by a sandstone member.

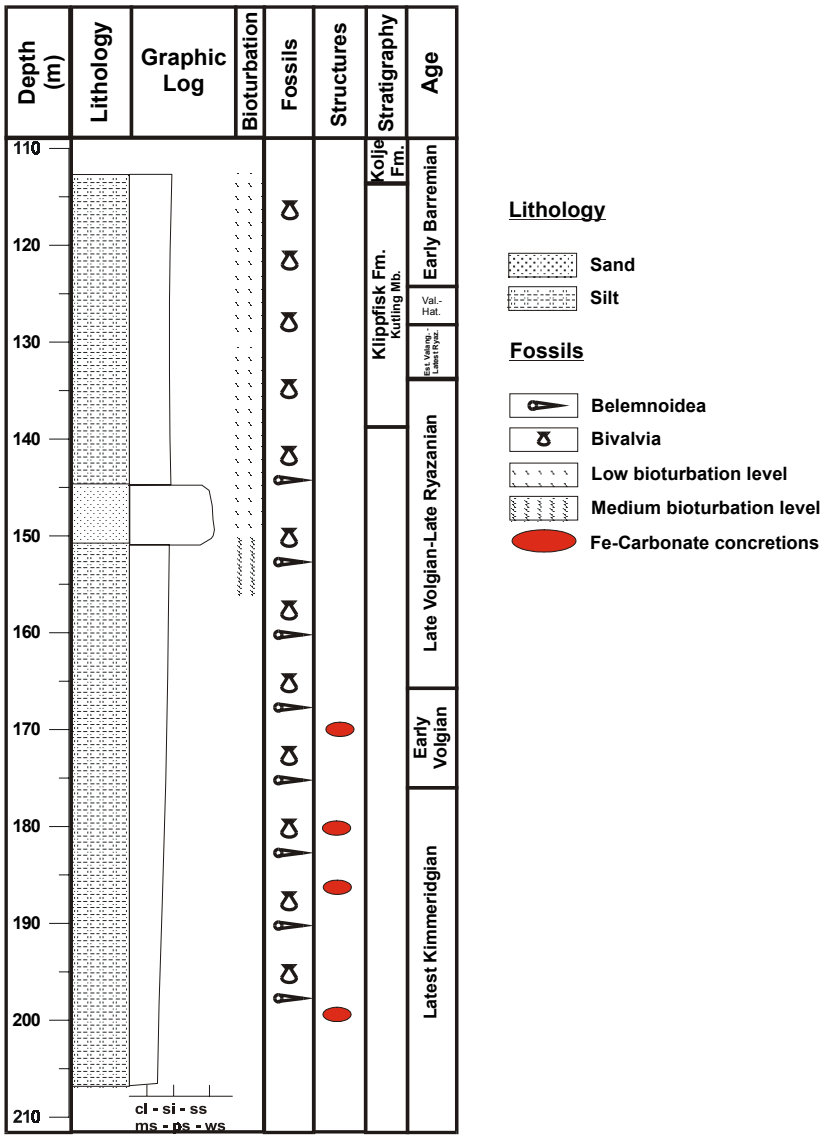

Figure 7 Stratigraphy of site 13/1-U-2

The core is subdivided in three units. The A unit from Lower to Mid.-Volgian is characterized by a black shale with a gradual increasing silt content reflecting a coarsening up trend. Bivalves and belemnites are common, whereas bioturbation is not documented. Carbonate cemented layers appear. The gradational succeeding subunit B consists of a green glauconitic fine grained-sandstone with bioturbation as well as belemnites and bivalves. The sharp base to the overlying subunit C at 145.5 m is identified as the Base Cretaceous Reflector (Smelror, 1989). Black shale with increased silt content characterize the subunit C. Bioturbation is common and bivalves, belemnites, and plant fragments were observed. The core has a paleolatitude of 43°N (Mutterlose et al. 2002).

3 Methods

An estimation of the diagenetic influence is essential and the values of the isotopes have to be examined in detail. These values depend strongly on the grade of diagenesis, as the values are considerably changing with increasing diagenesis. Therfore it is important to restrict the degree of diagenesis. To estimate the grade of diagenesis 34 distinctive shell-holding samples were chosen from the cores. They contain fragments of *Inoceramus*, *Buchia,* and belemnites. Comparative studies with the transmitted light-, polarization-, scanning electron-, and cathodoluminescence microscopy as well as geochemical analyses have been undertaken.

3.1 Microscopy

3.1.1 Scanning Electron Microscopy (SEM)

For the investigation of the structural development of the carbonate shell and diagenetic changes or new build ups the belemnite, inocerame, and *Buchia* shells were prepared for observations with a CamScan S44 EDitor scanning electron microscope at the University of Cologne. The samples were broken by hand or saw and sputtered with gold for two minutes.

3.1.2 Cathodoluminescence (CL)

The cathodoluminescence is an emitted visible radiation caused by energetic electrons bombarding of distinctive materials. In this study we used the cathodoluminescence to investigate the possible diagenesis of carbonate shells and the related chemical interaction. For cathodoluminescence samples from the same layers as for the SEM investigations were used. The samples were cut for thin-sections. They were fixed on a glass with araldite. The samples were polished with different grain-size powders (600 to 1000 μm) in a suspension of oil (Shell S4919) to prevent the clay minerals fom swelling. The slices were polished until they reached a thickness of 30 μm. For CL investigations the surface of the thin-sections has to be smooth to minimize the scattering of the electron-ray. Therefore the samples were polished again with different grain-size grinding and diamond-paste of 6-, 3-, and 1 μm each time for approximately 30 minutes. At last the thin-slices were sputtered with gold for two minutes.

At the University of Cologne a cathodoluminescence-microscope (HC2-LM) with a high sensitivity hot cathode was used. The high sensitivity hot cathode allows the observation of

low-intensity luminescence. Standard operation conditions were an accelerating potential of 14 kV at 0.1 mA beam current opening.

The carbonate minerals frequently exhibit luminescence. Bright luminescence is caused by the diagenetic incorporation of Mn^{2+} replacing Ca^{2+} in the crystal lattice (Barbin, 1999). Generally Mn^{2+} is the activator for luminescence and Fe^{2+}, Co^{2+} as well as Ni^{2+} are used to be quenchers (Marshall, 1988). CL intensities are controlled by absolute concentrations of Mn and Fe as well as Fe/Mn ratios (Walker, 1991). The activator- and quencher ions already show an effect even if their concentration lies below the detection-limit of the microprobe (Tucker, 1988). Walker (1991) mentioned a trigonal calcite with a bright luminescence containing Mn^{2+} in the amount of a few ppm up to 1% (Walker, 1991). Some combinations of the colours yellow, orange, and red describe the luminescence colour of calcite (Marshall, 1988). According to Tucker (1988) low Mg-calcites are yellow whereas Mg-rich calcites show an orange to red colour. Calcite with a very low Mn content as well as synthetic, pure calcite has a blue luminescence colour after a longer shelling (Richter and Zinkernagel, 1981). By Richter & Zinkernagel (1981) the colour depends on the amount of Mn either in the $CaCO_3$ -layers or the $MgCO_3$-layers. In the first case the colour will be yellow and in the second case it will be sooner red. Orthorhombic aragonite $CaCO_3$ contains Mn^{2+} as activator too, but the amount of Mn is not as common as in calcite or dolomite. The luminescence colour is described as yellow (Marshall, 1988) or yellow-green (Richter and Zinkernagel, 1981).

Before CL investigation the structures of the samples were investigated by transmitted light microscopy to compare a possible loss of the structure. Before any interpretation of the colours of the different carbonates it is always useful to characterize the facies of the samples and their chemistry related on trace elements like Mn, Fe, and Sr. The colour strongly depends on the chemistry, which again is related to the depositional facies and diagenesis.

3.2 Inorganic Geochemistry

A further step to characterize diagenesis is the estimation of the concentration of carbonate sensitive elements. Therefore analytical investigations with the electron microprobe are suitable to detect fluxes of carbonate sensitive elements. Mg in the shell would be degraded whereas elements of the bulk sediment and/or late diagenetic pore waters like iron and manganese would be incorporated (Veizer, 1983). Because of measuring problems strontium is not considered.

3.2.1 Electron Microprobe Analyses

Microprobe analyses were done with the same samples as usednfor the cathodoluminescence to allow comparative studies. Therefore the thin slices were cleaned from gold and renewed sputtered with carbon for the microprobe analyses. All samples were measured with a JEOL Superprobe JXA-8900RL with standard operating conditions of 15 kV accelerating voltage, 20 nA current, 5 μm probe diameter and ZAF data processing at the Institute of Mineralogy and Geochemistry at the University of Cologne.

3.2.2 OES-MS

33 bivalve samples were investigated by OES -MS with a PERKIN ELMER Optima 3000XL at the ICBM at the University of Oldenburg. We calculated diagenesis sensitive elements as Mn, Mg, Sr, Ca, and Na in the bivalves. Because of the small amount of *Buchia*- and inoceramid shell material of 50 mg in average, partly contaminated with clay particles, the carbonate was leached out with 1 N acetic acid. One day later only the clear solution was taken and all samples were diluted before measuring.

3.3 Stable $\delta^{13}C$- and $\delta^{18}O$ isotopes

The material for the investigation of the $\delta^{18}O$ and $\delta^{13}C$ isotopes was received in different ways. The material from the belemnites was drilled out by a dental drill of 0.5 mm in diameter. If possible the samples were taken from the apical line along the growth rings outside. The *Inoceramus* shell material was also drilled out. The preservation of the *Inoceramus* shell is well and prism-layers can be noticed without using a microscope. *Buchia* shells were lifted with a needle from the bulk sediment, because they were too small to drill them out. Additionally these samples were cleaned thoroughly off the adhering sediment. Beneath the measurement of the shell material the bulk was also investigated from the same depth as the shells. The bulk was crushed with a pestle to powder before measuring.
276 samples, of belemnites, inoceramids, *Buchia* fragments, and 320-bulk rock (black shales and limestone) were analyzed for $\delta^{18}O/^{16}O$ and $\delta^{13}C/^{12}C$ stable isotopes by using the "Kiel device" of the Leibniz-Laboratory in Kiel. The results are expressed in δ notation in ‰ relative to the Pee Dee Belemnite (PDB) of the Cretaceous in Carolina-USA. Calcite paleotemperature values were calculated using the equation of Epstein et al. (1953) and Craig (1965) modified by Anderson and Arthur (1983).

$$T(°C)= 16.0 - 4.14 (\delta_c-\delta_w) + 0.13 (\delta_c-\delta_w)^2$$

It is still in discussion if the Early Cretaceous yielded ice-building conditions. Therefore different assumptions have been undertaken for temperature estimation. Seawater of a non-glacial Cretaceous would have been isotopically lighter, whereas seawater of a glacial Cretaceous would have been isotopically heavier. Therefore we used different δ-seawater of –0,8‰ PDB, -1.2‰ PDB, and –1,5‰ PDB to cover the different circulation pattern, salinities, and other paleoceanographic scenarios. The error of temperature estimation is generally lower than 0,2°C resulting from a measurement error of maximal 0,05‰ PDB.

3.4 Colour litho-logs

Sediments are showing distinctive colours regarding to their facies. Investing lithologies and/or the search of sedimentary cycles by colour measurement is a frequent and non-destructive tool and gets more and more used (Schaaf, 1995; Weber, 1998; Nebe, 1999). There are different methods to measure colours. According to this physical data acquisition we hope to evolve a method to correlate the sites of the transect. This will be one major aim for an evaluation of climatic evolution. A spectrophotometer (Minolta CM-2002) that contains a spectral sensor with 40 single segments was used. This sensor measures received light from the object, for the different wavelength of the visible spectra. This information is transmitted to a microcomputer. The microcomputer determines the standard colour values from the reflection data of the sensor signal by integration. The result can be extracted both by numerical numbers or spectral curves. The spectrophotometer reveals a high resolution and short measurement times and is hence a fast logging tool. Sampling was done on the archive-halves with a sampling distance of one centimetre, if possible. The spectrophotometer transmits three different values of colour-analyses. The L*a*b* or CIELAB-system was applied. The CIELAB-system represents equidistant colour space, which was defined by CIE (Commission Internationale de l'Eclairage) in 1976. The colour values are calculated as follows.

Lightness L*: $L^* = 116 \left(\frac{Y}{Y_n} \right)^{1/3} - 16$

Colour-coordinates: $a^* = 500 \left[\left(\frac{X}{X_n} \right)^{1/3} - \left(\frac{Y}{Y_n} \right)^{1/3} \right]$

$$b^* = 200 \left[\left(\frac{X}{X_n} \right)^{1/3} - \left(\frac{Z}{Z_n} \right)^{1/3} \right]$$

with X , Y, Z: standard colour values (standard colour values XYZ for 2°- normal observation or $X_{10}Y_{10}Z_{10}$ for 10°-normal observation) and, Xn, Yn, Zn: standard colour value of an ideal lustreless white object (standard colour values XYZ for 2° normal observation or $X_{10}Y_{10}Z_{10}$ for 10°-normal observation).
If the quotient X/Xn, Y/Yn or Z/Zn small as 0,008856 following equations are valid:

$$\left(\frac{X}{X_n} \right)^{1/3} \text{ is substituted by } 7.787 \left(\frac{X}{X_n} \right) + \frac{16}{116}$$

$$\left(\frac{Y}{Y_n} \right)^{1/3} \text{ is substituted by } 7.787 \left(\frac{Y}{Y_n} \right) + \frac{16}{116}$$

$$\left(\frac{Z}{Z_n} \right)^{1/3} \text{ is substituted by } 7.787 \left(\frac{Z}{Z_n} \right) + \frac{16}{116}$$

The colour distance ΔE*ab in the L*a*b*-colour space indicates only the absolute value of the colour deviation, but not the direction

$$\Delta E^*_{ab} = \sqrt{(\Delta L^*)^2 + (\Delta a^*)^2 + (\Delta b^*)^2}$$

with ΔL*, Δa*, Δb*: differences of the L+a*b*-values between the colour of the sample and the colour of the reference

The L*-value is a reproduction of the lightness of the sediment and can be defined as a kind of grey value, whereas the other two values a* and b* are related to the colourfulness. Increasing L*values characterize more pale colours. Negative a* values are related to green dominated colours and positive a* values are dominated by a red colour. Blue colours are related to negative b* values, whereas positive values show a dominance of yellow colours. The sediment colour depends on many factors, which can be primary or secondary. Primary aspects can be the chemical or micropaleontological content and secondary their modification. The archive halves were measured directly with the spectrophotometer put on the core segment. We used the line scan method to keep statistical conditions. If possible a high-resolution sampling of one cm was done resulting in a total measurement of more as 22.000 colour values. Data from the colour litho-logs were used for frequency analyses with the "Speclab" program. The main tool in our investigations is the L* value for the lightness. Bivalves, mineral assemblages or other core contents can influence the L* value. A spline function was not used to keep our results authentic and random. The a* and b* values can be neglected with exception to special questions like e.g. the abundance of pyrite.

3.5 Frequency analyses

For spectral analyses we split the core sections into cycle sections with similar sedimentation rates. This is required for a consideration over a wider time span, which needs a quasi-stationary sedimentation system.

The change of physical, chemical or biological aspects in sediments can be often related to cyclic embedding. Normally geological processes are represented in a depth series with a various parameter described as a function of depth. Spectral analyses yield the assumption that a relation between depth and time is clearly certain and offers the possibility to represent cycles in a data set,given by transforming the depth series into a frequency series and describing the dominant frequencies/wavelength. Most of the software used to calculate the cyclicity of geological data sets is based on a Fourier-Transformation (FT). The result of a FT is the presentation of periodic oscillations in a time series. The amplitude Y_i is defined by the amplitudes of the frequency coefficients (α_n and β_n) at a distance X_i from the origin of the series.

Fourier-Transformation: $$Y_i = \sum_{n=1}^{\infty} \left(\alpha_n \cos \frac{2\pi n X_i}{\lambda} + \beta_n \sin \frac{2\pi n X_i}{\lambda} \right)$$

The Fast-Fourier-Transformation (FFT) is based on an algorithm for a more rapid calculation. This Transformation is restricted to a series of N data points with constant intervals X_i and an overall length of L. From this we calculate the Fourier coefficients α_n and β_n from the overall length as base wavelength, because the wavelet of the base oscillation is not known. The sum of the squared Fourier coefficients is the so-called power.

power: $S_n^2 = \alpha_n^2 + \beta_n^2$

The resulting power can be expressed graphically as power spectra plots representing the power against the frequency also mentioned as cycles/m.
The Nyquist frequency describes the shortest frequency that can be calculated by Fourier transformation.

Nyquist frequency: $f = 1/(2\Delta)$ with Δ = sample interval

Our sampling interval of one cm is clear below the Nyquist Frequency of ca. 20-30 cm in our studied cores to prove Milankovitch related cyclicity with a distinctive sedimentation rate of each site. For frequency analyses of single plot spectra and evolutionary spectral analyses the lightness data set was subjected to the "Speclab"-program (Port, 2000). This program for spectral analyses is based on the Lomb-Scargle-Fourier-Transformation-algorithm (LSFT) that yields the advantage to analyse inequidistant data sets too (Lomb, 1976; Scargle, 1982). In addition this method yields a high spectral resolution as well as a greater examinable frequency interval (Schulz, 1996). Beneath the bulk spectral analyses evolutionary spectral analyses (following ESA) have been done. This technique analyses a FT window, optional size in metres and it moves with a variable offset along the data set. These windows and the related offset then sample the whole data set. This technique has the advantage that changes of the orbital signal can be traced over a certain time span.

With the LSFT the single elements of the frequency pattern can be plotted against the amplitude. The significance of the allocation is the hierarchy of the configuration of the single elements. Berger (1977) mentioned the stability of this hierarchy to the Cretaceous. The program has the possibility to allocate the hierarchy pattern, that is defined by the time ratio of the single orbital factors of eccentricity, obliquity, and precession. In this study the ratios calculated from the maxima of the spectral energy are evaluated by hand and compared to the

Milankovitch ratios. If an agreement is observed an orbital control is very likely. Than a model explaining the orbital controlled signals is required.

Often cyclic sediment record is disturbed or modified due to variations of sedimentation rates, diagenesis, and tectonics (Peper, 1995; Oschmann, 1995). These processes can lead to a biased data set and false interpretations. Oschman et al. (1995) modified data sets for spectral analyses up to 20% simulating gaps, variations in the, diagenesis, tempestites, turbidites, slumping, erosion, bioturbation or condensed sections without destroying the orbital signals.

3.6 Milankovitch cycles

Periodic astronomical variations have multiple effects on earth (Mörner, 1994). This study only deals with the orbital control of insolation that affects a change of climate via temperature and precipitation, and hence the atmospheric and ocean circulation pattern on earth. The feedback results in changes of carbonate and organic matter productivity, changes in redox conditions, and fluxes of clastic input. The clastic input is controlled by the weathering conditions of the hinterland. Milankovitch (1920; 1930; 1941) was the first who described the orbital variations of the eccentricity, the obliquity, and the precession that are the most common types of cyclicity in sediments. Especially in the Quartenary and increasing for other periods Milankovitch cycles were established (Imbrie, 1985; Einsele et al., 1991; deBoer, 1994).

The eccentricity is caused by gravitational interactions with other planets of the solar system that create slight variations in eccentricity as the earth in its elliptical orbit itself rotates around the sun. The obliquity or tilt describes the angle of tilt between the Earth's axis and the ecliptic plane that undergoing small variations between 22° and 24°30'. The precession is characterized by the Earth describing a precessional movement as a result of the gravitational pull of the sun on the tilted equatorial bulge (Einsele et al., 1991) (Fig.8). It should be kept in mind that some interactions of these factors can force the effect like the precession index altering with the period of precession and the amplitude of eccentricity (Einsele et al., 1991).

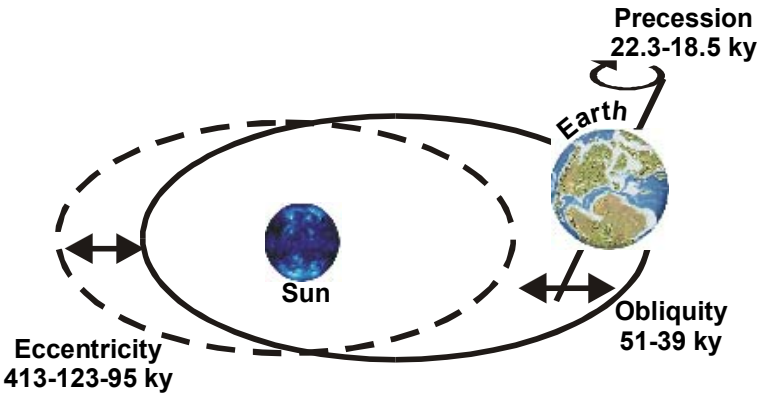

Figure 8 Cretaceous Milankovitch parameters of eccentricity, obliquity and precession (not to scale)

4 Results

4.1 Stratigraphy

The following three figures show the correlation of lithology, litho-logs, C_{org} content and $CaCO_3$ content of the three investigated sites of 7430/10-U-01, 6814/04-U-02 and 6307/07-U-02. The result is an agreement of the lithology and the litho-logs. In addition, a good correlation of the litho-logs and the C_{org} content is visible. Due to a low resolution of the carbonate content, the correlation with the litho-log is not very obvious.

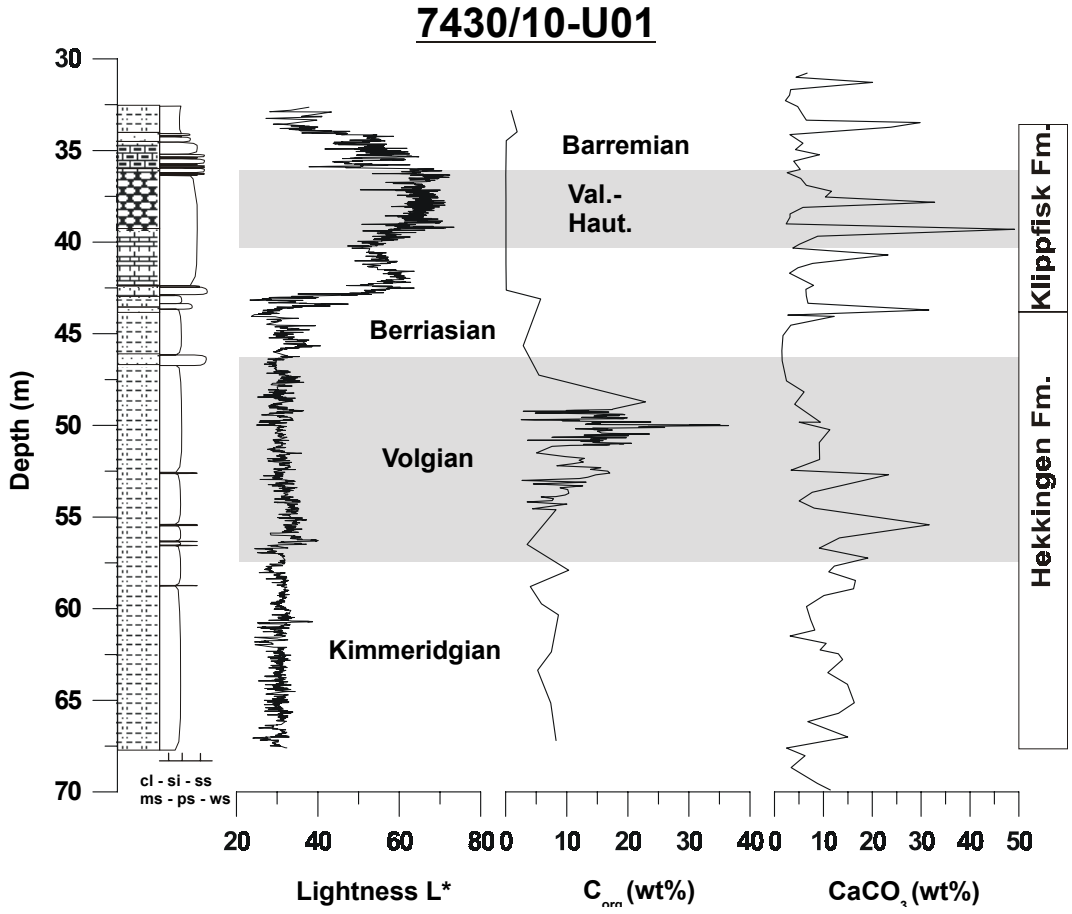

Figure 9 Stratigraphy, L* litho-log, Corg content (after Langrock, in prep.), and $CaCO_3$ content (after Lipinski, in prep.) of site 7430/10-U-01

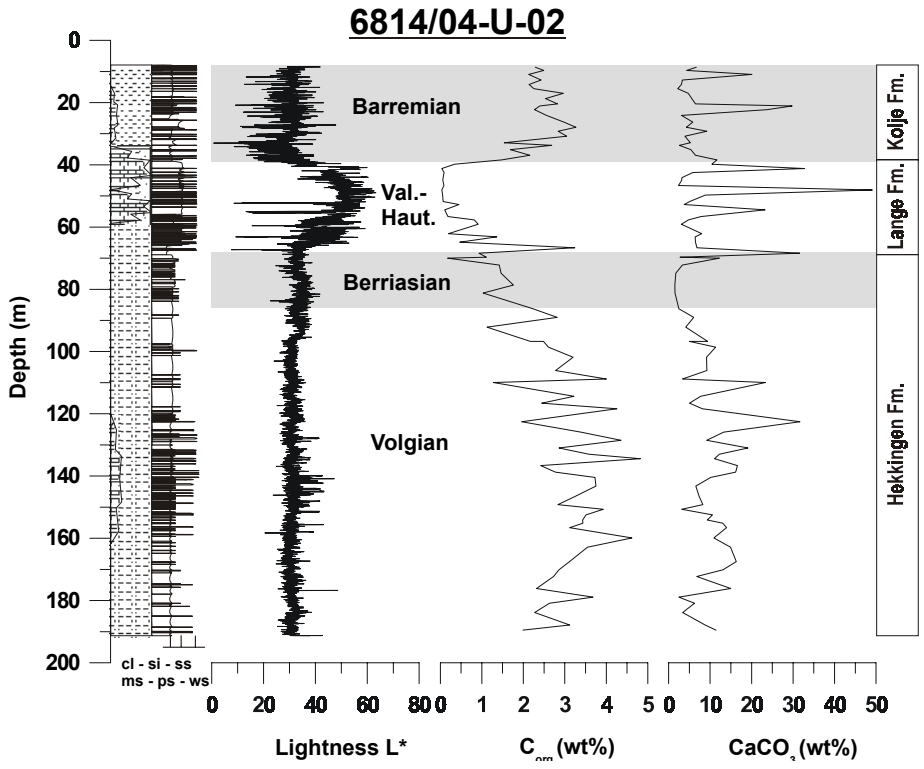

Figure 10 Stratigraphy, L* litho-log, Corg content (after Langrock, in prep.), and $CaCO_3$ content (after Lipinski, in prep.) of site 6814/04-U-02

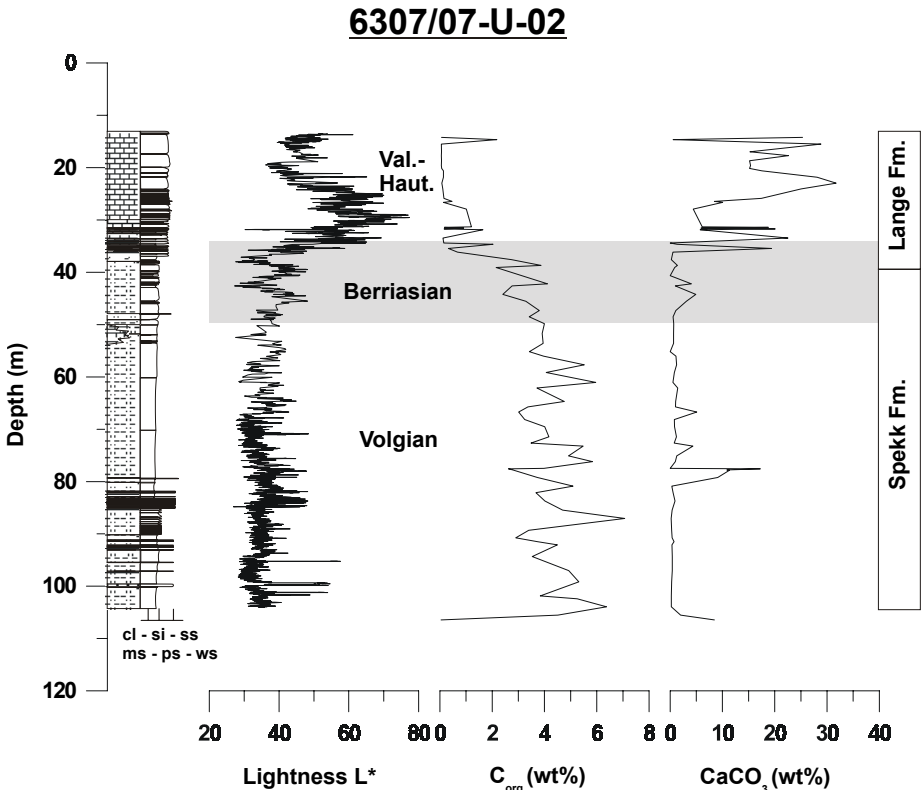

Figure 11 Stratigraphy, L* litho-log, Corg content (after Langrock, in prep.), and $CaCO_3$ content (after Lipinski, in prep.) of site 6307/07-U-02

4.2 Conditions of preservation

4.2.1 Stable $\delta^{13}C$- and $\delta^{18}O$ isotopes

4.2.1.1 Site 7430/10-U-01

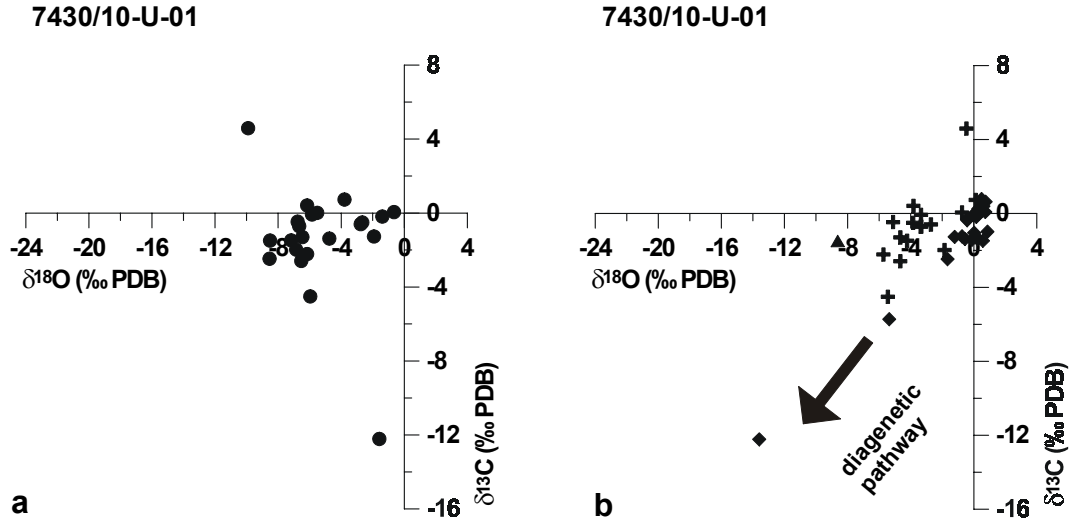

Figure 12 Isotope cross plots of bulk sediment (circles) and of belemnites (diamonds), inocerams (crosses) and *Buchia* (triangles)

The mean $\delta^{13}C_{bivalve}$ and $\delta^{18}O_{bivalve}$ values reveal differences in respective values. The oxygen-carbon isotope cross plots in figure12a show that the bulk sediment tends to more negative $\delta^{18}O$ values, whereas the $\delta^{13}C$ values are mostly arranged about 2 to –2 ‰ PDB.

	n ($\delta^{13}C$)	min	max	mean	n ($\delta^{18}O$)	min	max	mean
Buchia	1	-1,49	-1,49	-1,49	1	-8,62	-8,62	-8,62
Inoceramus	15	-4,51	4,59	-0,71	15	-5,72	0,13	-3,32
Belemnites	23	-12,22	0,78	-1,24	23	-13,6	0,88	-0,74
bulk	36	-15,49	0,33	-5,82	36	-11,13	-0,65	-5,61

Table 5 Statistics of stable isotope measurements in ‰ PDB

The *Buchia* and *Inoceramus* samples show a similar isotopic print about -4‰ PDB of $\delta^{18}O$. $\delta^{13}C$ values plot about 1‰ PDB. Elorza and Garmilla (1996) described relatively heavy inoceramid shells close to the bulk sediment, that lead to a possible "vital effect" which is often discussed. Generally, the $\delta^{13}C$ values of inoceramids are often described in our estimated range (Pirrie and Marshall, 1990; Elorza and Garcia-Garmilla, 1998; Pagani and Arthur, 1998). This is most likely related to an increase of secondary calcite, precipitated from pore water in the inner structure as visible under the CL. Inoceramid values less than –2 ‰, however, proclaim no alteration and are used for temperature estimation. The belemnites indicate values very close to the presumed original values. This can be related to the belemnite rostrum structure and the related surface area: volume ratio protects better than the open shell structures of bivalves where pore-fluids can easily infiltrate (Corfield, 1995). One example at 37.04 m reveals carbon and oxygen isotope values of up to –12,22 ‰ PDB and –13,6 ‰ PDB. These clear diagenetic values can be related to the bad preservation, as documented in the CL photograph. The belemnite $\delta^{18}O$ values, however, show no significant diagenetic alteration with a mean value of -0,74 ‰ PDB. The $\delta^{13}C_{bulk}$ isotope values indicate a possible influence of bacterial CO_2 either by terrestrial CO_2 of fresh water or CO_2 from marine methane-oxidizing bacteria.

For the bulk isotopes a general increasing trend of $\delta^{13}C$ is clearly visible in depth (Fig. 13). The $\delta^{13}C$ values are slightly more negative in the black shales. Some variations of a few per mill are also common. The trends of the shell and bulk samples are similar. The $\delta^{13}C$ isotope bulk samples of site 7430/10-U-01 display a range of –16‰ PDB with a decreasing trend with depth into the organic rich lithology. $\delta^{18}O_{bulk}$ variations are less expressed and do not confirm the decreasing trend with depth. The shell samples describe a closer variation of $\delta^{13}C_{shell}$ and $\delta^{18}O_{shell}$ with generally more positive values. No further correlations of isotope values and lithology are possible.

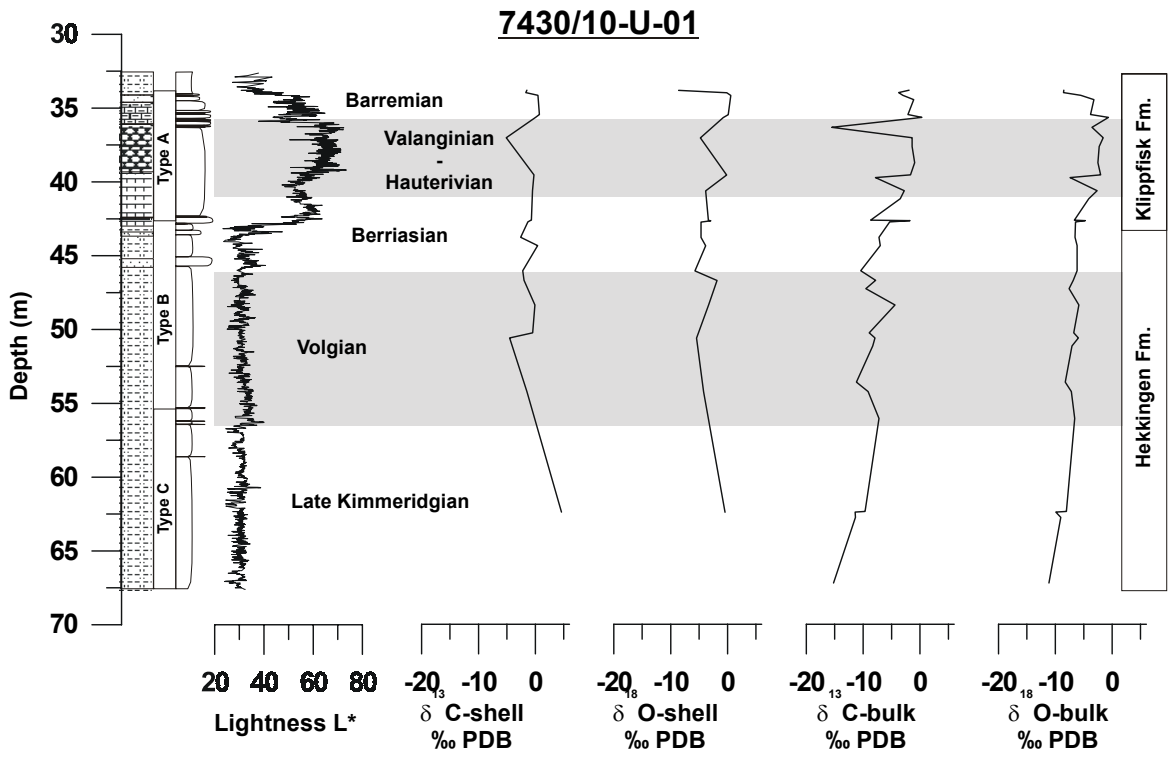

Figure 13 Site 7430/10-U-01 carbon and oxygen isotopes of shell material and bulk sediment related to depth (all $\delta^{18}O$ data are from inocerams, one *Buchia* sample, and five belemnite samples)

4.2.1.2 Site 6814/04-U-02

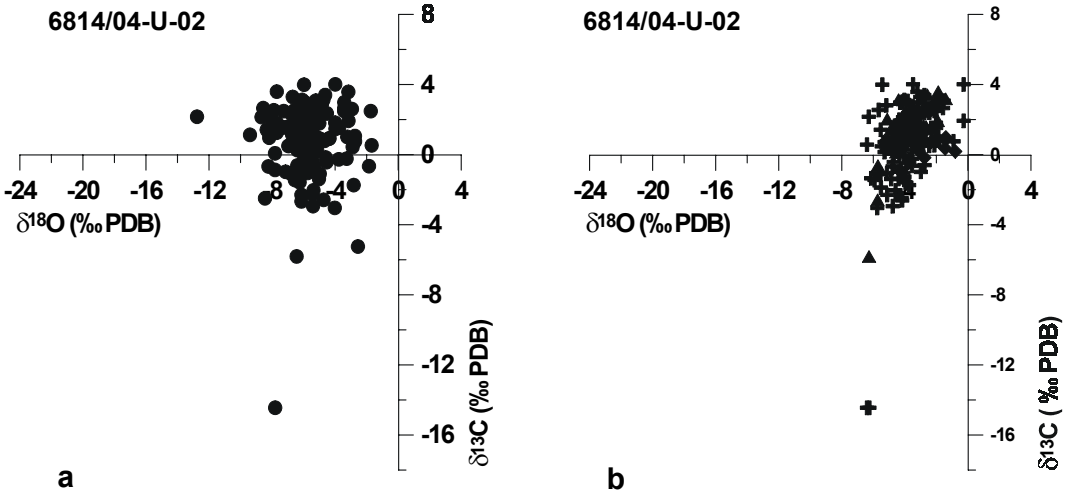

Figure 14 Site 6814/04-U-02 isotope cross plots of bulk sediment (circles) and of belemnites (diamonds), inocerams (crosses) and *Buchia* (triangles)

Mean $\delta^{13}C_{bivalve}$ and $\delta^{18}O_{bivalve}$ data are very similar to that of site 7430/10-U-01. The stable isotope values of this core are even slightly alterated by diagenetic effects (Fig.14). The *Buchia* samples show a more negative trend of $\delta^{13}C$ values, also reflected in the mean $\delta^{13}C$

value of 1,5 ‰ in contrast to 0,73 ‰ of the inoceramids (Tab.6). Well preserved inoceramid values from site 6814/04-U-02 were used for temperature estimation, as diagenetic alteration is not documented. This is expressed in $\delta^{18}O$ values up to –0,27‰ PDB (Tab.6). Most of the belemnite stable isotope values plot similar as the bivalve isotope values, indicating low diagenetic alteration. The values of the bulk sediment is comparable to that of site 7430/10-U-01, but shows an intern shift to slightly more positive $\delta^{13}C$ values and gives evidence for an introduction of light carbon.

	n ($\delta^{13}C$)	min	max	mean	n ($\delta^{18}O$)	min	max	mean
Buchia	33	-5,81	3,6	1,5	33	-6,27	-1,41	-3,61
Inoceramus	120	-14,45	4,01	0,73	120	-6,4	-0,27	-3,91
Belemnites	12	-0,17	1,58	0,73	12	-3,19	-0,8	-2,33
bulk	160	-12,77	1,86	-5,77	160	-12,76	-1,68	-5,61

Table 6 Statistics of stable isotope measurements in ‰ PDB

The $\delta^{13}C_{bulk}$ and $\delta^{18}O_{bulk}$ isotope curves of site 6814/04-U-02 also correlate (Fig.15). A decreasing trend of isotope bulk values in the black shales up to the Late Volgian/Berriasian (Ryazanian) is visible as well as the variations of up to 10 ‰ PDB. The shell samples do not express such a wide range of values as the bulk samples but also show rapid changes. The Hekkingen Fm.black shales are slightly more heavier than the calcareous Klippfisk Fm. and the shales of the upper Kolje Fm.. The site 6814/04-U-02 from the Ribban Basin even expresses variations up to 16 ‰ PDB in $\delta^{13}C_{bulk}$ but less in $\delta^{18}O_{bulk}$, and a certain correlation of both is noticeable. There is no trend of more negative values with depth but an increase to more positive values of both isotopes in the organic-rich lower part of the Hekkingen Fm., where also Fe-carbonate concretions and layers occur. The isotope data from shell material ranges around 0 ‰ for $\delta^{13}C_{shell}$ and around –4 ‰ PDB for $\delta^{18}O_{shell}$ without any context to lithology. The isotope curves of the bulk, as well as the shell samples, show a cyclic pattern throughout the whole core, most pronounced around 90 m.

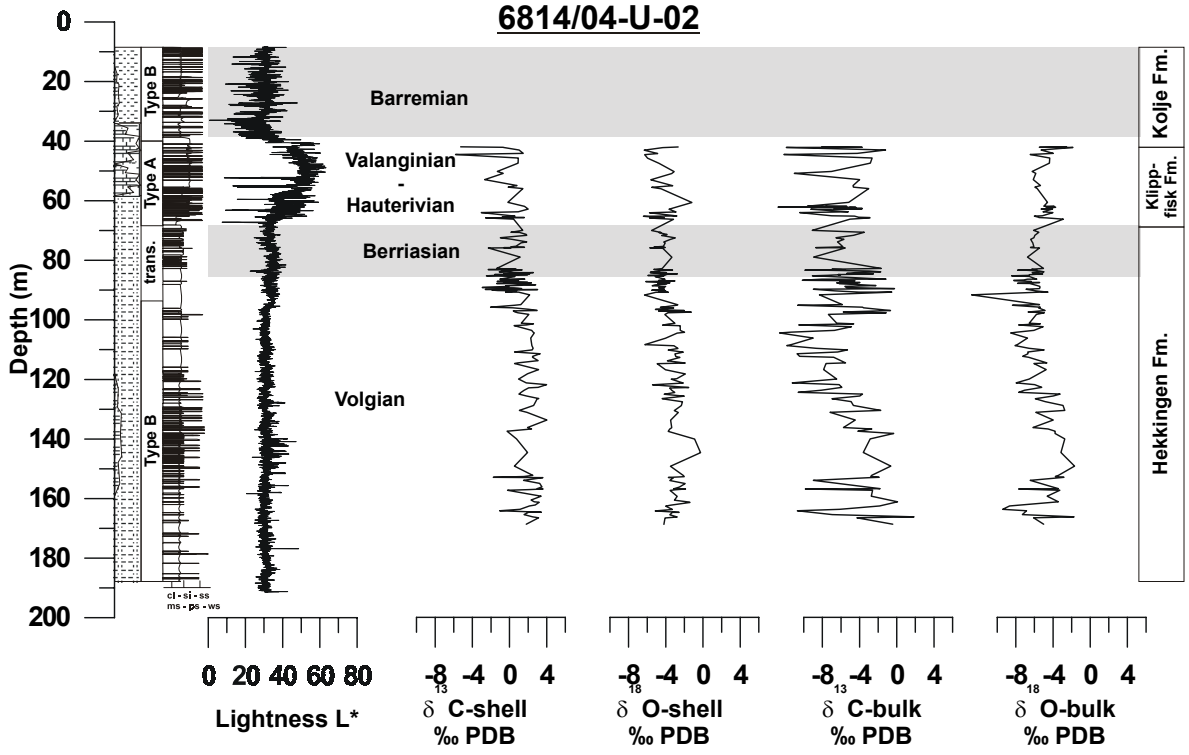

Figure 15 Site 6814/04-U-02 carbon and oxygen isotopes of shell material and bulk sediment related to depth (all $\delta^{18}O$ data are from inocerams, few *Buchias*, and three belemnites samples about 95m)

4.2.1.3 Site 6307/07-U-02

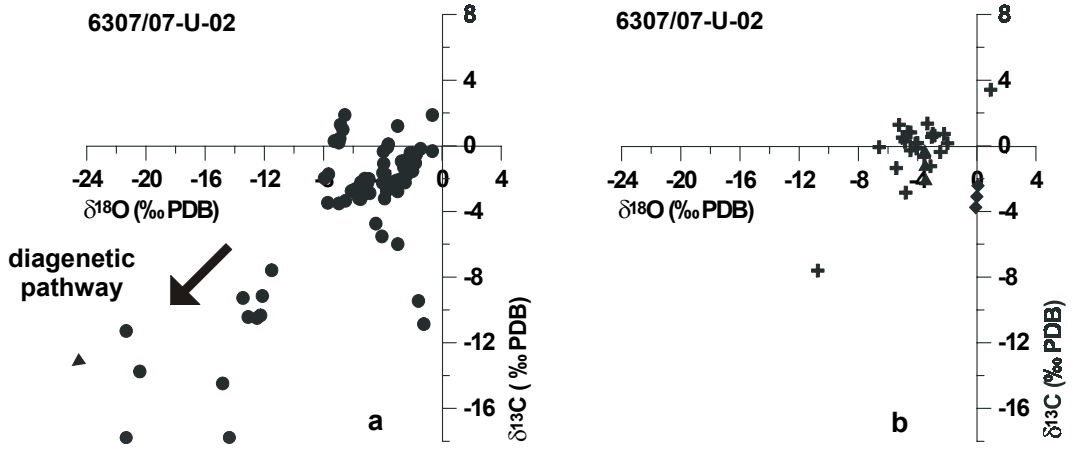

Figure 16 Isotope cross plots of bulk sediment (circles) and of belemnites (diamonds), inocerams (crosses) and *Buchia* (triangles)

Mean $\delta^{13}C_{bivalve}$ and $\delta^{18}O_{bivalve}$ values of site 6307/07-U-02 plot similar to the above mentioned sites (Fig.16). Two exceptions may be noticed. The belemnite $\delta^{18}O$ values plot at 0‰ PDB, but carbon values are slightly higher.

	n ($\delta^{13}C$)	min	max	mean	n ($\delta^{18}O$)	min	max	mean
Buchia	2	-2,04	-0,28	-1,16	2	-3,52	-3,45	-3,49
Inoceramus	23	-7,6	3,42	-0,13	23	-10,74	0,94	-4,05
Belemnites	2	-3,75	-2,43	-3,01	2	-0,07	0,08	0,00
bulk	72	-17,78	1,88	-3,24	72	-21,34	-0,65	-5,5

Table 7 Statistics of stable isotope measurements in ‰ PDB

The bulk samples are subdivided to samples very close to the shell values and samples that show very light carbon and oxygen values of ca. 16 ‰ and 18 ‰ PDB. Figure 17 demonstrates that the lightest values are related to the black shales of the Volgian. One inoceramid shows no diagenetic alteration and was suitable for temperature calculation. Site 6307/07-U-02 reveals $\delta^{13}C_{bulk}$ values about 0‰ PDB and similar, but less, $\delta^{18}O_{bulk}$values in the carbonaceous Lange Fm.. With increasing depth, the variation of isotopes becomes more significant and both curves turn to more negative values. As macrofossils are not documented in the Spekk Fm., the shell-isotope values are not as significant as the bulk values. $\delta^{13}C_{shell}$ and $\delta^{18}O_{shell}$ values, in contrast, do not show a significant correlation. There is a high frequent pattern about 20 m of the carbonaceous Lange Fm. which indicates cyclic sedimentation.

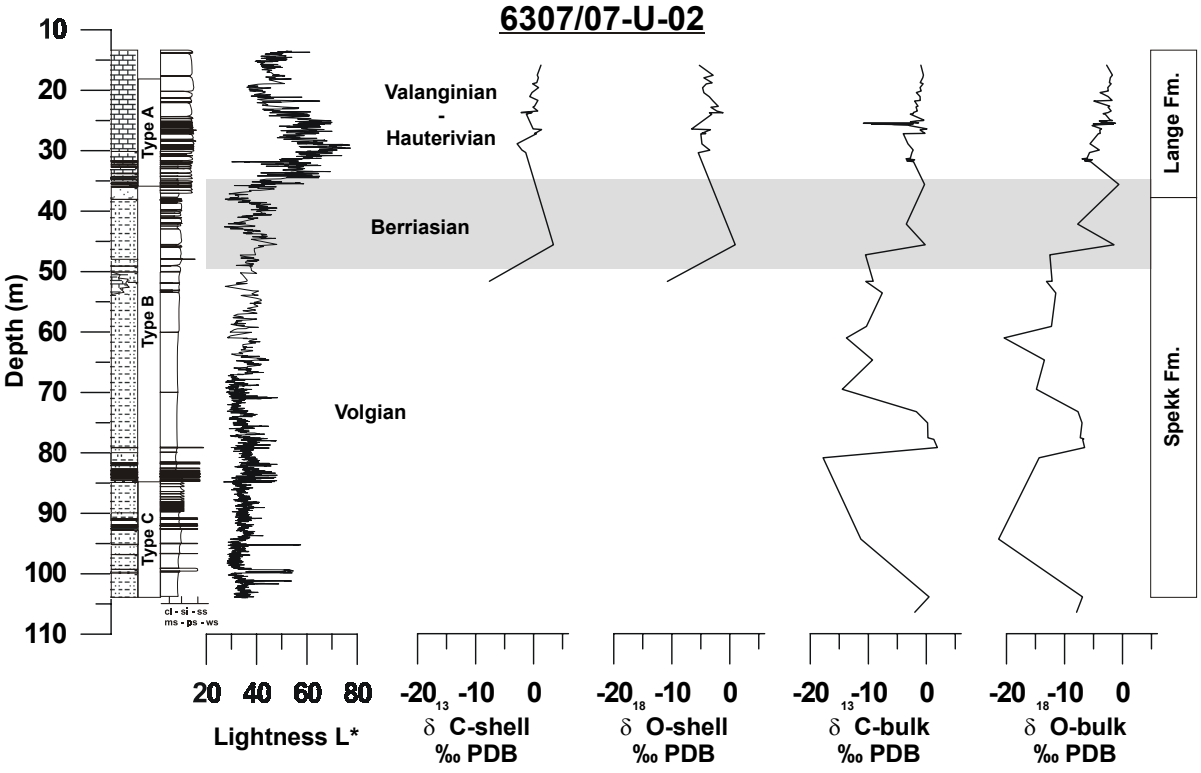

Figure 17 Site 6307/07-U-02 carbon and oxygen isotopes of shell material and bulk sediment related to depth (all $\delta^{18}O$ data are from inocerams, two *Buchias*, and one belemnite sample at 23,65m)

4.2.1.4 Site 13/1-U-2

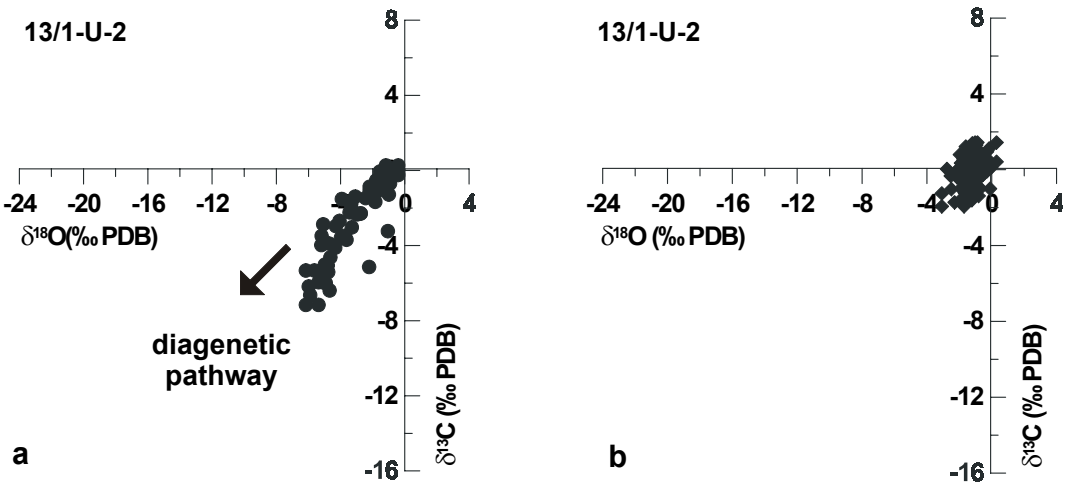

Figure 18 Isotope cross plots of bulk sediment (circles) and of belemnites (diamonds)

The stable isotope values of belemnites plotin cluster close to the origin value. The $\delta^{18}O$-$\delta^{13}C$ cross plots indicate that most of the belemnites are suitable for temperature estimation (Fig.18).

	n ($\delta^{13}C$)	min	max	mean	n ($\delta^{18}O$)	min	max	mean
Belemnites	188	-1,93	1,44	0,14	188	-3,08	0,3	-1,12
bulk	53	-7,16	0,27	-2,29	53	-6,16	-0,413	-2,75

Table 8 Statistics of stable isotope measurements in ‰ PDB

The southernmost site 13/1-U-2 shows a minor variation of the bulk samples of –6 ‰ PDB. The shell samples describe a highly frequent pattern about 155 m with an inner variation of –3 ‰ PDB both in $\delta^{13}C_{shell}$ and $\delta^{18}O_{shell}$ as well as in the bulk sediment. The high frequency pattern most likely indicate a distinctive cyclic variation. A correlation of lithology and shell isotope values is not obvious because the cycles occur at the transition from black shales to sand. The bulk isotopes seem to get lighter with the increasing sand content.

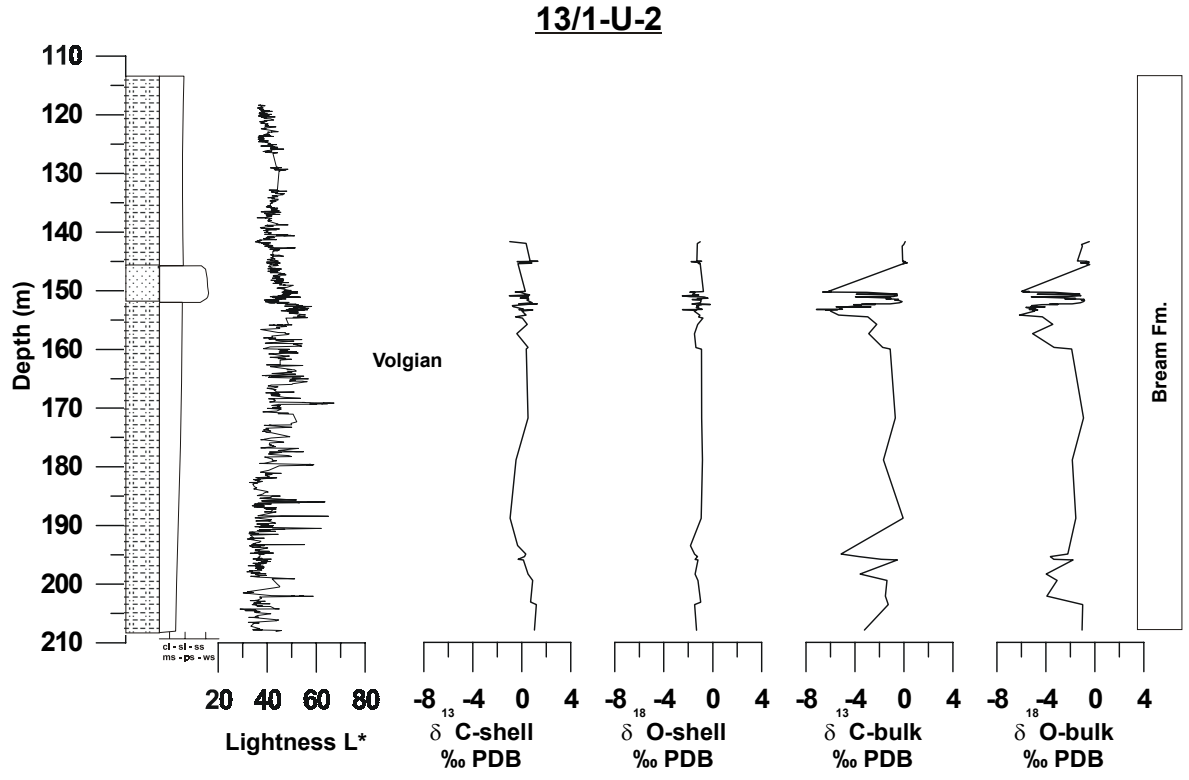

Figure 19 Site 13/1-U-2 carbon and oxygen isotopes of shell material and bulk sediment related to depth (all $\delta^{18}O$ data are from belemnites)

All sites reveal in general similar isotope trends. The bulk sediments indicate a more or less diagenetic pathway with increasing light values. Site 6307/07-U-02 shows the lightest carbon and oxygen isotope values. A correlation of $\delta^{13}C_{bulk}$ and $\delta^{18}O_{bulk}$ is visible, which is evident for diagenetic alteration and can be noticed from some linearity of the samples in the

plot. Inner fluctuations, as well as no notable progressive $\delta^{18}O_{bulk,}$ decrease with depth, with the exception of site 7430/10-U-01, whereas no diagenetic alteration is indicated. Therefore diagenesis with increasing burial temperatures can be excluded as the only or prime control on isotopic values (Jenkyns, 1997). $\delta^{13}C_{bulk}$ and $\delta^{18}O_{bulk}$ data are not suitable for temperature estimations but may contain primary features in form of inner fluctuations. With the exception of site 7430/10-U-01 all sites show a highly frequent pattern in different lithological sections. Site 6814/04-U-02 shows a highly frequent pattern in black shales, site 6307/07-U-02 reveal these rapid changes in the carbonaceous section.

All isotope values of bivalve samples plot in one cluster and show only minor trends to more positive values, which separates them from the bulk values. The belemnite samples contain the most origin values with rarely observed exceptions.

Brand & Morrison (1987) described oxygen isotope variation in belemnites from the Cretaceous up to –2 ‰ PDB of $\delta^{18}O$. Specimens with oxygen isotope values in that range vave been used for temperature estimation, even for bivalves.

Oxygen isotopic values rarely increase during diagenesis and decreases are expected in a non-marine environment or at elevated temperatures (Hudson, 1977). Inocerames investigated by Pirrie and Marshall (1990) include median $\delta^{18}O$ values of -2,59 ‰ and -2,45 ‰ PDB as well as $\delta^{13}C$ values of 3,33 ‰ PDB for calcite. The isotope data of belemnites reveal median $\delta^{18}O$ and $\delta^{13}C$ values of -0,45 ‰ and 2,05 ‰ PDB. Pirrie and Marshall (1990) interpreted this difference in terms of a stratified water column, whereas pore waters expelled from the underlying compacting volcaniclastic sediments modify the benthic bivalve isotope signals. Isotopic carbon values change with fluids in the presence of carbon, derived from the decomposition of organic matter (Hudson, 1977). The decomposition of organic matter leads to a decrease of $\delta^{13}C$, because $\delta^{12}C$ is getting enriched and CO_2 is transferred to surrounding water. Increasing salinity results in higher $\delta^{18}O$ values (Wefer, 1985).

4.2.2 Scanning Electron Microscopy

Under SEM the calcite prismatic layers of the shells seem to be well preserved and without evidence of neomorphism or secondary calcite. The samples of belemnites and inoceramids in figure 20 show simple prismatic calcite and a characteristic polygonal and well-defined honeycomb morphology, perpendicular to the long-axis of the calcite prisms. The grain boundaries are also well defined.

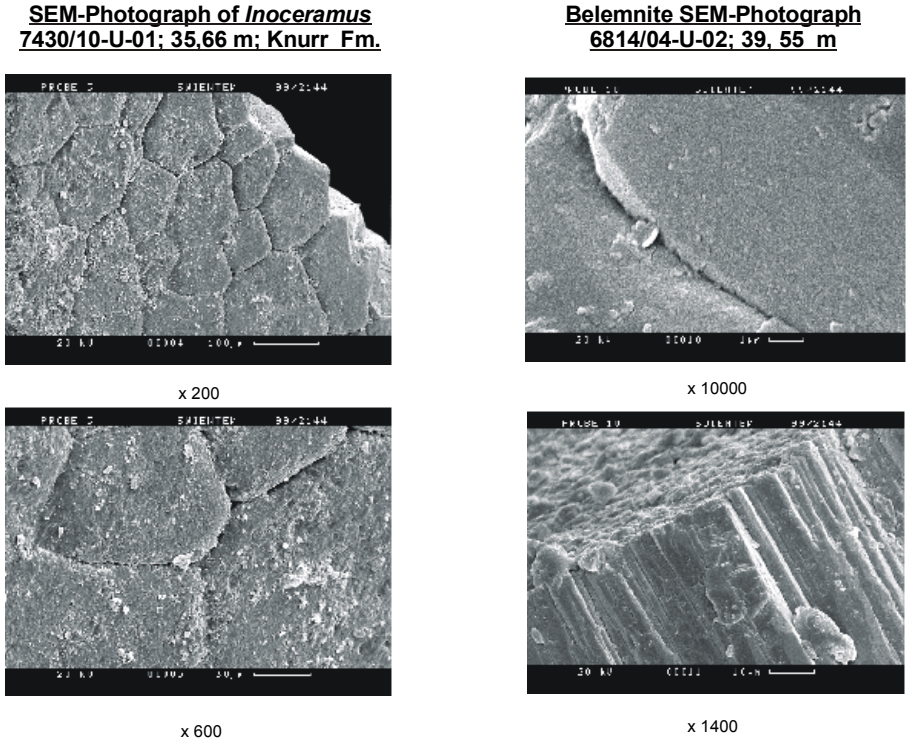

Figure 20 SEM-photographs of an *Inoceramus* shell and of a belemnite. Note the well-defined prism boundaries.

Small pits, as a result of carbonate dissolution or the loss of organic filaments originally present within the prisms are visible at a higher magnification of 6000. This primary structure geometries was described as a non-intense diagenetic alteration. Pirrie and Marshall (1990) described geochemical altered inocermids, which appeared well preserved under SEM. A *Buchia* shell sample from the Hekkingen Fm. at 50,25 m of 7430/10-U-01 shows a well-preserved nacreous sheet at a fresh breaking. No calcite prisms are observed in this sample. Another sample of *Buchia* at 48,62 m from the Hekkingen Fm. of site 7430/10-U-01 shows the lamellar structure of this bivalve. Pits with a size at 1 μm are expressed within the laminae, producing a significant porosity.

SEM-Photograph of *Buchia*
7430/10-U-01; 48,62 m; Hekkingen Fm.

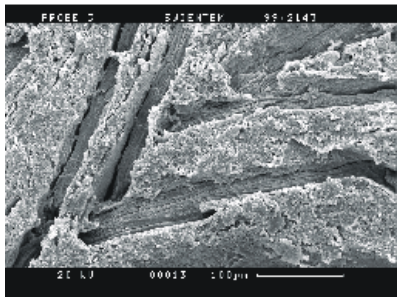

x 270

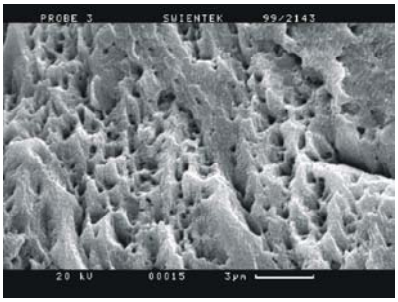

x 6000

Figure 21 SEM-Photograph of a *Buchia* shell. Note the secondary dissolution pits leading to a significant porosity.

Cross laminae of a nacreous layer can be observed at the deepest sample at 162,51 m of site 6814/04-U-02. Parts of a new built calcite cement are also visible.

There are two distinctive diagenetic features that can be noticed in transmitted light. The first is the new building of blocky calcite in shell fracture zones. This was only observed in one *Inoceramus* sample, so that this feature can be neglected. The second are brownish alterated (or opaque) zones covering the primary structures of *Inoceramus* and belemnite samples. These zones are not linked to particular structures.

4.2.3 Cathodoluminescence

Five belemnite and bivalve samples of core 7430/10-U-01, three samples of 6814/04-U-02, one sample of 6307/07-U-02, and 12 samples of 13/1-U-2 were investigated under CL. Diagenetic features are usually more pronounced where pore fluids were able to affect the shell, as along fractures. The latter are mosr likely caused compaction, tectonic movements, and at the rim. CL investigation reveal not significant variation among the belemnite samples. Concentric structures of the rostrum are visible under CL and transmitted light. The rostrum is build up by radial arranged calcite prisms. The background shows a very dull red colour or is non-luminescent. The zone near to the apical line, radial cracks, and the outermost growth ring show a bright orange to sometimes yellow colour, most likely due to suggesting diagenetic influence in this zone (Fig.22).

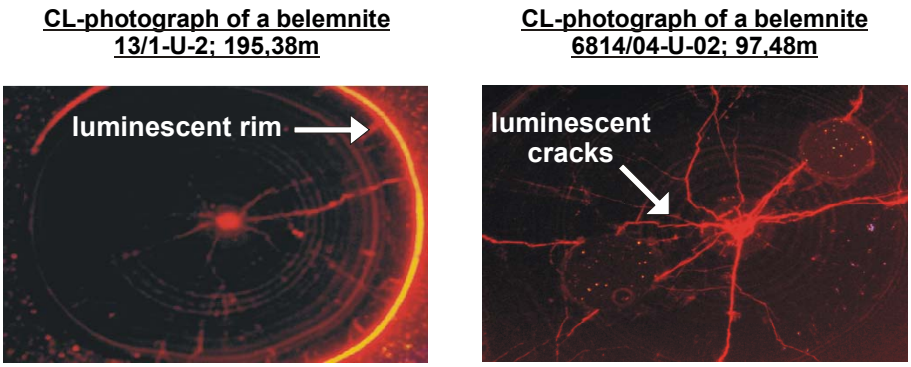

Figure 22 Cathodoluminescence-photographs of a belemnite. Note the diagenetic influenced areas.

Saelen and Karstang (1989) described the same feature as cements. Some growth rings have a dull to sometimes bright red colour caused by an infill of the secondary porosity developed from the decay of organic matter. Saelen (1989) discussed the dissolution of the intercrystalline organic material and a subsequent recrystallization of early cement resulting in bright luminescent cthodoluminescence colours. But most of the growth rimgs are not as bright as the cracks or the apical zone. These rings are also visible under transmitted light as brownish alterated (or opaque) concentric rings. Only two samples of site 7430/10-U-01 of a total number of investigated 20 belemnites show differences from the general belemnite features. These examples show a recrystallisation effect where the clear concentric structure is sometimes lost under the CL and display a bright orange to yellow colour. Belemnites of site 6814/04-U-02 reveal hardly any luminescence with the exception of bright orange cracks. The non-luminescence of these belemnites could also be caused by a high Fe content, which is a

cathodoluminescence quencher. The only belemnite sample of site 6307/07-U-02 exhibits a bright orange luminescence next to the sediment filled phragmocone. Site 13/1-U-2 shows similar effects as mentioned above.

Inoceramids and *Buchia* draw a contrasting picture. Visible calcite prisms of inocerams both in CL and transmitted light do not indicate a strong diagenesis.

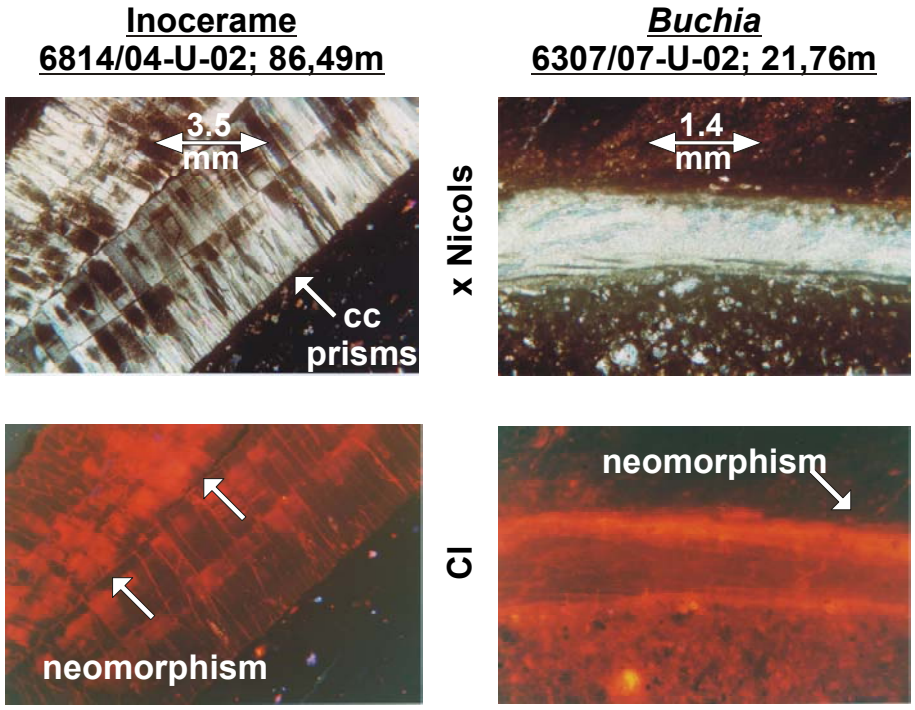

Figure 23 Transmitted-light and cathodoluminescence photograph of an inocerame shell and a *Buchia* shell. Note the opaque areas in the inocerame shell under crossed Nicols corresponding to the neomorphism in the cathodoluminescence.

There is no observation of an inner aragonitic nacreous shell layer of inoceramids as described by other authors (e.g. Pirrie and Marshall, 1990). The inocerams show a bright orange to yellow luminescence whereas there are also non-luminescent patches in the inner zones of the calcite prisms. Elorza and Garcia-Garmilla (1998) recognized similar patterns from inoceramids of different localities in the Basque country. The strongest luminescence of inocerams occurs between the single prisms, the two prism layers, and a patchy luminescence within the prisms itself. After the dissolution of the organic material, pore fluids can easily infiltrate between those prisms. Yellowish lines in greater fractures give evidence of new built calcite. These parts are clearly visible in transmitted light as bright stripes and are mentioned as neomorphism. Elorza and Garcia-Garmilla (1997) consider inoceramid shells not to be good paleoenvironmental indicators because they do not preserve the original isotopic signal

during severe diagenesis. But only CL analyses are not sufficient to discovers the degree of diagenesis.

Buchia have a different mineralogy to the belemnites and inocerams. Their shell layers are also constructed by aragonite, which was thought to be intact because of the nacre lustre of *Buchia* by the sampling campaign (Brand and Morrison, 1987). Neither in transmitted light nor under CL aragonite was visible. Diagenetic influences in *Buchia* shells are indicated by a bright red to mostly yellow colour. The inner structures of lamellae are sometimes visible under transmitted light, but are not expressed in CL photomicrographs. The loss of the internal structure is often marked by altered brownish appearing zones under transmitted and polarized light (Fig.23). Yellow lines appear in between the lamellae not likely due to the loss of organic compounds and the replacement by new diagenetic calcite. The grade of diagenesis rather seems to be a function of changing bedding conditions than of depth, because there is no relationship of preservation and depth. The best-preserved *Buchia* samples are from site 6814/04-U-07, where luminescence is not as strong expressed as in the other sites.

4.2.4 Inorganic Geochemistry

Belemnites precipitate low magnesium calcite, which is thought to have low trace element concentrations (e.g. Veizer, 1974). A Fe/Mn cross plot is used to display diagenetic alteration features. Anderson et al. (1994) propose that calcite shells with Fe contents above 1000 ppm and Mn contents above 100 ppm are diagenetically altered. According to this estimation, the samples of site 6814/04-U-02 and site 7430/10-U-01 have to be excluded (Fig.24).

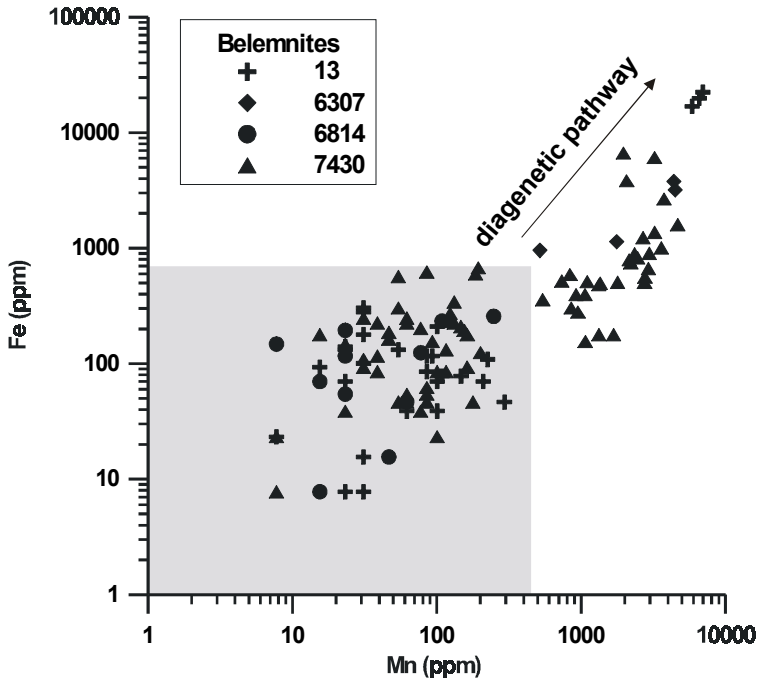

Figure 24 Scatter diagram of Fe vs. Mn trace element concentration in belemnites. Shaded area indicates the typical concentrations of modern marine LMC shells from Miliman, 1974 and Morrison and Brand (1986).

In a $\delta^{18}O$/Mn cross plot the belemnite values show no trend of diagenetic alteration which would be expressed by decreasing $\delta^{18}O$ values and increasing Mn values (Fig.25), with exception of two samples from site 6814/04-U-02 and three samples of site 7430/10-U-01 with an elevated Mn content. In a $\delta^{18}O$/Mn cross plot the bivalve values follow the diagenetic pathway with decreasing $\delta^{18}O$- and increasing Mn-values (Fig.25).

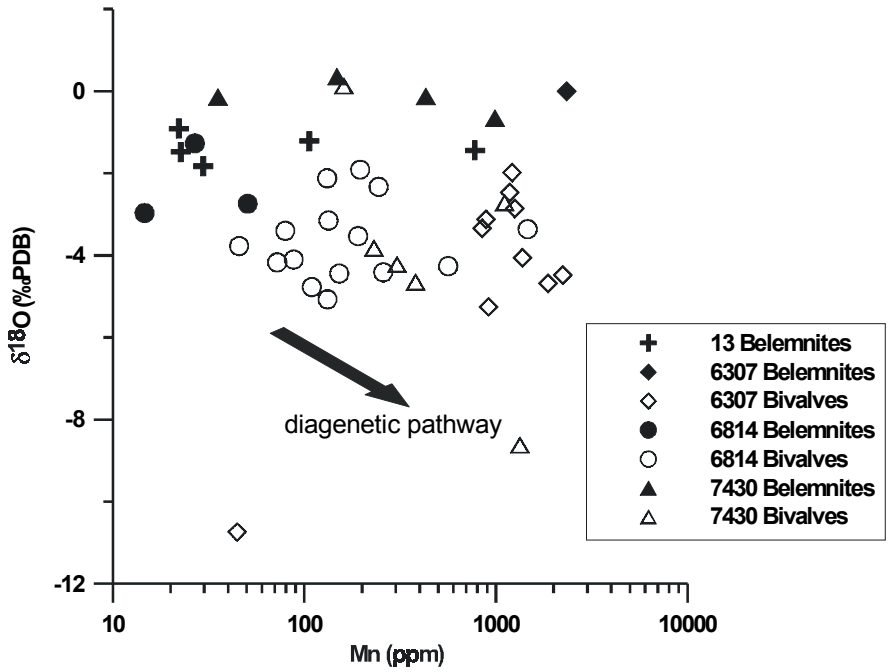

Figure 25 Diagram showing $\delta^{18}O$ (‰ PDB) versus Mn (ppm) for belemnites and bivalves. Note the diagenetic pathway with progressive increase in Mn and decreasing $d^{18}O$ for bivalve samples.

The Fe/Mn cross plot (Fig.24) draws a different picture, in accordance to the CL investigation. Some belemnite samples plot outside the field of well-preserved belemnites (Anderson et al., 1994). These samples are diagenetic altered and most likely represent infilled cracks or zones near the rim or the apical line of the belemnite.

Elemental variations between the shell material and adjacent bulk material are well expressed in element distribution-profiles by means of EMPA. In some of the graphs the content of Fe and Mn differ significantly from the content in the shells, whereas the content of sodium and manganese does not change significantly. Therefore a strong diagenetic influence can be excluded. By Morrison und Brand (1988) the measured Mg- and Mn-values of the shells plot in the field of origin values with natural chemical variations and hence do not represent diagenetic altered shells.

The OES-MS data of bivalves show that Sr/Ca, Mn/Ca, and Na/Ca relations are more or less close to values for low Mg-calcite or mixed mineralogy (aragonite-LMC) precipitated in equilibrium with modern seawater (Fig.26; Pagani and Arthur, 1998). This seems to be in contrast with the CL investigations, which show diagenetic effects.

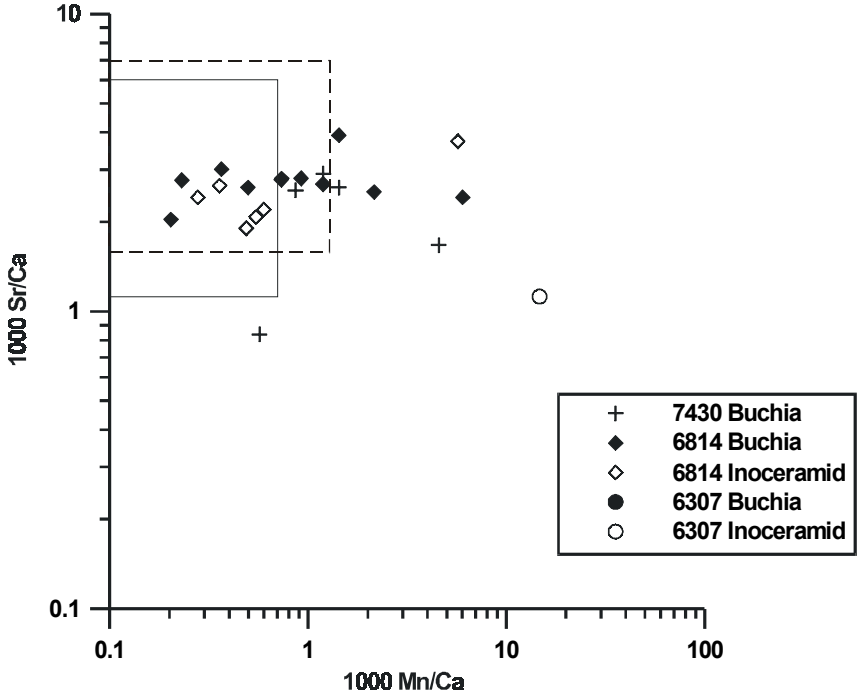

Figure 26 Sr/Ca vs. Mn/Ca trace element cross plot of Inoceramids and *Buchia*. Solid-line box indicates the chemical range for bivalves with low Mg calcite shells (Milliman, 1974; Morrison and Brand, 1986); dashed-line box indicates the chemical range for bivalves with mixed mineralogy (aragonite-LMC)(Morrison and Brand, 1986).

4.2.5 Colour logs and sedimentary cycles

With exception of site 13/1-U-2 the colour litho-logs give a similar picture in the logs (Fig.27).

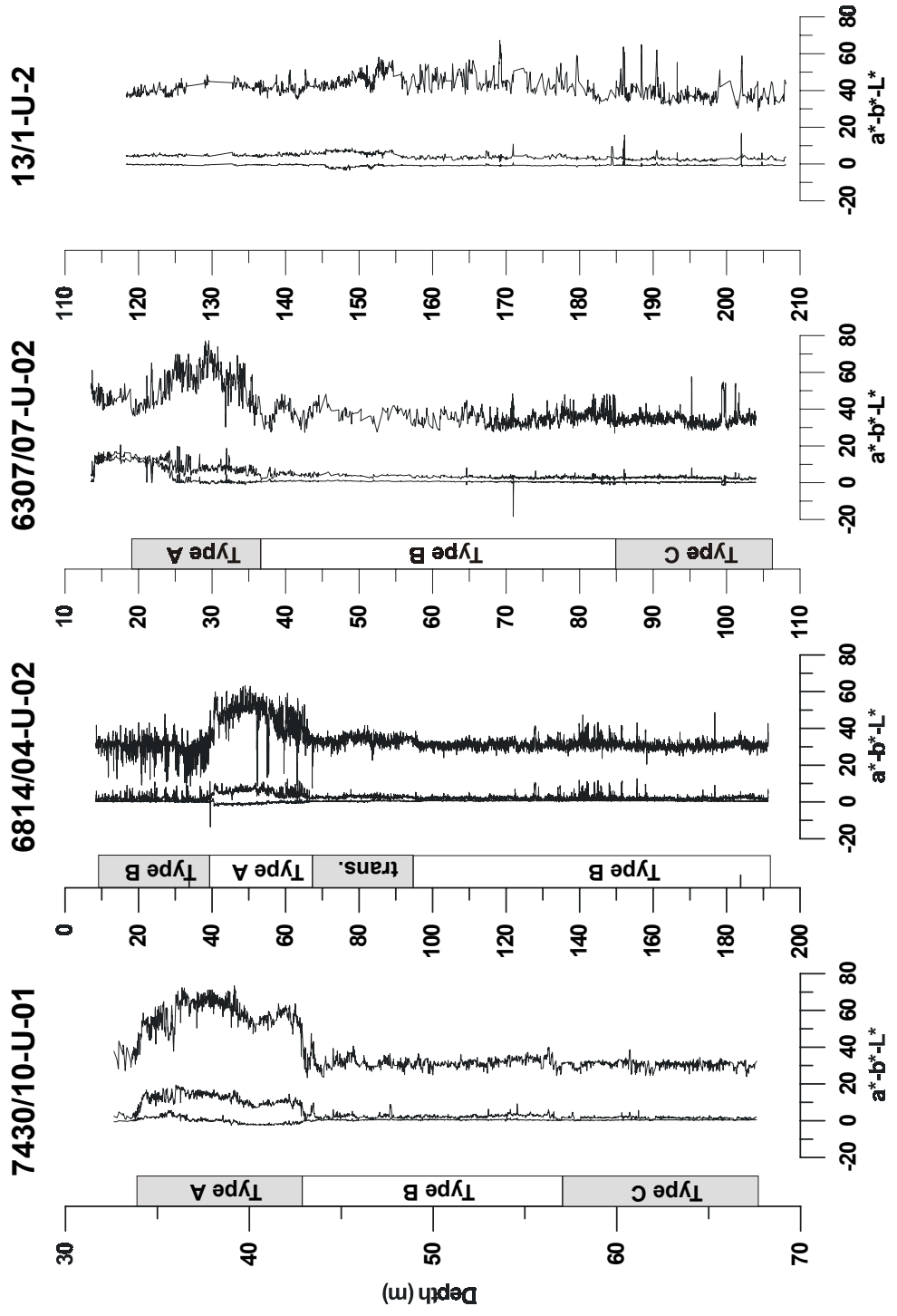

Figure 27 a* (green to red), b* (blue to yellow), and L* (black to white) values from left to right of site 7430/10-U-01, 6814/04-U-02, 6307/07-U-02, and 13/1-U-2

The similar chronological sequences permit a comparison of the different sites from Norway to the Barents Sea, and indicates a genetically relation of the sediments. With exception of site 13/1-U-2 the deposits show a similar lightness pattern with a significant maximum in the Valanginian/Hauterivian and other peaks in the Volgian, which can be used to correlate the sites. The litho-logs express the black shale sequences with L*-values about 25-35 with relative constant cyclic variations around a value of 5. The subsequent carbonaceous sections establish L*-values about 50 or more and a cyclic pattern with even higher variations around 10-15. The more silty shale at the base of site 6307/07-U-02 and 7430/10-U01 contains L*-values of 30-40 and in parts a cyclic embedding.

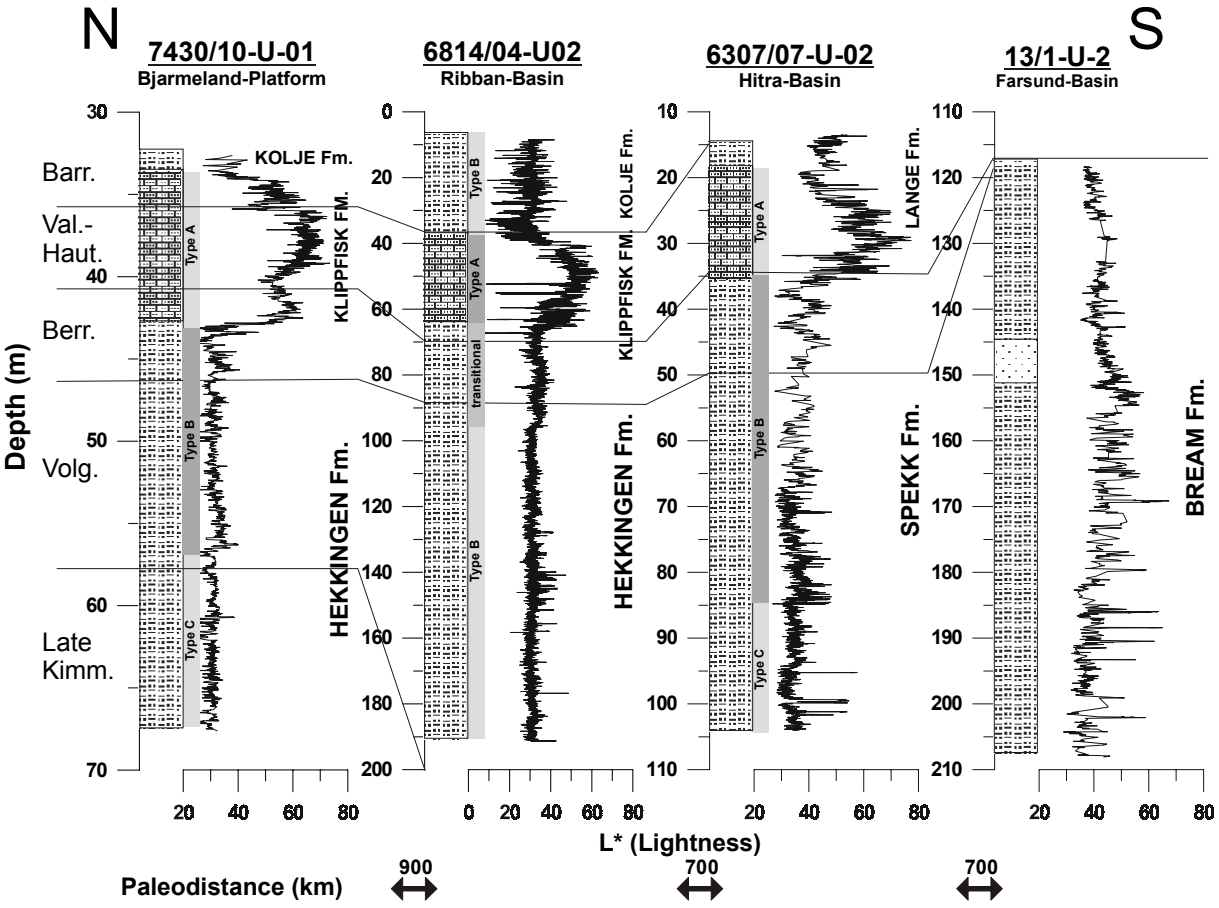

Figure 28 Biostratigraphical and cycle correlation of stratigraphy and L* litho-logs of investigated sites in a transect from North to South.

The spectrophotometer recognizes minimum changes in sediment colour which are otherwise not visible. The calculated colour values of L* (black-white component), a* (red-green component), and b* (yellow-blue component) combined with a detailed core description can be assigned to lithology parameters in a first approximation. The L* value e.g. shows positive

correlations with the carbonate content in carbonaceous sections or with the silt/sand content of shales. TOC-rich shales are in general darker than carbonates. Nebe (1999) postulated that the lightness value reveals a good estimation of the sediment content if it is defined before. In our case low L* values give a good estimation inverse to the organic rich shales and high L* values to proportional inverse carbonates.

Quasi-periodic cycles occur in various forms as described by e.g. Einsele et al. (1991). In this study the focus is on such types of cycles, which can be classified as dominantly allocyclic cycles without influence of the sedimentary processes itself. Allocyclic systems are created by factors which are not linkable to local effects, but dominant to climatic changes, tectonic processes or eustatic sea level changes (Einsele et al., 1991). The observed allocyclic cycle types can be distinguished as follows.

Most of the cyclic bedding pattern can be noticed by visible bed scale lithology changes, whereas other cycles are not obvious because the sediment seems to show a monotone colour. The main cyclic pattern based on changes in lithology and related bioturbation pattern are from top to bottom Typ A - carbonate productivity cycles, Type B - organic-rich concretionary cycles, and Type C - silt dilution cycles. The differentiation of these types of cycles is mainly based on changes in lithology and related colour changes (Swientek and Ricken, 2001b).

The Type A cycle is characterized by transitional variations in the carbonate content of 5 to 50% during a steady contribution of clay. The nannoplankton-carbonate rich intervals reveal an intensive bioturbation with *Planolites*-like structures whereas the carbonate-poor and C-organic richer intervals contain *Zoophycos* and *Chondrites*. The tiering pattern structure indicates a continuous growing of the sediments (Savrda, 1994) and can be attributed to an allocyclic genesis, best described as a change from oxic to dysoxic conditions. This type of cycle can be grouped into carbonate or calcareous redox cycles as proposed by Einsele et al., (1991) and Savrda (1991). Microscopic observations show a mud to wackestone matrix with some organic components. These Type A cycles occur in each of three sites. In 7430/10-U-01 from 34-44 m, in 6307/07-U-02 from 20-36 m, and in 6814/04-U-02 from 40-67 m where limestone layers appear in form of limestone/marl alternations are common (Fig.29). Type A cycles show L*-values of 35-80.

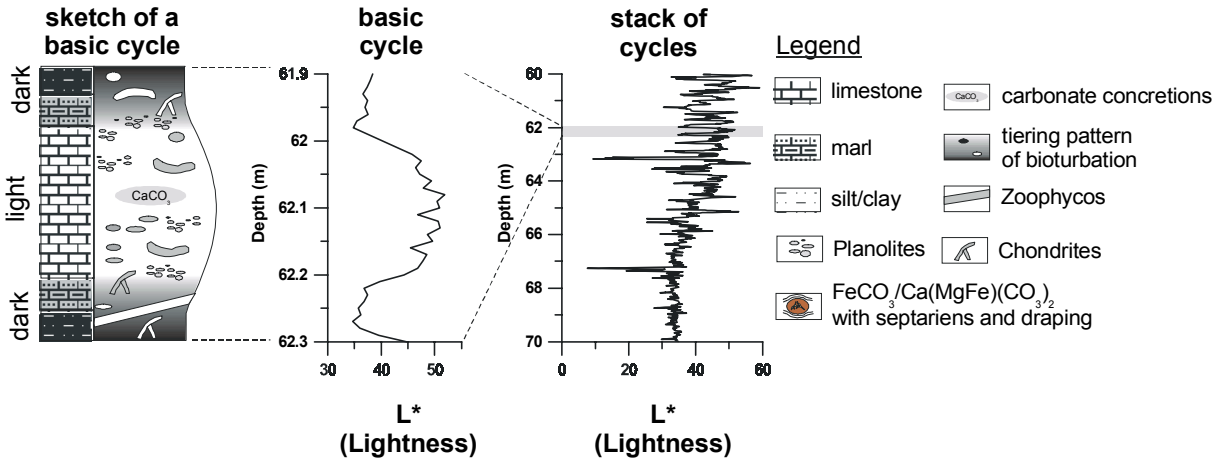

Figure 29 idealized Type A cycle section; lithology data are from site 6814/04-U-02

The organic-rich concretionary Type B cycles are dominated by laminated black shales with intercalated carbonate beds and concretions of calcite, siderite, and ankerite mainly at site 6814/04-U-02. The cyclicity within these laminated black shales is expressed by a faint colour differentiation. Some concretions, partly with blocky calcite infillings of shrinking veins reach 15 cm in length and visible draping structures indicate their foration prior to compaction. Bundling can be expressed by stacking with layers of smaller concretions. These Type B cycles occur in 7430/10-U-01 from 44-57.5.m, in 6307/07-U-02 from 67-85.m, and in 6814/04-U-02 from 9-40.m and from 96-192.m. The section from 67-96.m of site 6814/04-U-02 is marked by a transition between Type A and B cycles. Type B cycles show L*-values of 25-55.

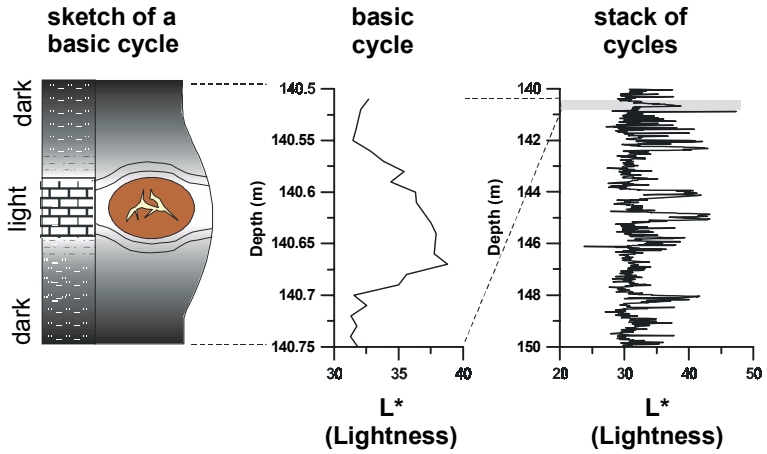

Figure 30 idealized Type B cycle section, lithology data are from site 6814/04-U-02

The Type C silt dilution cycles of the siliciclastic dominated basal sequences of site 6307/07-U-02 and 7430/10-U-01 are characterized by a succession of small-scale graded events of

silt/mud couplets. The quantity of silt changes throughout the cycle section, but not the quality. The texture is build up by non-rounded silt grains of mainly quartz that are embedded in a matrix of clay and organic matter. There is no visible change in lithological components. The lamination, clearly macroscopically visible, is sometimes wavy, but mostly not visible in microscopic observation. These events dilute the organic-rich sedimentary background. Some events are grouped to cycles of 4 to 8 events. Type C cycles show L*-values of 30-45. These cycles are assigned as dominantly allocyclic cycles, because of their orbital pattern in the spectral analyses. The existence of the silt dilution cycles indicate continental climatic changes with periodic supply of clastic material.

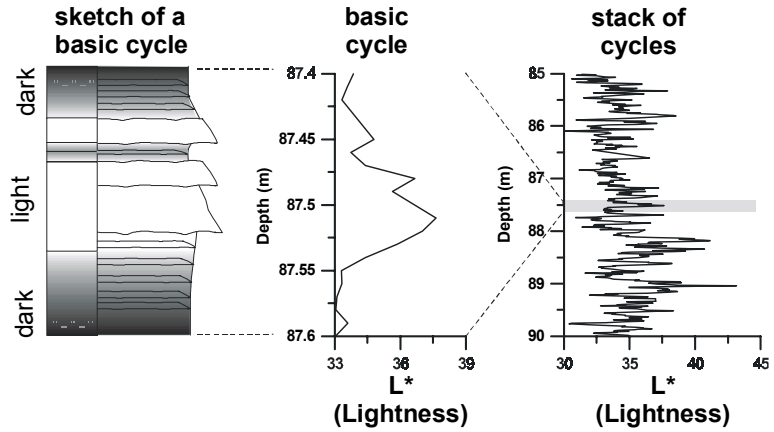

Figure 31 idealized Type C cycle section; lithology data are from site 6307/07-U-02

All cycles show a bundling effect with 3 to 6 cyclic beds per bundle, which most likely show a hierarchy pattern in cyclicity. Type A bundles display a variation in carbonate content, Type B in redox variations and/or stacked concretionary beds and Type C in stacked siliciclastic events.

4.2.6 Frequency Analyses and Milankovitch Cycles

The spectral analyses investigates a given time controlled function or time series to periodic parts as e.g. Milankovitch cycles (Oschmann, 1995). Spectral-analyses with the "Speclab" program (Port, 2000) show that orbital forcing dominantly drives the observed cyclic bedding rhythms. The program was run with distinctive data as the high resolution L*-values of the spectrophotometer and different physical well logs measured by the SINTEF Petroleum Research-Norway. Only high-resolution logs yield useful data for determination of cyclic bedding pattern. The resolution of common borehole logs is limited and hence they are mostly

not suitable for high-frequency analyses. Fischer (1990) proposed that logs are still useful in tracking low-frequency cycles, which can be partly confirmed by this study.

Generally we do not use any kind of spline functions or filtering with the exception one of evolutionary power spectrogram. Those well logging data were filtered through a low pass FFT-Filter with a smoothing of 50. The filtering was necessary to avoid internal periodicities of the "base-line". This is accompanied by the disadvantage of loosing long periodicities signals, like the E3-eccentricity, for the benefit of a better representation of short period signals. In our single plot spectra we use only peaks with significance above a power of 0.2 for interpretation. According to Nebe (1999) we tolerate a deviation of 3,5% of the match of Milankovitch cycles to the peak position in our single plot spectra, leading to a security interval of 93% of Cretaceous orbital cycles. Cretaceous Milankovitch cycles show signals of 413 ka (E3), 123 ka (E2), and 95 ka (E1) for the eccentricity, 51 ka (O2) and 39 ka (O1) for the obliquity, and 22.3 ka (P2) as well as 18.5 ka (P1) for the precession (Berger, 1977; Berger, 1989). The periodicities of these orbital features for the Cretaceous time are summarized in table 9.

Duration (kyr)	Orbital-period	Precession P1	Precession P2	Obliquity O1	Obliquity O2	Eccentricity E1	Eccentricity E2	Eccentricity E3
18.5	P1	1	1.21	2.11	2.76	5.14.	6.65	22.32
22.3	P2	0.83	1	1.75	2.29	4.26	5.52	18.52
39	O1	0.47	0.57	1	1.31	2.44	3.15	10.59
51	O2	0.36	0.44	0.76	1	1.86	2.41	8.1
95	E1	0.19	0.23	0.41	0.54	1	1.29	4.35
123	E2	0.15	0.18	0.32	0.41	0.77	1	3.36
413	E3	0.04	0.05	0.09	0.12	0.23	0.3	1

Table 9 Orbital periods of Mid-Cretaceous Milankovitch cycles (after Berger, 1977 and Berger et al. 1989a,b) and their internal ratios

4.2.6.1 Spectral analyses

Our results show a general coherence of the sedimentation rate based on the biostratigraphic frame and itself based on the observed and related Cretaceous hierarchy pattern of frequencies. Table 10 exemplifies for each cycle type the sedimentation rates estimated from biostratigraphy and spectral analyses.

	linear sedimentation rates per stratigraphic interval based on biostratigraphy	average sedimentation rates per investigated section based on the attributed peaks of spectral analysis
Type A (Early Valanginian)	3.8 ± 0.8 m/ma	4.4 ± 0.2 m/ma
Type B (Late Volgian)	19.0 ± 7.6 m/ma	16.2 ± 0.4 m/ma
Type C (Early Volgian)	6.7 ± 2.5 m/ma	8.2 ± 0.4 m/ma

Table 10 Biostratigraphically-based sedimentation rates follow the time scale of Hardenbol et al. (1998); Type A and B (lower part) cycle data are from site 6814/04-U-02 and Type C cycle data are from site 6307/07-U-02

This study presents some single power spectra which clarifies the orbital control of the sedimentary cycles. The periods of the cycles correspond with the Milankovitch frequencies. All ratios are normalized to the E1 eccentricity signal. Generally we divide the core in three sections related to the containing cycle pattern. Spectrograms are presented from North to South.

7430/10-U-01

Type C Cycles

The cycles are given by the pale-dark contrast and hence there are a function of the TOC and silt content. The resulting cycles are silt dilution cycles. Microscopical investigations show an argillaceous texture with silty inlets whereas clear lamination is lacking. Spectral analyses show a clear orbital forcing, showing that these cycles have to be allocyclic. The orbital control is shown in Fig.32 as well as the ratios of periods with an assumed sedimentation rate about 2,3 m/Ma. Beneath a well-developed precessional signal the eccentricity can also be

observed. Obliquity is also well expressed. The ratio of 4.12-1.31-1-X-0.37-0.3-0.21 indicates an orbital controlled pattern after Milankovitch.

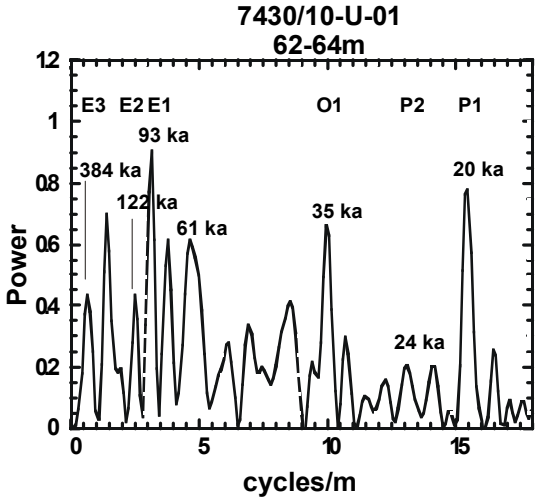

Figure 32 Power spectrogram of Type C cycles of site 7430/10-U-01 (62-64m) and allocated orbital signals

Type B cycles

In the black shales the carbonate content is low and dysoxic conditions are documented by the dark sediment colour and pyrite resulting from sulphate reduction. Therefore the litho-log is thought to reflect redox cycles, whereas the TOC-content controls the L*-value. With an assumed sedimentation rate about 1,6 m/Ma the orbital signals are well developed. The ratio is 4.51-1.41-1-0.54-0.41-0.26-0.2. Besides the well-expressed eccentricity, obliquity, and precession are also visible. Precession is not as good developed as in the Type C cycle section.

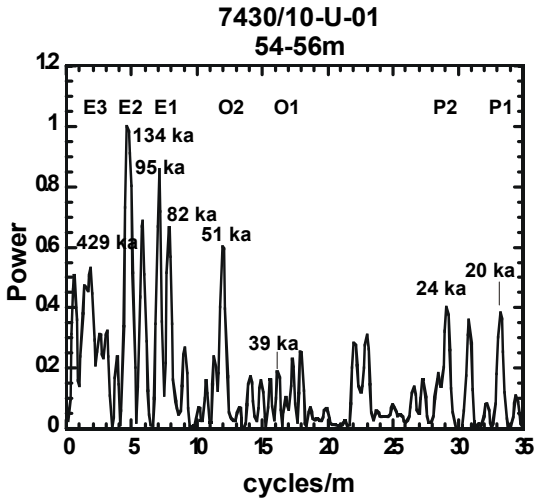

Figure 33 Power spectrogram of Type B cycles of site 7430/10-U-01 (54-56m) and allocated orbital signals

The carbonaceous Type A cycle section is subdivided in grey/reddish brown marls and limestones. These units also show orbital driven sediment pattern. The carbonate productivity cycles are characterized by change in the nannoplankton content. The L* litho-log is a function of the carbonate content and the background sedimentation. The assumed sedimentation rate is 1.2 m/Ma. The ratio of 4.57-1.37-1-0.54-0.45-X-X documents an orbital control of sedimentation. In contrast to the Type B and C cycle spectrograms, the spectrogram of the Type A section reveals no precessional peak and a very low eccentricity (Fig.34). Therefore the obliquity is very strong evolved.

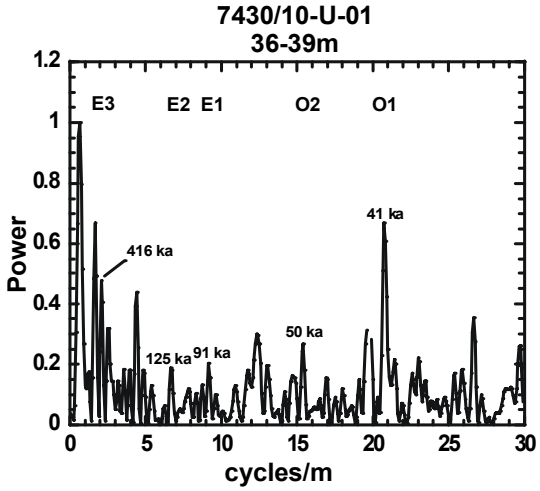

Figure 34 Power spectrogram of Type A cycles of site 7430/10-U-01 (36-39m) and allocated orbital signals

6814/04-U-02

The Type B cycle sections can be divided in parts with and parts without concretions. The lower part ranges from 120-170 m and the upper part from 16-40 m. Both parts are characterized by $FeCaCO_3$-concretions. The upper part with an assumed sedimentation rate of 4.18 m/Ma shows the ratio of 4.12-1.27-1-0.52-0.38-0.25-0.19.

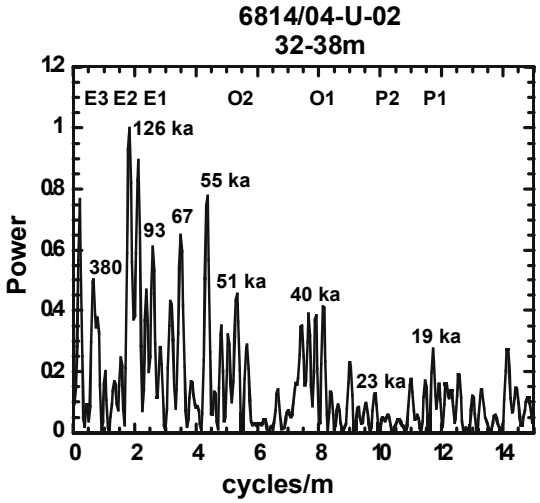

Figure 35 Power spectrogram of Type B cycles (upper part) of site 6814/04-U-02 (32-38m) and allocated orbital signals

The lower part also indicates Milankovitch ratios with 4.36-1.37-1-0.66-0.44-0.25-0.2. The sedimentation rate is assumed to be about 16 m/Ma.

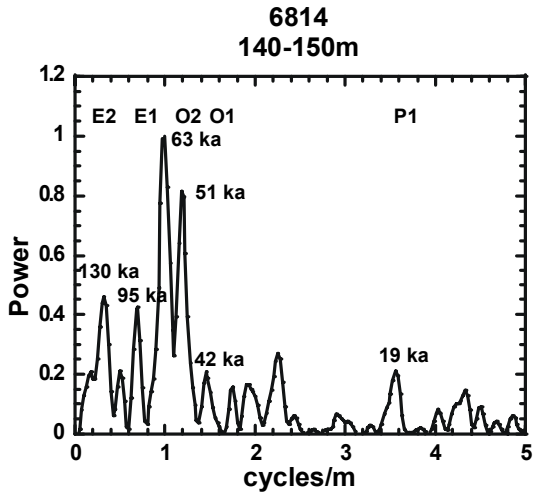

Figure 36 Power spectrogram of Type B cycles (lower part) of site 6814/04-U-02 (140-150m) and allocated orbital signals

The structure of both spectrograms is similar. The succession of the hierarchy pattern is eccentricity and obliquity with minor power of precession. The two Type B cycle parts with an intercalated Type A cycle describe a superior cycle, but cannot be explained due to the core limitation.

Type A cycles show similarities to the Type A cycle of site 7430/10-U-01 with a clear dominance of obliquity and a ratio of 3.79-1.17-1-0.58-0.44-X-X.

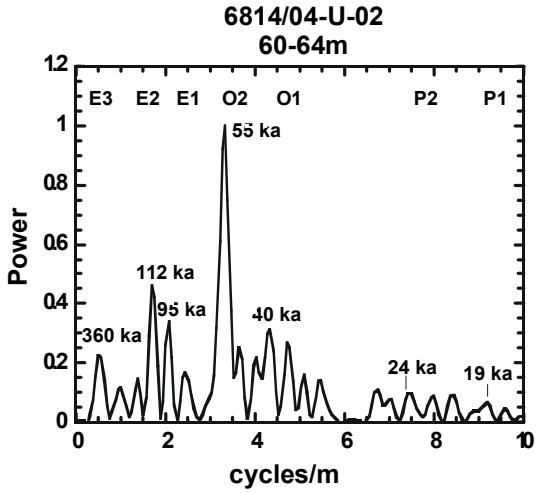

Figure 37 Power spectrogram of Type A cycles (upper part) of site 6814/04-U-02 (60-64m) and allocated orbital signals

6307/07-U-02

Further the Type C cycle section of this site is comparable to that of site 7430/10-U-01 as can be observed by a dominance of eccentricity and precession. The ratio is 4-X-1-0.51-X-0.24-0.2 with a sedimentation rate about 8 m/Ma. This Type C section is characterized by a well-developed precessional signal, similar to the Type C cycles of site 7430/10-U-01.

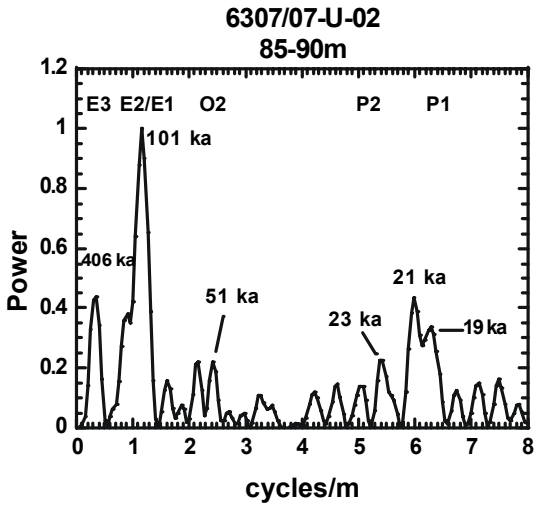

Figure 38 Power spectrogram of Type C cycles of site 6307/07-U-02 (85-90m) and allocated orbital signals

For this Type B cycle section a sedimentation rate of 5.7 m/Ma was established. A ratio of 3.7-1.25-1-0.52-0.34-0.23-0.18 indicates an orbital controlled sedimentation with a strong dominance of the obliquity.

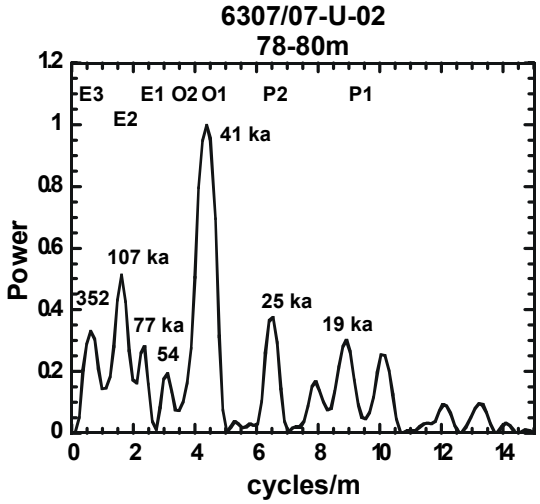

Figure 39 Power spectrogram of Type B cycles of site 6307/07-U-02 (78-80m) and allocated orbital signals

Type A cycles of site 6307/07-U-02 show comparable to Type A cycles of site 7430/10-U-01 and 6814/04-U-02 a certain dominance of obliquity beside the eccentricity. With an assumed sedimentation rate around 2.3 m/Ma the following pattern was calculated: 3.7-1.25-1-0.54-0.38-X-X.

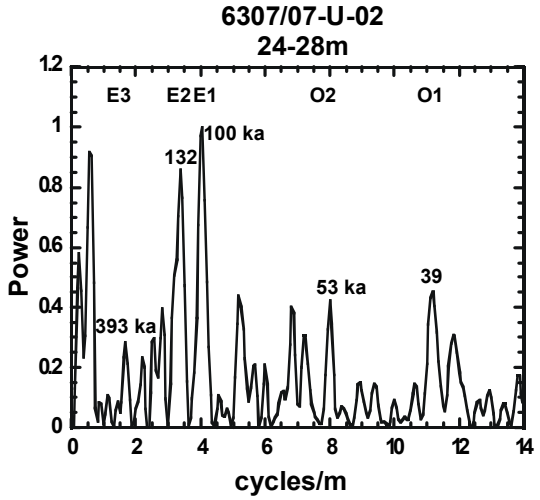

Figure 40 Power spectrogram of Type A cycles of site 6307/07-U-02 (24-28m) and allocated orbital signals

A certain comparability of site 6307/07-U-02 and site 7430/10-U-01 is visible in the Type A and Type C cycles. Although the L*-pattern of site 6814/04-U-02 shows a genetic relationship to the other sites it is somewhat different and will be discussed later.

It should be emphasised that spectrograms change with each cycle type and each cycle type have a very similar hierarchy pattern throughout the different sites of the transect, like e.g. the obliquity dominance of Type A cycles. This fact supports the genetic relation of the

different sites like the correlations of the L* (lightness) pattern above. Moreover, it is obvious that the spectrograms change with stratigraphy and that there is no evidence of the preference of distinctive cycle types with latitude.

4.2.6.2 Evolutionary spectral analyses (ESA)

Evolutionary spectral analyses offers a coherent observation of the evolution of cycles with time. Therefore a moving window technique is applied. Distinctive spectra (window size) are calculated and shifted along the depth scale in a defined interval (windows offset) to illustrate the stability of the spectra with time. Hence, the allocation of power and its stability can be estimated. The alternating appearance of cyclicity within a distinctive cycle type section can be pointed out. Additionally, changes of the sedimentation rate can be observed.

7430/10-U-01

The carbonaceous Klippfisk Fm. Type A cycle sequence of core 7430/10-U-01 from 34-44m was run with a window size of one metre and a window offset of 0.05 m. First the ESA seem to be very complex and that there are no stable orbital cycles. Rapid changes are common. There are clear signals of eccentricity both of 400 and 100 ka. Beneath the E signal the 70 ka and obliquity are even getting stronger whereas the eccentricity generally lowers. The 400 and 100 ka eccentricity signals mainly characterize the carbonaceous section. The eccentricity dominates in general this orbital controlled section, but two exceptions exist in the Valanginian (39-41 m) and the Mid.-Hauterivian (36.10-38.55 m), which are also dominated by obliquity and the 70 ka period as well as the precession. Note two stratigraphic gaps about 10 m, 36 m and 39 m, which split this section in three parts. The first is an eccentricity dominated part in the Later Berriasian (Ryazanian) (up to 41.50 m) turning into a shorter eccentricity and 70 ka as well as obliquity in the Early Valanginian (39-41 m). The second part covers the obliquity and recession dominated Mid.-Hauterivian. Between the first and the second part a lithologic change from a more marly to a nodular limestone occurs. Described by Einsele et al. (1991), nodular limestones are formed by early concretionary cementation of bioturbated carbonate muds, which do not necessarily modify orbital signals. These are formed by pressure solution during later stages of diagenesis. This stage of diagenesis is not fulfilled in our sites for direct reading of a vitrinite reflectance of R_0 0.3-0.35% and low maturity parameters of organic geochemistry (Bugge, 1988). Although this site seems to be the most diagenetic influenced, the signal is not characterized by lower frequencies. The third part of the Barremian is again characterized by the eccentricity.

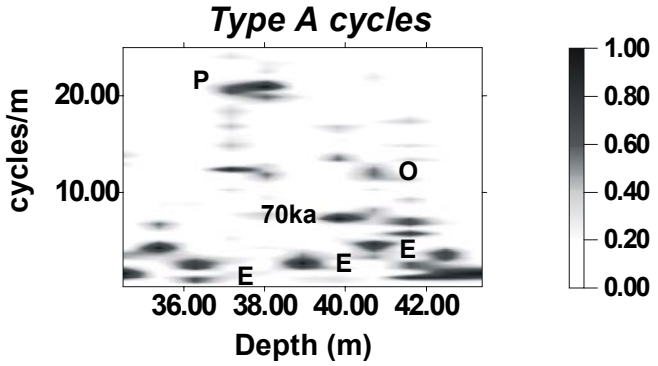

Figure 41 Evolutionary power spectrogram of Type A cycles of site 7430/10-U-01 and allocated orbital signals

Type B section cycles (44-57.5 m)

The run was done under same conditions as above (1/0.05). The most dominant signal over the section is the E3. The E2 signal sometimes coexists, like from 51-54 m and above 46 m. The E1 signal is very prominent from 53 m to the end of the section and is visible around 50 m and around 46 m. The obliquity is most pronounced in domains where the E3 vanishes. e.g., aaround 48 m. Precession is also evolved around 46-48 m. A visible shift can be estimated at ca. 53 m where the 70 ka cycle is evident. This change marks the Early Volgian/Late Volgian transition.

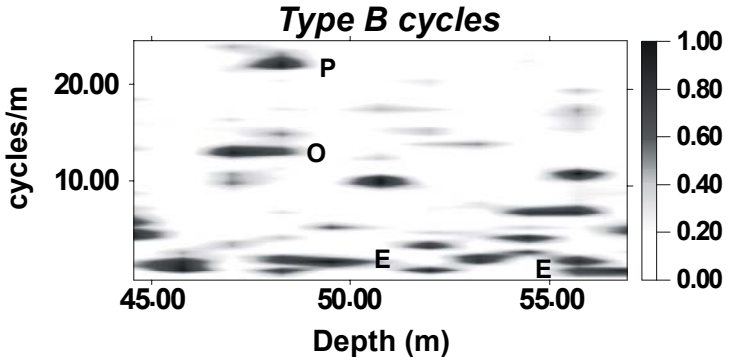

Figure 42 Evolutionary power spectrogram of Type B cycles of site 7430/10-U-01 and allocated orbital signals

Type C cycle section (52.5-67.6 m)

The run was undertaken with 2/0.1 window size/offset. This Early Volgian section is the most complex of site 7430/10-U-01. The eccentricity is marked very well throughout the section with the exception of two hiati from 65-63 m and from 61-60 m. In those times obliquity and

precession dominate the section. The 70 ka period is also well shown in the first break and it is also expressed at 60 m.

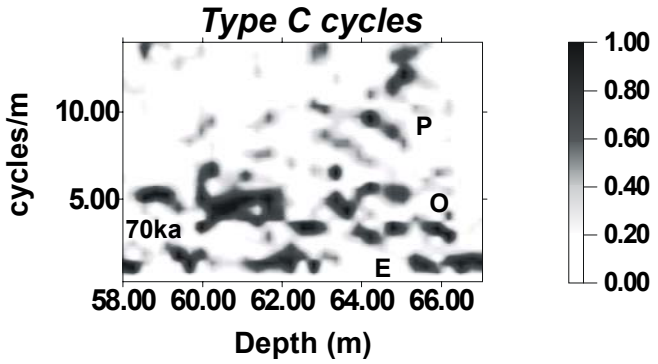

Figure 43 Evolutionary power spectrogram of Type C cycles of site 7430/10-U-01 and allocated orbital signals

6814/04-U-02

Type A cycle 6814/04-U-02 (40-64 m)

The run of the Type A cycle section was done with 3/0.1 window size/offset. The section starts with the dominance of the E2 period. A strong period of the 70 ka signal and partly obliquity up to ca. 61 m follows. From that the E3 eccentricity signal rules up to 47 m where E2 gives the strongest signal up to 41 m. Again the eccentricity is the most dominating signal with the exception of the Earliest Valangian part, which is characterised by the 70 ka cycle and obliquity.

Type B cycle section

Upper part up to 40m: The upper part reveals some strong signals that are discontinuous related to depth. The eccentricity of E3 and E2 shows the strongest signals.

Transitional part up to 96 m:

The transitional part also uncovers an eccentricity dominated spectra and a particular E3 signal.

Lower parts to the bottom: The first part (96-120 m) shows a dominance of obliquity and partly of precession from 96 to 103 m. Up to 158 m obliquity is also pronounced over a wide part but E2 is prominent from 120 to 168 m and 146 to 158 m. Precession occurs alike. In the last part up to the bottom of site 6814/04-U-02 eccentricity is the most dominating part with alternating eccentricities. In some parts precession also occurs.

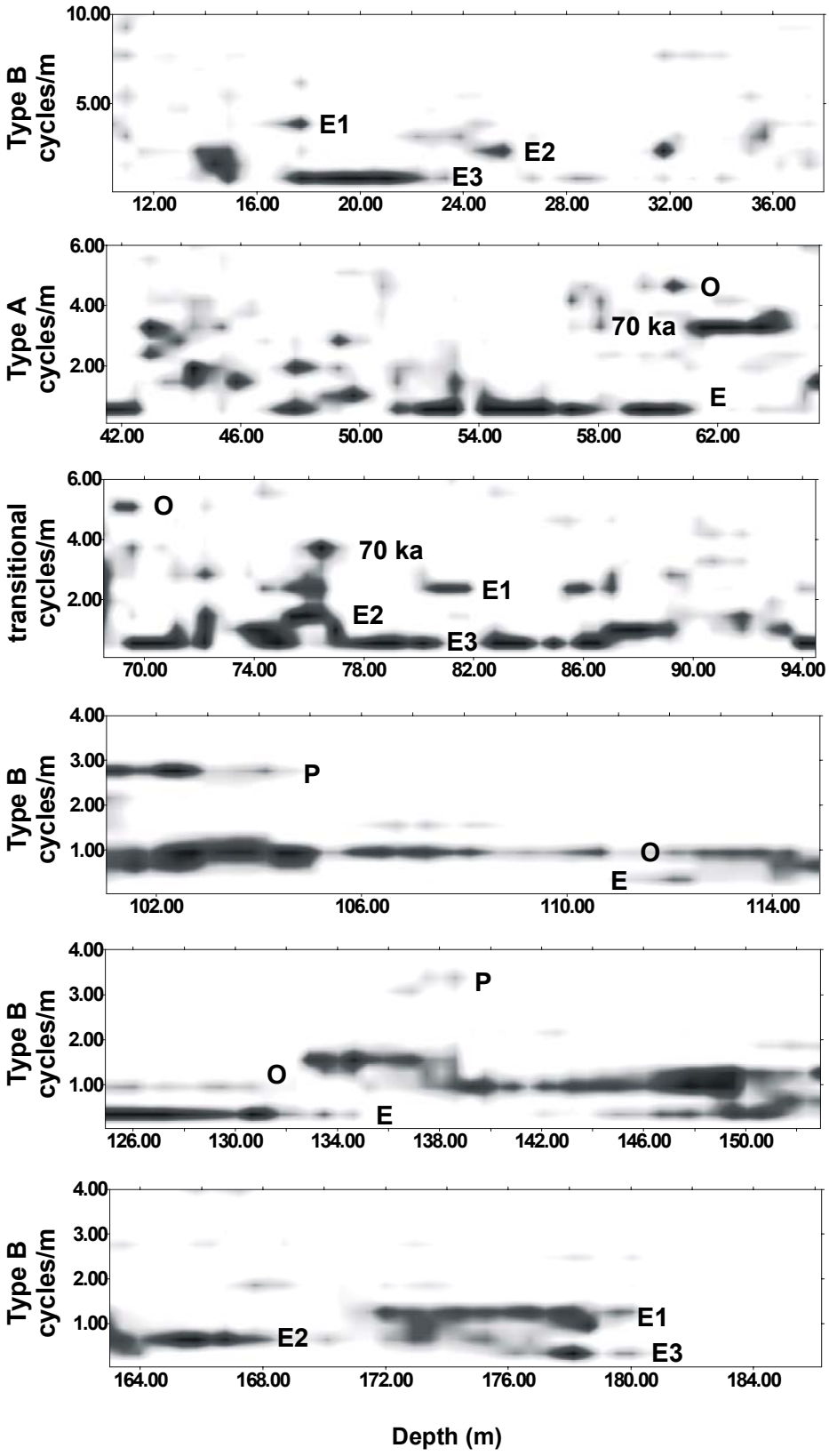

Figure 44 Evolutionary power spectrogram of Type A and Type B cycles of site 6814/04-U-02 and allocated orbital signals

Type B cycle sections are also ruled by eccentricity in both sequences of site 6814/04-U-02 with the exception of the $FeCaCO_3$ concretion section from 132-160 m where obliquity dominates. Primary bedding features can be diagenetic overprinted, e.g. by compaction cementation, precipitating in pore spaces and so on. This leads to enhancement, modification or sometimes obliteration of the structure (Einsele et al, 1991). Fölmi et al. (1991) described concretions frequently belong to layers deviated from the normal sediment e.g. by high TOC contents, high porosities, and low sedimentation rates. Our concretions can also be related to a high TOC content and slow sedimentation rates. Draping structures indicate a near surface or shallow development and not due to a late diagenetic stage. The concretionary layers follow an orbital pattern that is shown in the frequency analyses, whereas two different patterns are common. In the upper Type B cycle section of 6814/04-U-02 the E2 and E1 control the concretionary layers, whereas obliquity dominates minor colour changes expressing TOC- or carbonate content variations. The lower section is characterized by an E2 signal for the concretions, but the dominating signal is the obliquity showing layers of filled bioturbation which can be described as horizons of more ventilated and more oxygenised water. A weak signal of precession most likely exclude the fact of carbonate mobilization to defined horizons, which might be thought to be pseudo-cyclic.

6307/07-U-02

Type A cycle section 6307/07-U-02 (20-36 m)

The run was done with 2/0.05 window size /offset. There is a clear and dominant 100 ka eccentricity signal up to 28 m where the signal gets indistinct and intercalations of 70 ka y obliquity get in without an eccentricity signals. From 24-28 m is a recognizable shift from grey to red shales at the Berriasian (Ryazanian)/Valanginian transition. The grey shales have, in contrast to the red shales, a greater TOC content and might be related to warmer climate with higher productivity. This fits to the higher estimated temperatures for the Late Berriasian (Ryazanian)/Early Valanginian by Swientek and Ricken (2001a). From 24 m to the top of the eccentricity shows the strongest signal. Due to the assumption that precession is an often-characteristic feature in lower latitudes the lacking precession in the southernmost core 6307/07-U-02 can be explained by a lower resolution of the measured data. The lower resolution is caused by a poorer quality of the archive-half for our measurements. Therefore the high frequency signals, as precession lack, whereas obliquity is expressed.

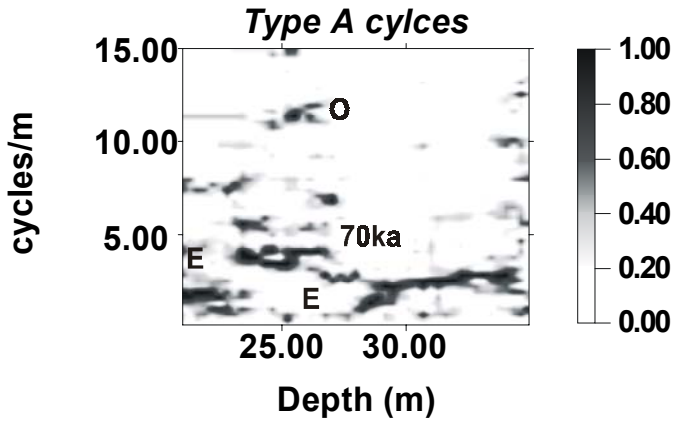

Figure 45 Evolutionary power spectrogram of Type A cycles of site 6307/07-U-02 and allocated orbital signals

Type B section cycles 6307/07-U-02 (36-85 m)

The run was done with the same conditions as the Type A cycle section above. The archive halves were not well preserved in parts of the core for colour measurements. Therefore we can only present the section from 67-85 m from Early to Mid.-Volgian times. The section starts with a mixed signal of eccentricity and the 70 ka signal. From 78-81 m the mixed signal changes into an eccentricity and obliquity signal succeeded by an eccentricity signal to the upper end of the section. A new mixed and indistinct signal of eccentricity and obliquity is expressed from 73 m possibly marking the onset of the Mid.-Volgian turning into an eccentricity signal at the end of the spectra.

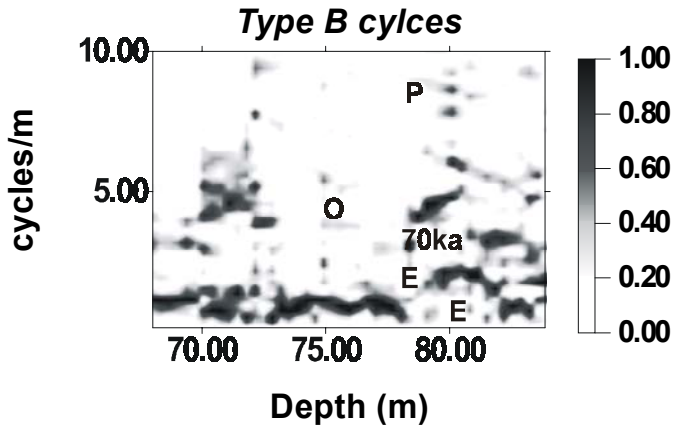

Figure 46 Evolutionary power spectrogram of Type B cycles of site 6307/07-U-02 and allocated orbital signals

Type C cycle section 6307/07-U-02 (85-104 m)

The run was done of 2/0.05 window size/offset. The main signal in the spectra is the eccentricity. Precession is strong from 98m to the upper end of the section, whereas obliquity occurs between 90 and 98m. The 70ka period gets also stronger in times where eccentricity gets weaker. Type C cycle sections of 6307/07-U-02 and 7430/10-U-01 show each a complex but similar pattern. Precession, obliquity, a 70ka cycle, and eccentricity appear in certain combinations. Changing of dominance indicates different colours expressed by the lithological content. There is no macroscopic evidence visible while the spectrophotometer recognizes it and even microscopic investigations suggest changes in the silt content.

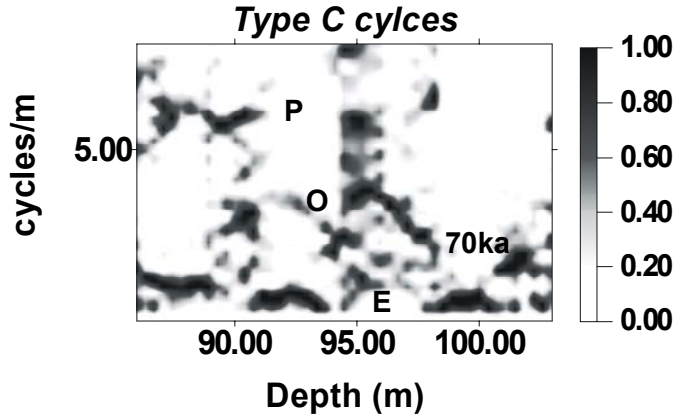

Figure 47 Evolutionary power spectrogram of Type C cycles of site 6307/07-U-02 and allocated orbital signals

The ESA are generally a good illustration of the different orbital signals and their stability through time. Changes in the sedimentation rate and changing bedding patterns prevent a continuous signal in the ESA. A change in the sedimentation rate lead to a shift of the signal, which is characterized by a diagonal pathway, e.g., the precession signal in figure 47. Type C cycles represent the most nervous appearance of cyclicity with signals jumping forth and back. Tis might be due to a change in the lightness pattern and hence lithology, most likely indicating a change in the orbital hierarchy. Type B and A cycles exhibit more stationary occurrences of power sections than Type C cycles, due to more stable oceanographic conditions for Type B and especially for the Type A cycles, which represent typical oceanic productivity cycles.

4.2.6.3 Well logs

Geopysical well log data are set up available from the SINTEF Petroleum Research Trondheim/ Norway. Suitable logs with a resolution in the range of Milankovitch were used for spectral analyses. Furthermore, the logs support climatic interpretation (Goldberg, 1997). For spectral analyses only the geophysical well logs from site 6814/04-U-02 were useful. The generally low sample rate of the logs of 10 cm in best cases is usually too small for the visualization of cycles. Site 6814/04-U-02 is an exception because of the higher sedimentation rate. Note the change to a lower sedimentation rate at ca.100m (Fig.48).

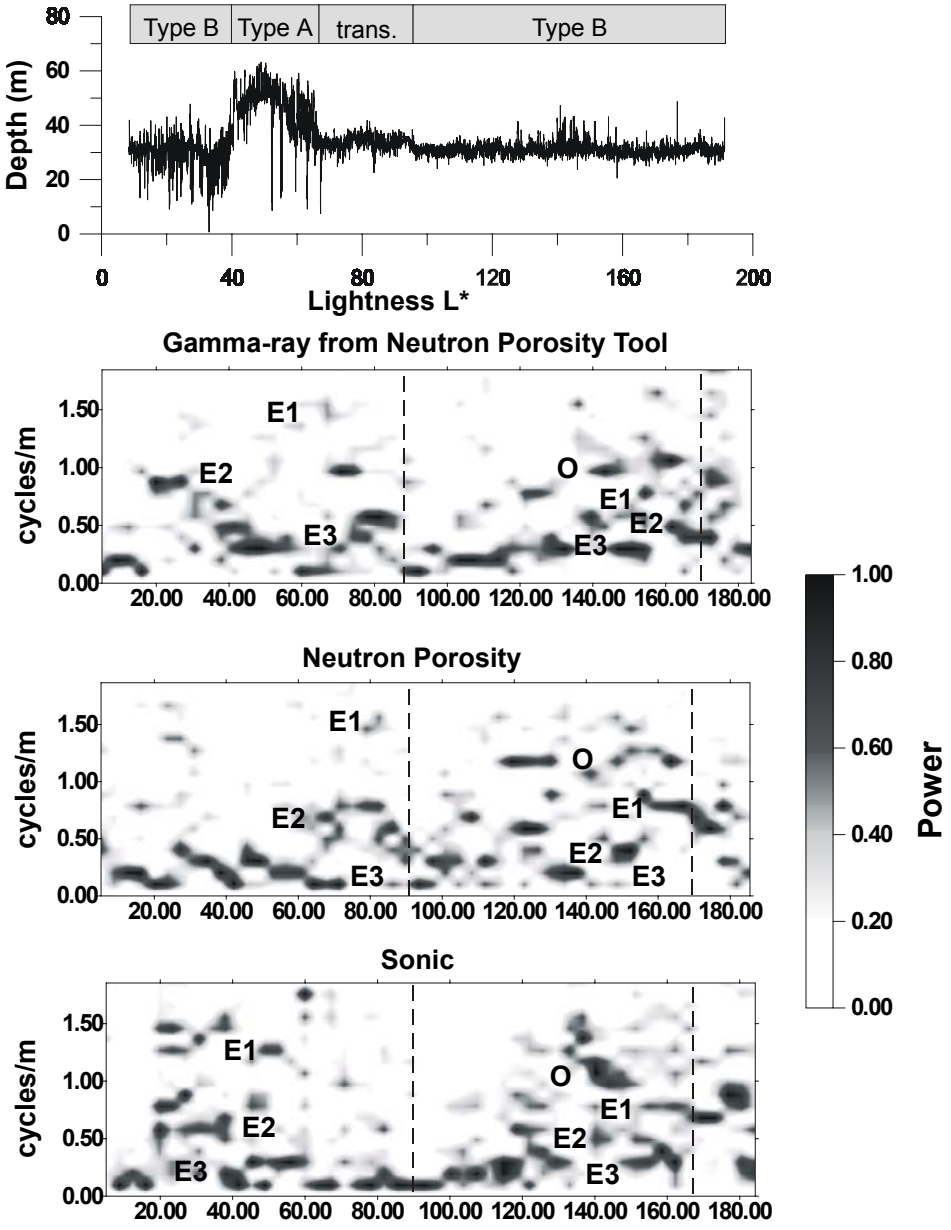

Figure 48 Lightness-Log and evolutionary power spectrogram from well logging of site 6814/04-U-02 and allocated orbital signals

The sonic velocity log is well expressed in bedding cycles of concretion bearing sections. Velocity is a function of density, which gets higher in compacted horizons like concretions. The ESA shows, independent from the L* values, the same orbital control for the sonic log in concretionary sections. The eccentricity controlled laminae of about 20 m and the obliquity dominated concretions of about 140-150 m reveal the same signals, both in L* and sonic log. The very prominent signal of E1 eccentricity of L* is also pronounced in the neutron porosity log between 150 and 180 m. Neutron porosity is used as an indicator for hydrogen and hence water or hydrocarbons. But these latter features cannot be cyclic itself. Therefore the cyclic signal is usable as a shale indicator and the cycles most likely show clay content and related bounded water. The gamma ray log (calculated from neutron porosity) demonstrates a loss of obliquity due to the decrease of the sedimentation rate. The gamma ray response can be used as a shale indicator and hence as a C_{org} indicator in the carbonaceous section indirectly. The gamma ray can estimate a clear E3 dominance, consistent with the L* spectral analyses. It is noteworthy that the L* values can be also described as a function of C_{org}. The L* litho-logs were the most suitable logs for identifying Milankovitch cyclicity due to the high resolution and the detectable changes in lithology.

5 Discussion

Before starting the discussion, some figures are presented. The following three figures give a good overview of the most important parameters, which will be discussed in this chapter. The figures contain information about stratigraphy, lithology, geochemistry and data from geophysical well logs.

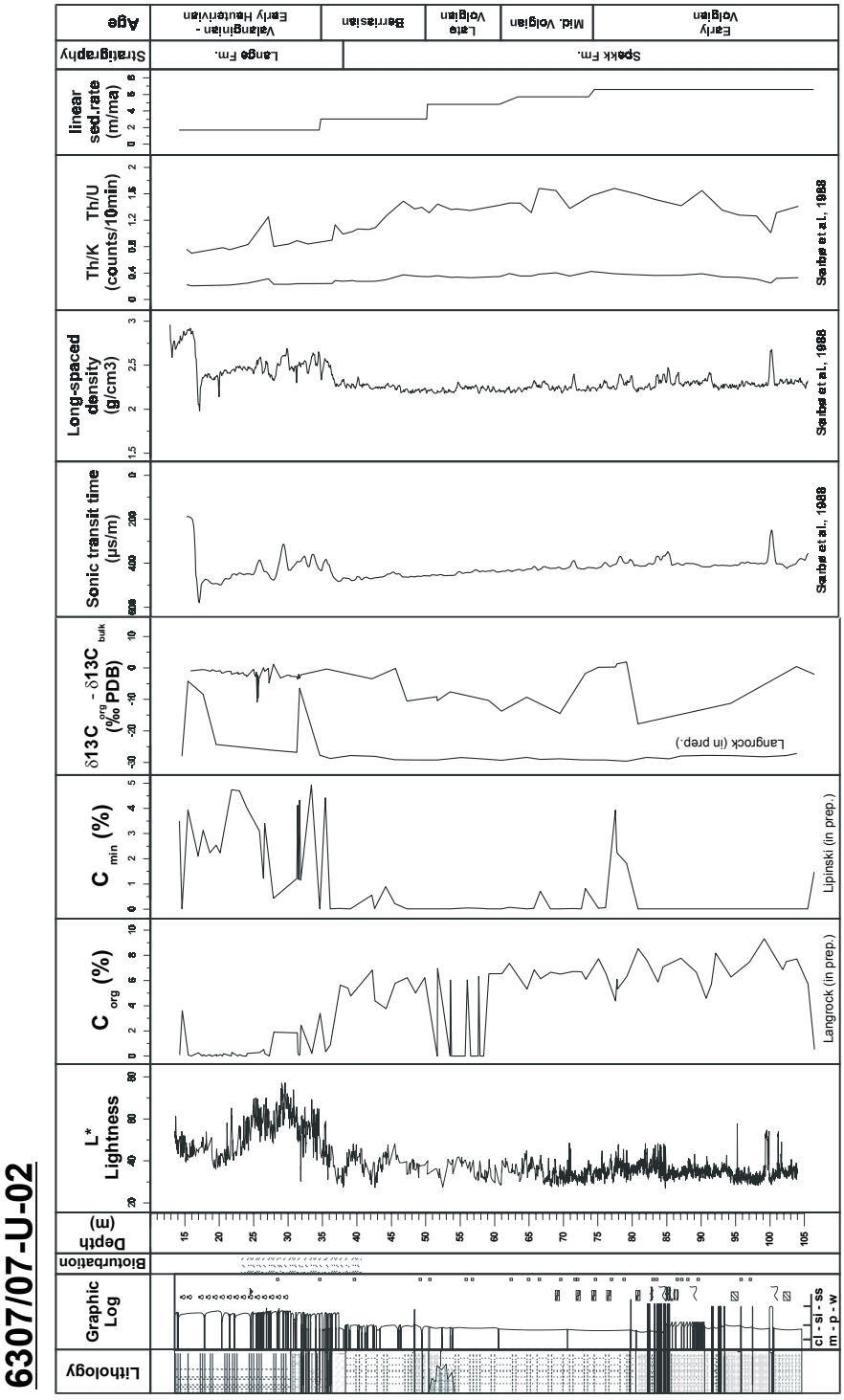

Figure 49 Lithology, geochemistry, petrophysics and stratigraphy of site 6307/07-U-02

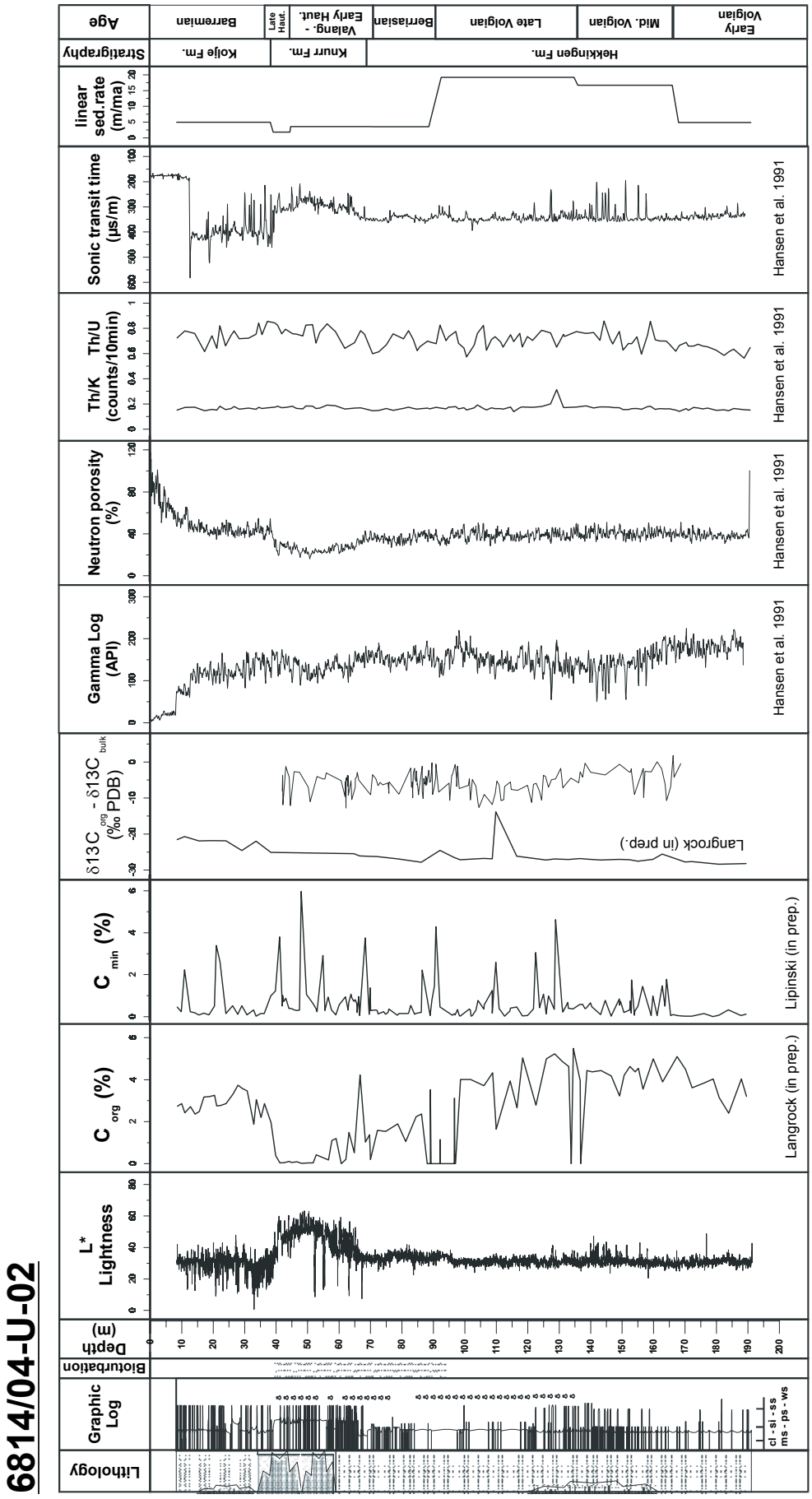

Figure 50 Lithology, geochemistry, petrophysics and stratigraphy of site 6814/04-U-02

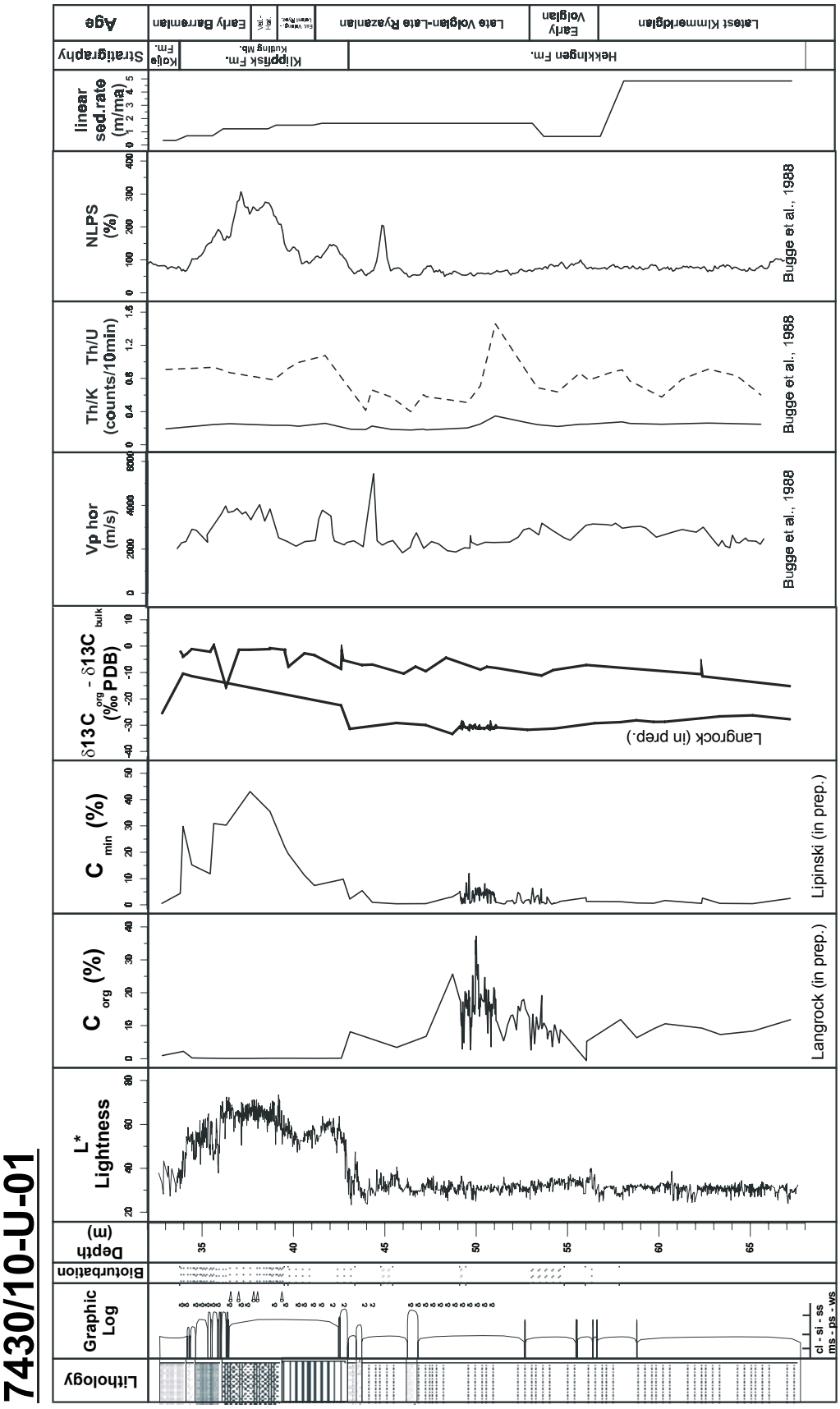

Figure 51 Lithology, geochemistry, petrophysics and stratigraphy of site 7430/10-U-01

5.1 Climatic control on stable isotope data

Combined cathodoluminescence and geochemistry analyses reveal diagenetic processes and show a clear difference between the belemnite and bivalve samples (Swientek and Ricken, 2000). The majority of the belemnite values express no diagenetic influence. They are good examples for specimen, which are unaffected by possible diagenesis. Diagenetic influence is in contrary, visible in the bivalves.

Different mechanisms can provide a shift to negative $\delta^{18}O$ values as observed in different sites on the current study. Primary or origin control on stable isotope data and secondary or diagenetic control are dicussed in the following.

Primary control: Different δ_w of seawater causes different $\delta^{18}O$ values in shells and related bulk sediment. Therefore different assumptions of the Cretaceous seawater have to be taken in consideration. Non-glacial seawater would be indicated by lighter values, whereas glacial seawater would reveal heavier $\delta^{18}O$ values. Different paleoceanographic scenarios show δ-seawater variations of –0,8‰ PDB, -1.2‰ PDB, and –1,5‰ PDB. The resulting temperatures are listed in Table 11.

Fresh water influence can explain the observed shift in isotope values. Especially site 7430/10-U-01 may be influenced by brackish or fresh indicated by freshwater algae after a breakdown of the stratified water column by tsunamis, which are related to the Mjølnir meteorite impact at the Jurassic-Cretaceous boundary (Smelror et al., 1999). If at all, fresh water influences in site 7430/10-U-01 and 6814/04-U-02 were triggered by uplifting events in the Late Cretaceous/Tertiary.

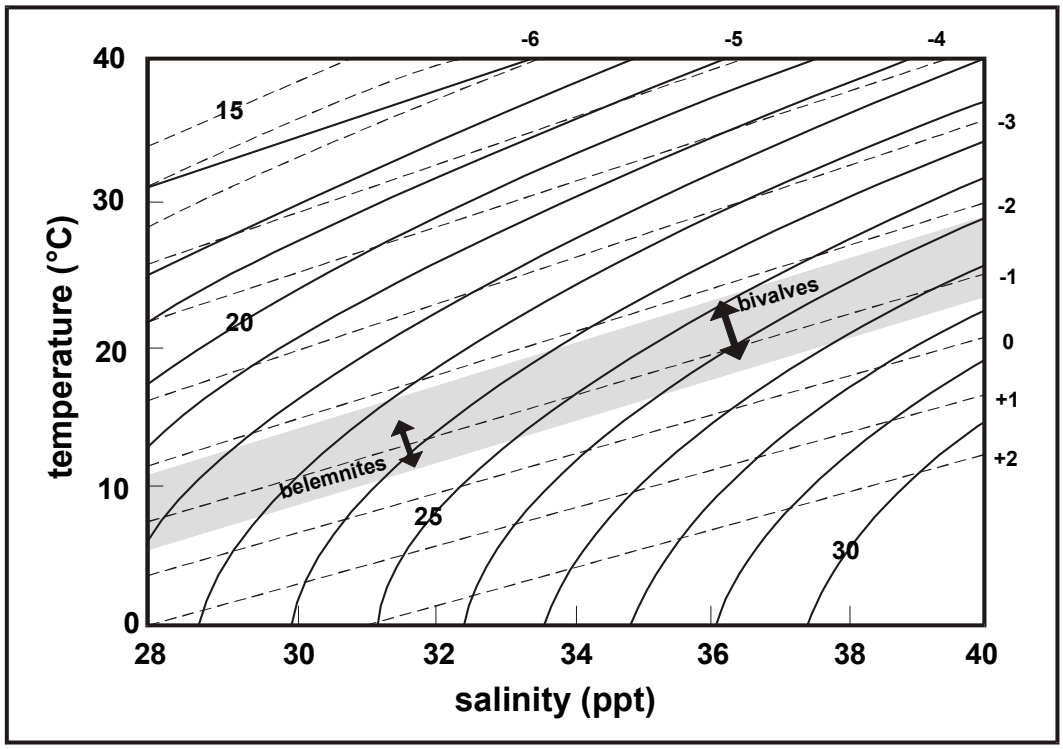

Figure 52 Variation in the $\delta^{18}O$ composition of well preserved belemnites and bivalves (*Buchia* and inocerams) for the Greenland Norwegian Seaway estimated from all sites after the model of Railsback (1989) and for an ice-free earth with a dw of -1 after the model of Railsback (1989) and for an ice-free earth with a δw of –1‰. Heavy dashed lines are isopleths of calcite $\delta^{18}O$ values. The T-S combinations for seawater describe the isotopic equilibrium with calcite of that composition.

The assumed distribution field of belemnites and bivalves are displayed in Fig. 52. The bivalves, mainly inocerams, tend to warmer and more saline water than the belemnites. This may indicate relatively warm saline bottom water and relatively cold surface water influenced by fresh water input. These aspects point to an estuarine circulation.

Hydrothermal activity may explain shifted isotope variation described by Mutterlose et al. (2002) for site 7430/10-U-01, but not for site 6814/04-U-02 with a very similar isotope signature.

Secondary control: Organic-rich sediments display low $\delta^{18}O$ and $\delta^{13}C$ values, as a result of organic matter degradation under reducing conditions. This would require a source of relatively light oxygen (sulphate ions and organic matter) and the sink of heavier oxygen like bicarbonate and solid carbonate (Sass and Ahuva Almogi-Labin, 1991). Generally this reservoir is characterized by an exchange of C_{org} and carbonate. The black shale sequences contain TOC values of 7 wt% at site 6307/07-U-02, 5 wt% at site 6814/04-U-02, and 36 wt% at site 7430/10-U-01 (Mutterlose et al., 2002). The incorporation of isotopically negative respiratory CO_2 may lead to isotopically lighter carbonate (Marshall, 1992). Barron et al.

(1980) described South Atlantic black shales with carbonate component composed of recrystallized foraminifera with calcite overgrowth. Hence, they attribute the depletion of $\delta^{18}O$ to increasing temperature with burial depth and pore water $\delta^{18}O$ depletion resulting from the formation of authigenic silicates. But neither a clear correlation of $\delta^{18}O$ values with depth nor significant authigenic silicate minerals are obvious. Even pore filling carbonate cements can lead to a similar isotope print. The influence of a high temperature diagenesis can be excluded by various facts, e.g. thermal immaturity of organic matter, low vitrinite reflectance or lack of authigenic diagenetic mineral assemblages as well as non-dehydration of clays (Skarbø et al., 1988; Bugge et al., 1988; Hansen et al., 1991). Site 7430/10-U-01 shows a vitrinite reflection of R_0 = 0.3%, most likely caused by a very early and weak diagenetic process (Bugge, 1988). An even low R_0 of <0.4 was obtained by Skarbø (1988) from site 6307/07-U-02 indicating a rather weak diagenesis. Various parameters, e.g. a R_0 of 0.43 to 0.53, indicate a burial depth of site 6814/04-U-02 of 1.8-2.5 km (Hansen, 1991). Therefore it seems most likely, that altered samples are influenced by the degradation of organic matter by sulphate ions in reducing environments as mentioned by Sass and Almogi-Labin (1991). In addition cementation may also attribute to the low isotope values.

5.2 Estimation of temperature based on $\delta^{18}O$ isotopes

Representative samples without diagenetic effects for temperature estimation have been choosen from the collected specimen (Tab.11). The following temperature estimation is based on a δ_w seawater of –1,2‰ for an ice-free Cretaceous environment, assuming that the ocean water content has not changed through the investigated time.

Site	Material	Depth (m)	Stage	$\delta^{13}C_{shell}$	$\delta^{18}O_{shell}$	$\delta^{13}C_{bulk}$	$\delta^{18}O_{bulk}$	Fe ppm	Mn ppm	T°C (δ_w-0,8‰)	T°C (δ_w-1.2‰)	T°C (δ_w-1.5‰)
7430/10-U-01	inocerame	35,46	Early Barremian	0,73	0,13	-2,13	-3,79			12,26	10,72	9,60
	inocerame	35,66	Early Barremian	0,05	-0,74	0,33	-0,65			15,75	14,12	12,93
	inocerame	46,7	Late Berriasian	-1,98	-1,85	-7,81	-6,85			20,49	18,75	17,46
	inocerame	62,4	Late Kimmeridgian	4,59	-0,46	-11,43	-9,90			14,59	12,99	11,82
	belemnite	33,98	Early-Mid- Barremian	-0,89	-1,67	-3,55	-8,54	198,64	51,63	19,72	17,99	16,72
	belemnite	34,16	Early Barremian	-0,76	0,45	-3,02	-5,52	69,44	32,79	11,02	9,51	8,41
	belemnite	37,04	Mid. Hauterivian	-1,24	-1,24	-1,38	-1,58	690,88	970,40	17,83	16,15	14,91
	belemnite	39,55	Early Valanginian	-0,30	-0,02	-1,21	-1,39	241,90	430,62	12,83	11,28	10,14
	belemnite	42,66	Late Berriasian	-0,76	0,36	-1,78	-4,75	290,38	148,26	11,39	9,87	8,76
6307/07-U-02	inocerame	22,71	Valanginian-Hauterivian	0,16	-1,98	-1,43	-2,22			21,07	19,31	18,02
	inocerame	45,63	Berriasian	3,42	0,94	-0,18	-1,45			9,19	7,74	6,67
	belemnite	23,75	Valanginian-Hauterivian	-3,09	0,00	-2,23	-2,49	1812,66	2331,25	12,76	11,21	10,07
6814/04-U-02	inocerame	60,71	Valanginian-Hauterivian	-0,17	-1,19	-5,16	-4,59			17,63	15,96	14,73
	inocerame	104,27	Late Volgian	2,53	-1,99	-11,38	-7,89			21,11	19,35	18,06
	inocerame	110,93	Late Volgian	0,54	-2,12	-6,35	-6,71			21,69	19,92	18,62
	inocerame	114,6	Late Volgian	0,90	-1,92	-5,51	-4,66			20,80	19,05	17,76
	Buchia	118,27	Late Volgian	1,93	-1,91					20,76	19,00	17,72
	inocerame	122,78	Late Volgian	3,08	-1,54	-5,91	-5,22			19,13	17,42	16,17
	inocerame	140,09	Mid. Volgian	0,76	-0,91	-2,86	-2,73			16,46	14,81	13,60
	inocerame	144,69	Mid. Volgian	1,93	-0,27	-3,60	-3,15			13,84	12,26	11,10
	Buchia	155,07	Mid. Volgian	3,24	-1,92					20,80	19,05	17,76
	inocerame	156,91	Mid. Volgian	3,60	-1,88	-9,82	-7,70			20,62	18,88	17,59
	inocerame	161,19	Mid. Volgian	2,66	-1,58	0,08	-3,42			19,31	17,59	16,33
	inocerame	161,42	Mid. Volgian	3,19	-1,41					18,57	16,88	15,63
	belemnite	97,48	Late Volgian	0,86	-1,43	-4,73	-6,28	15,59	18,67	18,64	16,94	15,69
13/1-U-02	belemnite	171,75	Early-Mid. Volgian	0,35	-0,91	-0,70	-0,93	43,86	22,13	16,46	14,82	13,61
	belemnite	188,84	Early-Mid. Volgian	-0,95	-0,94	-0,06	-1,56			16,58	14,93	13,72
	belemnite	193,51	Early-Mid. Volgian	-0,35	-1,83			128,61	29,57	20,38	18,64	17,36
	belemnite	194,95	Early-Mid. Volgian	0,00	-1,48	-5,14	-2,22			18,86	17,15	15,90
	belemnite	195,84	Early-Mid. Volgian	-0,83	-1,43	-1,84	-3,36			18,67	16,97	15,73
	belemnite	195,96	Early-Mid. Volgian	0,13	-1,21	-0,53	-1,78			17,72	16,04	14,81
	belemnite	198,36	Early-Mid. Volgian	0,51	-1,44	-3,58	-3,98	2307,98	776,59	18,70	16,99	15,75
	belemnite	199,45	Early-Mid. Volgian	0,88	-1,21	-1,39	-3,09	105,71	106,11	17,71	16,04	14,80
	belemnite	203,54	Early-Mid. Volgian	1,14	-1,48	-1,28	-1,00	79,67	22,59	18,87	17,16	15,91
	belemnite	207,9	Early-Mid. Volgian	0,79	-1,32	-3,23	-1,06			18,17	16,48	15,24

Table 11 Mean values of specimens used for temperature estimations

Based on the above mentioned assumptions on $\delta^{18}O_{seawater}$, the Latest Kimmeridgian of site 7430/10-U-01 shows an estimated paleotemperature span from 11.8° to 14.6°C. The obtained temperature value is in agreement with the proposed general global warming trend during the Kimmeridgian (Podlaha et al., 1998). Spicer and Corfield (1991) assume an equator to pole temperature gradient of 0.15°C/degree for the Cretaceous. The estimated gradient of this study of 0.13°C/degree fits well to the paleotemperature of 12.3°C given by Ditchfield (1997) for Svalbard (i.e. the Kong Karls Land/Svalbard) further north. The Early and Mid.-Volgian of site 13/1-U-2 shows mean temperatures of 14.6°C and 17.5°C, whereas the estimated mean temperature obtained from inoceramids of the more northern site 6814/04-U-02 is 15.2°C. The Upper Volgian shows higher mean temperatures of 15.1°C to 18.8°C from a belemnite and 19°C from inocermids at site 6814/04-U-02. Hence, the Upper Volgian confirms the highest temperatures in these high latitudes. Subsequently to this maximum, a drastic temperature fall is observed at site 6307/07-U-02 with a temperature drop to 6.7-9.2°C for the Early Berriasian (Ryazanian). Paleotemperature proxies increase again through the Late Berriasian (Ryazanian) as observed by a mean value of 16.3°C at site 7430/10-U-01. Temperature estimations for the northernmost site 7430/10-U-01 in the Barents Sea reveal a mean value of 16,2°C in the Early Valanginian. The following Valanginian-Hauterivian section of site 6307/07-U-02 shows a temperature range of 10.1-12.8°C obtained from a belemnite, which seems to be more realistic than the mean value from 18-21.2°C calculated from an inocerame. Assuming the gradient of Spicer and Corfield (1991), Price et al. (2000) give a similar belemnite-based paleotemperature estimation of 10-15°C for Speeton/England further south. Ditchfield (1997), however, suggested mean paleotemperatures of 8,1°C based on belemnites from Svalbard. Site 7430/10-U-01 also shows similar temperatures for the Mid.-Hauterivian (10.5-13.2°C) comparable to that of Price et al. (2000) for Speeton (12-15°C). The latter observation is in agreement with Mutterlose & Kessels (2000), which estimated relative paleotemperature proxies by changing nannofossile assemblages of sites 6307/07-U-02 and 7430/10-U-01. The Early Barremian at site 7430/10-U-01 illustrates paleotemperatures of 8.7-11.4°C, estimated from belemnites and 9.6-15.8°C from inoceramids. Some authors suggested that temperature reconstructions from inoceramids may indicate temperature overestimations (e.g. Pirrie and Marshall, 1990; Saltzmann and Barron, 1982). Our temperature estimations exhibit a similar trend. In addition, a warmer and more saline bottom water cause a sluggish circulation also resulting in temperature overestimations.

All sites of the studied rift basins are located on the same (Eurasian) continental block. As the relative distance between the sites did not change significantly through time by strike

slip movements (Mutterlose et al., 2002), the temperature gradients were estimated from the above calculated temperatures. For the estimation mean values from each site for corresponding stages were used. All calculated temperatures (for a δ_w of –1.2‰), e.g. for the Early Volgian of site 13/1-U-2, were combined to one mean value. Boreal temperature data from other authors like Podlaha et al. (1998), Price et al. (2000), and Ditchfield (1997) complement this data set to confirm the estimated temperature gradients. Two main stages of the investigated time slice are divided: the Latest Jurassic (Latest Kimmeridgian-Latest Volgian) and Earliest Cretaceous (Early Berriasian (Ryazanian)-Mid.-Barremian). The temperature gradient for these stages were calculated from our data sets and from the data of the above mentioned authors. Fig. 53 illustrates two temperature gradients: a gradient of 0,13°C/degree latitude for the end of the Jurassic and a lower value of 0,08°C/degree latitude for the beginning of the Cretaceous.

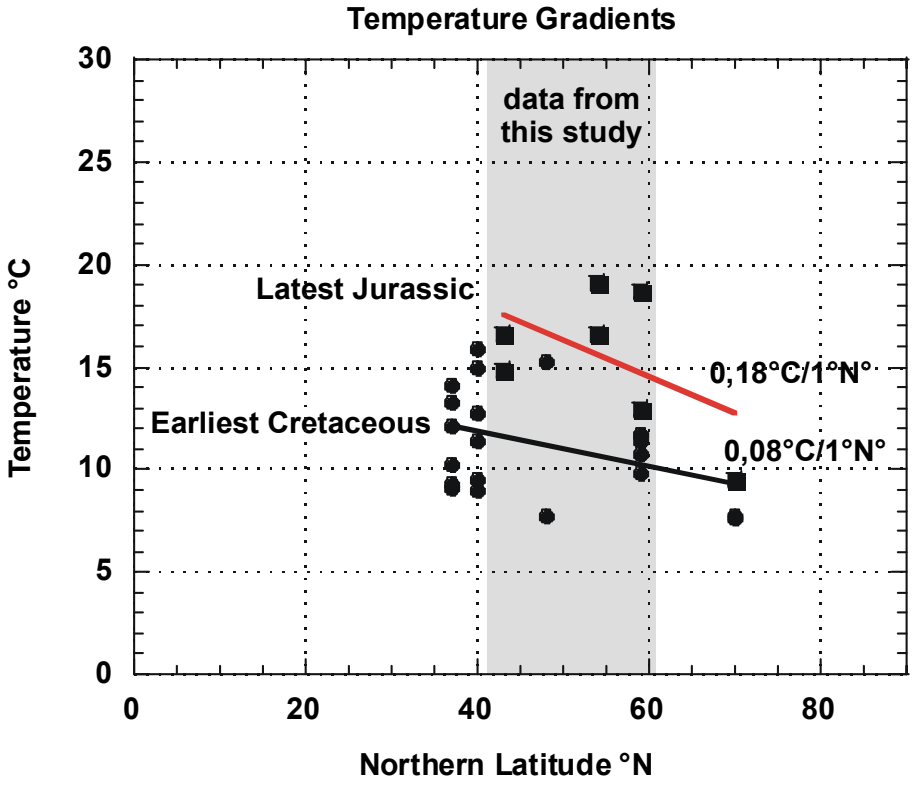

Figure 53 The temperature-gradient diagram from 0°-90°N latitude indicates possible temperature gradients under the assumption of a δseawater of –1,2‰; estimated from this study, (1) Ditchfield, P. W., 1997(70°N), (2) Price et al., 2000 (40°N), (3) Podlaha et al. 1998 (40°), and (3) Podlaha et al. 1998 (37°N).

Afterwards a simple matrix of our calculated temperatures together with those temperatures calculated from Podlaha et al. (1998), Price et al. (2000), and Ditchfield (1997) and the corresponding latitudes was composed. For time slices without temperature values those were calculated with the estimated temperature gradients of 0,13°C/degree latitude for the end of the Jurassic and of 0,08°C/degree latitude for the beginning of the Cretaceous.

		S ←					→ N		
				13/1-U-02	6307/07-U-02	6814/04-U-02	7430/10-U-01		
Stage	Age	37°N	40°N	43°N	48°N	54°N	59°N	70°N	T-gradient
L. Barrem.	125,12	*12,17*	*12,72*	12,48	12,08	11,6	11,36		0,08
M. Barrem.	126,06		*15,9*	12,87	12,63	12,15	**11,75**		0,08
E. Barrem.	127	*14,08*	*11,45*	12,05	11,65	11,17	**10,77**		0,08
L. Haut.	129,84	*10,27*	*9,56*	9,32	8,92	8,44	8,04		0,08
M. Haut.	130,92	*9,36*		12,63	12,23	11,75	**11,35**		0,08
E. Haut.	132	*9,15*	*9*	8,76	8,36	7,88	7,48		0,08
L. Valang.	135,67	*13,26*		12,78	12,38	11,9	11,5		0,08
E. Valang.	137		*15,00*	14,6	**14,2**	12,1	**11,7**	*7,7*	0,08
L. Berrias.	140,05			11,15	10,75	10,27	**9,87**	*7,6*	0,08
E/M. Berrias	144,2			8,13	**7,73**	7,25	6,85		0,08
L. Volg.	145,99			18,17	20,19	**19,11**	**18,74**		0,18
M. Volg.	148,74			**17**	**16,67**	**16,58**	15,68		0,18
E. Volg.	150,7			**17,5**	**17**	15,92	15,02		0,18
L. Kimmeridg.	154,1			15,87	14,97	13,89	**12,99**	*9,5*	0,18

Table 12 Temperature matrix of our stable isotope analyses (bold), the analyses of Podlaha et al. (1998), Price et al. (2000), and Ditchfield (1997) (*italics*) and interpolated temperatures. Interpolation was done with the specified temperature gradient in the last row. Arrows, mainly from south to north, indicate direction of interpolation. Only where southern values are missing interpolation took place from north to south.

Figure 54 and 55 illustrate temperature trends and show a significant similarity of the trend from site 7430/10-U-01, which is only estimated by mean values (bold values in table 12) and the interpolated trend. The data in figure 54 are only from site 13/1-U-2, 6307/07-U-02, 6814/04-U-02, and 7430/10-U-01 for the corresponding stages. In addition figure 55 reveals the temperature curves including the interpolated data.

In figure 54 two major trends can already be identified: an increasing trend of warm temperatures in the Late Jurassic and relatively colder temperatures in the Early Cretaceous

succession. Furthermore the Early Cretaceous is characterized by significant variations in temperature.

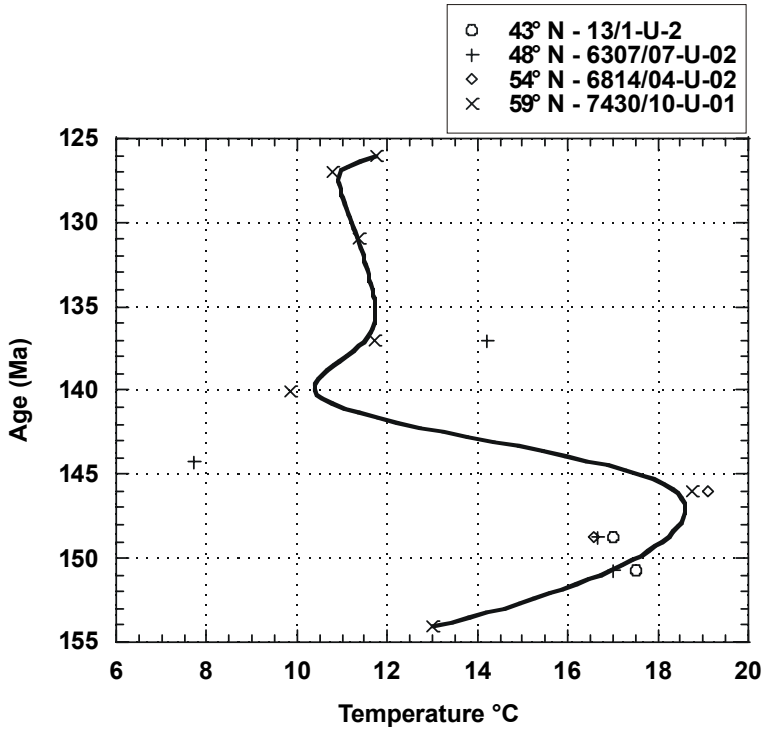

Figure 54 Estimated temperatures from stable isotope analyses of this study (mean values of each site for the corresponding stage). Note the trend of the northernmost site of 7430 /10-U-01 and the higher temperatures of the Late Jurassic.

Figure 55 shows the interpolated temperature curves of site 13/1-U-2, 6307/07-U-02, 6814/04-U-02, and 7430/10-U-01 calculated with a gradient of 0,13°C/degree latitude for the end of the Jurassic and a lesser temperature gradient of 0,08°C/degree latitude for the beginning of the Cretaceous.

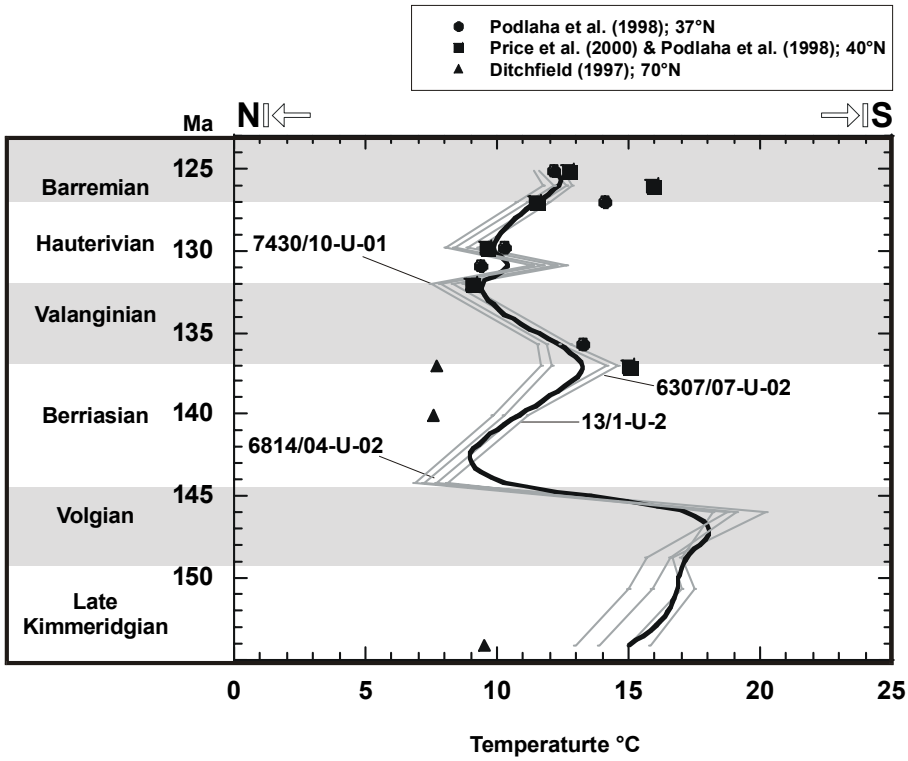

Figure 55 Model of calculated temperature curve and spline function from data of site 7430/10-U-01, 6814/04-U-02, 6307/07-U-02, 13/1-U-2 and from Ditchfield, P. W., 1997; Price et al., 2000 and Podlaha et al. 1998

These interpolated data (Fig.55) show also a major cooling trend from Late Volgian to Berriasian (Ryazanian)/Barremian time. This trend describes the change from the warm Late Jurassic to the relatively cooler beginning of the Cretaceous. The observed dominant pattern may reflect the isolation of the Boreal seaway from warm Tethys waters caused by restricting marginal and intrabasinal highs. This has been widely described in literature and is therefore assumed to be the effect of a global trend. Among others, Frakes (1999) described the Early Cretaceous cooler as the warming of the Albian, Turonian/Coniacian, and Late Maastrichtian. Our data set has a higher time resolution than the one of Frake (1999) and indicates additional warmer intervals in the Late Volgian, the Late Berriasian (Ryazanian)/Early Valanginian, Mid.-Hauterivian, and Barremian as well as relatively cooler phases in the Early Berriasian (Ryazanian), Early Hauterivian, and Early and Late Valanginian. The general warming up trend from the Berriasian (Ryazanian) to the Barremian is accompanied by transgressive conditions leading from clastic black shales to hemi-pelagic calcareous sediments. Minor temperature trends may be related to increasing volcanic tectonic activity and increased CO_2 emission leading to enhanced temperatures.

Black shale events related to C_{org} rich sediments (like anoxic events) are characterized dominantly by positive $\delta^{13}C$ values (Weissert and Mohr, 1996). They are possibly associated

with an increase in weathering, erosion, and run-off rates and hence to an elevated nutrient transfer into the ocean. This events are most likely associated with warm transgressive periods. The stable carbon isotope data of the biota and bulk sediment of the investigated sites are modified by diagenesis. Therfore the absolute $\delta^{13}C$ values cannot be compared to black shale events, but the superior trends are still suitable for interpretation. However, Price et al. (2000) also described $\delta^{13}C$ data of such light carbon isotopes for the Speeton area. Some transgressive signals can be read from the relative $\delta^{13}C_{bulk}$ data in site 6307/07-U-02, 6814/04-U-02, and 7430/10-U-01 for the Latest Kimmeridgian to Late Volgian and from the Berriasian (Ryazanian) to the Mid.-Barremian. Haq et al. (1988) also proposed a major transgression for the end of the Jurassic.

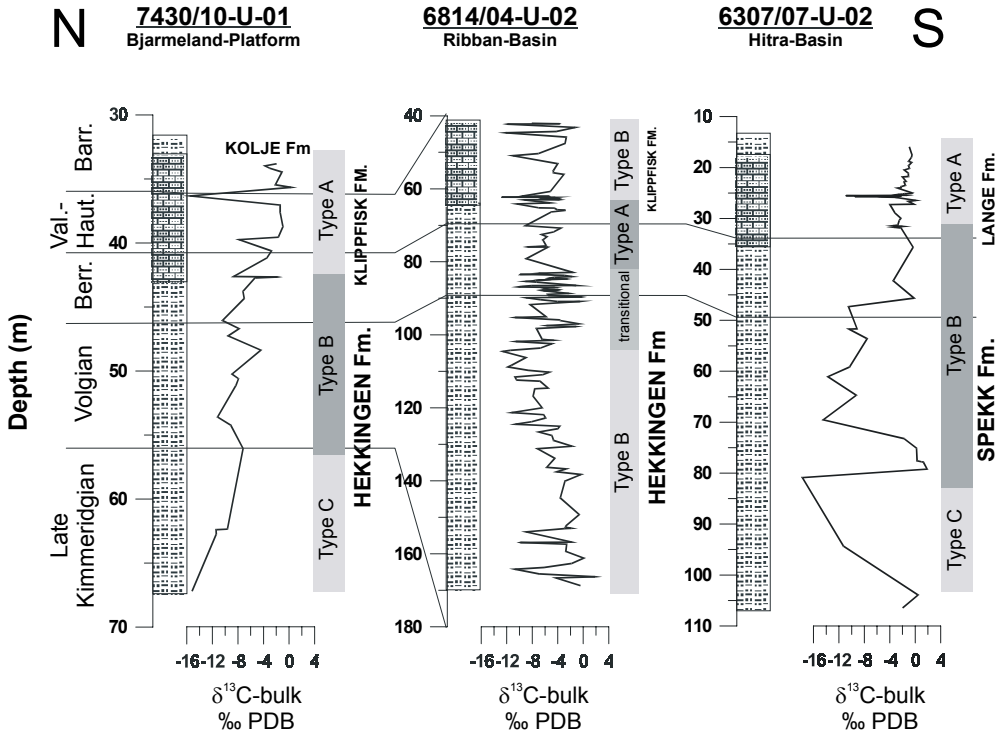

Figure 56 Correlation of $\delta^{13}C$ values based on biostratigraphy and on similar cyclic sequences. The cyclic sequences of Type A, B, and C cycles are based on the L*litho-logs.

There is a general agreement between our paleotemperature estimations and that of other authors in the Boreal Early Cretaceous (Ditchfield, 1997; Podlaha et al., 1998; Price et al., 2000; Abbink, 2001). However, it cannot be excluded that some of the $\delta^{18}O$ data reflect regional or local trends. Local effects may depend on a regional basin structure, related to a different paleoceanography. Haq et al. (1998) proclaim a global second order sea-level low

stand for the Early Cretaceous, resulting in restrictions of shallow seas in rift basins (Ziegler, 1990). Dysoxic conditions most likely result from these second order low stand.
The Latest Jurassic in general indicates warmer temperatures than the Early Cretaceous from the Berriasian (Ryazanian) to the Late Barremian. Mutterlose et al. (2002) discuss a major transgressive period from the Berriasian (Ryazanian) to the Barremian based on microfossils, geochemistry, and sedimentological observations. Our increasing temperature trend and associated $\delta^{13}C$-trends most likely reflect this transgression.

Estimated temperatures are further supported by various arguments: The Late Volgian was the warmest period and reveals the highest C_{org} and gamma ray values at several sites (e.g. 7430/10-U-01 and 6307/07-U-02). The highest TOC content suggests the influence of a dominance of stagnant near-shore conditions associated with relatively warm water masses and a higher surface productivity. Smelror et al. (2001) described an increase in gamma ray readings for site 6814/04-U-02, related to slow sedimentation and/or condensation during this period. The regressive Berriasian (Ryazanian) was accompanied by a decreased gamma ray (i.e. increasing flux of silt), a decrease in TOC content, and increased incoming of Kerogen type III (Smelror et al. (2001). Abbink et al. (2001) proclaim a temperature maximum in the Late Kimmeridgian and Portlandian for the southern North Sea area and a following climatic shift in the Earliest Ryazanian comparable to our Early Berriasian (Ryazanian) climatic shift to cooler conditions. Hallam (1991) mentions low kaolinite abundances all over Europe from the Late Kimmeridgian interval onwards as an indicator of aridity. Moore et al. (1992b) describe the Kimmeridgian/Tithonian as a warm and arid climate caused by a high CO_2 content in the atmosphere. Kornpihl (2001) postulates an increase of kaolinite for site 7430/10-U-01 and 6307/07-U-02. The following regressive phase to the Late Berriasian (Ryazanian)/Early Valanginian in our calculations is also proven by Smelror et al. (2001) by a decreased gamma ray (increasing silt content), a decrease in TOC content, and increased incoming of Kerogen type III. Rawson and Riley (1982) and Doré (1991) point out a regression in the Berriasian (Ryazanian) and a subsequent transgression in the Late Berriasian (Ryazanian)/Early Valanginian. Furthermore Braduchan et al. (1986) declare a regressive event in the eastern Barents Sea and the Western Siberian Basin. The temperature increase in the mid and end of the Hauterivian is associated with transgressive pulses as suggested by microfossil and ammonite assemblages (Mutterlose & Kessels, 2000). In contrast to other authors (Rawson, 1994) this study suggest a continuous major transgressive trend from the Berriasian (Ryazanian) to Mid Barremian. This trend may be superimposed by smaller scale transgressive and regressive variations at a higher frequency pattern. In addition Smelror et al.

(2001) suggest a Barremian transgression after the condensed Valanginian-Hauterivian section because of transgessive dark grey shales of the site 6814/04-U-07. An increased TOC content in the Late Barremian might reflect this transgressive trend. Hence, warmer conditions most likely demonstrate the onset of the Barremian-Aptian arid phase in NW Europe (Mutterlose and Kessels, 2000). Dominant patterns of temperature variations may be related to some transgressive-regressive tracts of the sea-level chart of Ruffell (1991) for NW Europe, showing transgressive phases in the Late Volgian, the Mid.-Hauterivian, and the Mid.-Barremian. The Early Valanginian lacks in his chart, but a transgressive phase is indicated. Our temperature results are also similar to the data set of van de Schootbrugge et al. (2000) for the Vocontian Trough in the Thetys realm. They estimated warm temperatures in the Early Valanginian, subsequent cooling in the Late Valanginian and Early Hauterivian and a renewed warming in the Late Hauterivian corresponding to our Mid.-Hauterivian section.

Climate archives in sites from the Polar Regions are used to solve key questions in controlling the Cretaceous atmosphere/ocean system. This study investigates a transect of 43° to 63° paleolatitude. Therefore polar climates cannot be estimated directly, but estimations are possible by incorporating selected localities of the Boreal zone to the south (i.e. Speeton) and to the north (i.e. Svalbard). Temperature estimations are succeeded by linear extrapolation of the derived paleotemperature gradients to areas close to the assumed pole. For the Greenland Norwegian Sea and the Western Barents Sea shelf the possibility of paleotemperatures <10°C is suggested for the Early Berriasian (Ryazanian), the Early, and Late Hauterivian times. This is in agreement with the lowest presumed paleotemperatures near the Hauterivian-Barremian boundary by the basis of low-latitude data of Douglas and Savin (1975). Within regional settings and an estimated error of 0,2°C these proxies for paleotemperatures most likely suggest sub-freezing conditions in latitudes close to the pole.

It is very difficult to characterize the paleoceanographic settings of the Early Cretaceous. The assumption that the Cretaceous does not yield ice caps, complicates an explanation of sea-level fluctuations by a glacio-eustatic control. Furthermore a glacio-eustatic control would imply a distinctive circulation pattern initiated by a thermohaline contrast like the today conveyor belt with sinking of cold water at the poles and warm saline surface currents. Some authors proclaim ice-yielding conditions in the northern hemisphere (e.g. Kemper, 1987; Frakes and Francis, 1988 and Price, 1999). Valdes (1995) illustrates that at least the southern hemisphere permited metre scaled sea-level variations. Stoll and Schrag (1996) propose evidence for glacial control of rapid sea level rises. The tectonic evolution of the investigated

area is a further explanation for sea level fluctuations. But a tectono-oceanographic context is difficult to establish due to the complex structures of the Greenland Norwegian Seaway. Ziegler (1990) describes the major eustatic sea-level fluctuations in combination with increased tectonic instability. This gives rise to regional unconformities as well as regressions and transgressions. It should be kept in mind that the Greenland Norwegian Sea was an active area of rifting throughout the Late Jurassic/Early Cretaceous and especially the Berriasian (Ryazanian) of the Late Cimmerian phase. This may have been accompanied by sea-level changes due to increased oceanic crust and later subsidence. Hallam (1988) proposes, that many eustatic sea-level fluctuations for the Jurassic of the North Sea are superimposed by a regional tectonic noise of uplift and subsidence. The tectonic subsidence of passive margins is thought to be slow and gradual but tilted fault block taphrogenic tectonic and associated sedimentation is widespread at rifting seaways (Hallam, 1988). Other authors, like Moore et al. (1992a), may restore sea-level fluctuations to the Kimmeridgian/Tithonian to expanded continental rifting and increased sea floor spreading. They relate the culminating sea level of Haq et al. (1988) in the Late Jurassic directly to increased sea floor spreading rates. But, as discussed above, this study estimated temperature gradients and interpolated a temperature curve over more than 2000 km paleodistance. There is a correlation of temperature estimated from this study and transgressions/regressions according to other authors (Haq et al. 1988; Smelror et al. 1998; Jacquin et al, 1998; Mutterlose and Kessels, 2000; Smelror et al, 2001). This is most likely documented in 2nd order sea-level rises by Haq et al. (1988), which is in accordance to our highest temperatures in the Late Volgian/Ryazanian and the renewed sea-level rise throughout the Early Cretaceous. The Early Cretaceous rise is related to increasing temperatures that correlate to the first and second major transgression cycle at Andoya, Northern Norway (Dalland, 1981). 3rd order transgressive/regressive systems can also be related to climatic shifts as mentioned above. This can be compared e.g. to Rawson (1994), which proved that ammonite faunas were triggered by rapid sea level rises.

5.3 Cyclicity and orbital forcing

5.3.1 Isotope cycles

The different cylces in the lightness-logs are based on various assumptions, e.g. the dependence of the colour from the C_{org} and carbonate content. Hence, they are controlled by the amount of bioproductivity of carbonaceous or organic walled organisms. This may has been triggered by the nutrient supply from the hinterland. Some higher resoluted sections of the isotope curves also show variations, which are most likely cyclic (Fig. 57).

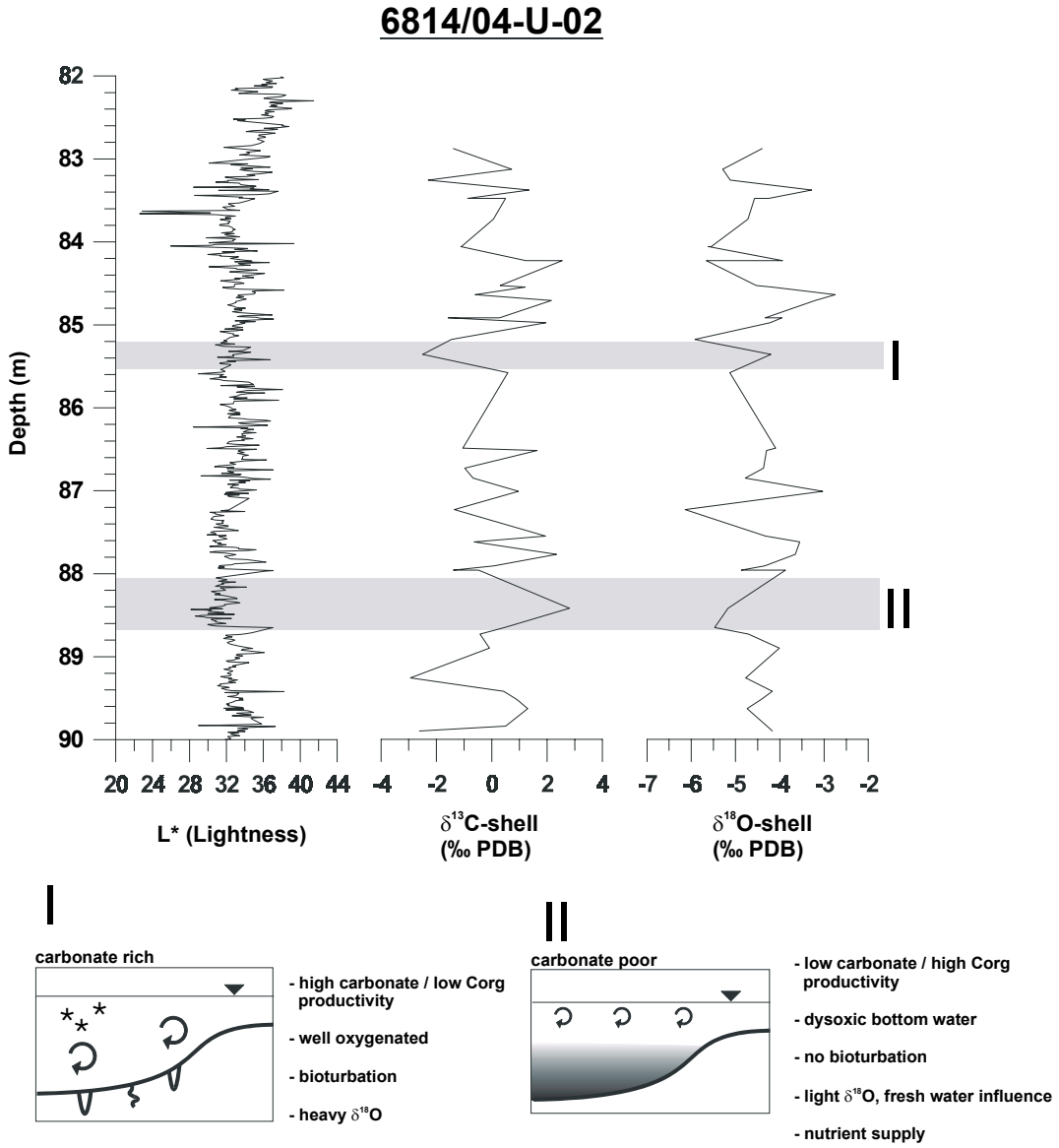

Figure 57 Close up figure of Type A cycles of site 6814/04-U-02, related cycle pattern of $\delta^{13}C$ and $\delta^{18}O$ stable isotopes, and possible corresponding oceanographic scenarios

In the Type A cycle section of site 6814/04-U-02 both, the absolute values of the $\delta^{13}C$ and $\delta^{18}O$-curves of bivalves (mainly inocerams), are slightly modified by diagenesis. The reservoir is in general characterized by an exchange of C_{org} and carbonate. The variations of $\delta^{13}C$ values most likely indicate times of higher carbonate productivity with more positive values. More negative values are presumably caused by the abstraction of light carbon by photosynthesis of organic walled plankton. Corresponding to this are the heavy $\delta^{18}O$ values in carbonate rich sections and light $\delta^{18}O$ values in carbonate poor sections. An elevated C_{org} content in the sediment most likely caused a lighter oxygen isotope source due to diagenesis. That would lead to a higher deviation of the isotope signal in dependence to the C_{org} content. Therefore these data are not suitable for exact temperature estimations, but they are still useful to interprete some trends. In addition the $\delta^{18}O$ values can be used as a salinity indicator, as the light $\delta^{18}O$ values indicate an enhanced fresh water influence, which could cause an estuarine circulation pattern. The low resolution of these isotope data sections is in general not sufficient to establish an oceanographic model or to identify Milankovitch cycles.

5.3.2 Lightness-log cycles

Milankovitch cycles must be amplified to produce a sedimentary signal due to the small seasonal effect of insolation, e.g. by climatic-oceanic feedback systems (Kerr, 1981; Ruddiman and McIntyre, 1984; Fischer, 1989; Einsele et al., 1991). A summary of important feedback systems is given in Einsele et al. (1991). The most important example for the Pleistocene is the build up and vanish of ice sheets (Berger, 1984). It is still discussed in literature if the Early Cretaceous prevail ice-building conditions or not. Which model could be used to explain the different cycles in case of an ice free Early Cretaceous? Evaporation and related circulation patterns, as described by Schwarzacher (1993) seem to fullfil the requirements. Precipitation, run-off, and evaporation balance most likely changed regularly under orbital control from estuarine anoxic conditions into anti-estuarine circulation. A relationship between the orbital signals and latitude is often described by other authors e.g. by Schwarzacher (1993) or Einsele et al. (1991).

The various ESA show that the different cycles are imaged very similar over the facies and time and describe an oceanographic pulse, which modulates all sedimentological systems in a similar way. The appearance of orbital forced sediment characteristics depends on many processes and the preservation of cyclicity in the sediment is not always obvious. The ESA

show some characteristics, reminding of a relaxation or a rebound system, like the sharp change from eccentricity domination to a simultaneous occurrence of precession and obliquity and back. This is also known from other climatic aspects, like the liberation of methane hydrates or rapid CO_2 liberation caused by volcanic activity.

Eccentricity has a small direct effect on insolation but it controls the intensity of precession and the growth of major ice sheets in high latitudes caused by variation in north summer temperatures leading to snow melting or not (Valdes, 1995).

Obliquity is well developed in our sites and it occasionally occurs to our warm phase. Waterhouse (1995) proposed that in the Late Jurassic Kimmeridge Clay of Dorset/UK the obliquity controlled the marine system with currents, productivity, and preservation conditions via climate. These features are caused by a high obliquity and the related greater seasonality contrast from a lower pole to equator insolation gradient and less atmospheric and marine currents. Without any obliquity ocean currents do not yield anoxic conditions via climate. The obliquity is often described to be most effective in higher latitudes >40° and intensifies the contrast of seasonality (deBoer, 1994).

Schwarzacher (1993) and deBoer (1994) relate the precessional signal to alternating oxidation and reduction conditions, whereas the obliquity forces evaporation, precipitation, and run-off. Furtheron the precession is responsible for the influence on the terrestrial system, due to the shift of climatic belts and related variations of boundaries between wet and arid zones (Waterhouse, 1995). The precession arranges the balance between monsoonal and zonal wind circulation and hence vegetation and erosion. Waterhouse (1995) also described a reworking of sediments particularly in the sensitive zones of 20-40° latitude. An elevated run-off caused by precession can lead to a stratification of water masses on the shelf and influence the currents by the salinity contrast as well as the productivity by higher nutrient supply. Park and Oglesby (1990) describe that a variation in the precipitation (subtracted by the evaporation) leads to cyclic variations of anoxic waters in shallow basins and in the fluctuation of terrigenous input on the shelf. Waterhouse (1995) retracts facts that both orbital signals are interfering to an overlap of latitudes. The same effect is seen in Type A carbonate productivity cycles. Giraud (1995) interpreted their strong obliquity signal in the Valanginian-Hauterivian Vocontion Trough (with a paleolatitude of 30° N) as caused by a connection to Boreal seas and their signals.

Many of the ESA are not well developed because of instabilities in the depositional environment, which prohibit clear imaging of cyclicity. Some sections, on the other hand, show nearly ideal sequences and allow a very good interpretation. The interpretation of the

evolutionary spectral data is based on the assumption that orbital signals do not change their significance within cycle categories A, B, and C.

Beneath the often quoted genetic relation of sedimentation, site 7430/10-U-01 and 6307/07-U-02 express strong precession and obliquity signals. The signals are most pronounced where the cycles are well documented in the site. The obliquity therefore prevails the marine signal expressed in anoxic conditions, lacking bioturbation, and hence preservation of organic matter. Three factors control the illustration pattern mechanism of these sediments: the general transgressive time of the Late Jurassic/Earliest Cretaceous, the tectonic related basins and swells of a passive continental margin and the orbital forcing mechanisms. This leads to variability in clastic input, nutrient supply, restricted circulation, and preservation conditions. This study shows, that weathering and clastic input as well as nutrient supply is most likely related to a warm climate.

The Type C cycle ESA of all sites contain mostly autocyclic signals, which are related to the relative high energetic environment and instabilities in the depositional environment. There are only a few examples where dominant frequencies are not related to those of orbital cycles. One of them is the 70 ka frequency maximum, which cannot be explained merely by the known cyclic variation of orbital parameters, indicating that Milankovitch forcing is clearly not the only process that influences a sedimentary signal (Rose, 1999). The 70 ka signal was also detected in several Cretaceous sites, as the Piobbico core from the Apennins/Italy, $\delta^{18}O$ data from several sedimentary sequences, and the Kirchrode cores from Germany (Muller and MacDonald, 1995; Rose, 1999). The reason for that frequency is still in discussion and not inherits with the Milankovitch Theory. Muller and MacDonald (1995) discuss periodic variations of the inclination and in 1997 they propose that this frequency characterizes a non-linear interaction of the eccentricity and obliquity. Single power spectra of the related colour measurements of a* (amount of red colours) and b* (amount of yellow colours) even show a dominance of the 70 ka cycle at the sites of this study, whereas there is no explanation for the formation of it. Therefore the often quoted 70 ka signal in this study may be related to secondary processes of pyrite and Fe-carbonate formation which cannot be depicted without further analyses. But also the 70 ka cycle may be a natural frequency of the related basins, e.g. controlled by subsidence.

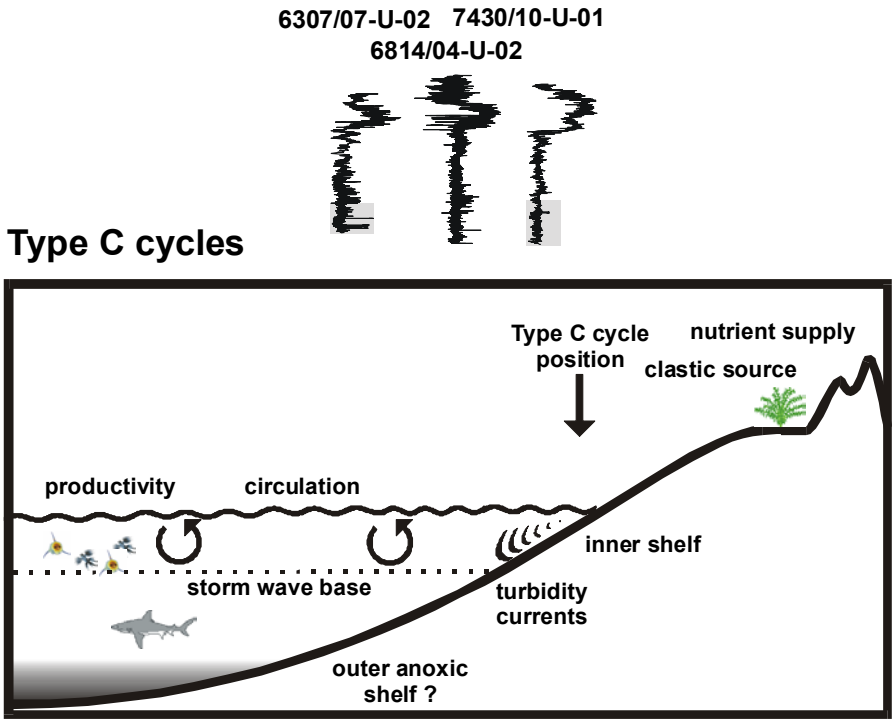

Figure 58 Sketch of the generalized depositional environment of Type C cycle sections

The above mentioned data sets lead to an oceanographic model, which is graphically displayed in figure 58 and explained in the following. The precession most likely is responsible for the terrestrial signal from the hinterland, like the clastic source of silt. The silt diluted the clayey background sedimentation and is often coupled to the eccentricity signal. The deposition occured under near-shore conditions above the storm wave base. Near-shore conditions are shown by grain size distribution of silt, a relative high sedimentation rate (three times higher than the remaining core), grain size distribution, and type of organic matter as well as a high zirconium signal (Mutterlose et al., 2002). Obliquity causes ocean currents, providing ascending and descending anoxic conditions on the shelf, which reflect preservation conditions. These conditions are coupled directly with the precession controlled nutrient supply and hence elevated primary production, which increases the organic matter preservation to more than 10% of site 7430/10-U-01 and up to 9% of site 6307/07-U-02. The precession controls in addition the clastic input of silt to the sedimentation space. Site 7430/10-U-01 reveals a dominance of obliquity in times of the Late Berriasian (Ryazanian)/Early Valanginian and the Mid.-Hauterivian, where even the precession shows a strong signal. These periods are also characterized as relatively warm by Swientek & Ricken (2001a), most likely due to a relationship between warm climate and higher frequency signals.

Furthermore, a genetic connection from the southernmost core 6307/07-U-02 and the northernmost core 7430/10-U-01 appears probable.

Site 6814/04-U-02 does not show Type C cycles. The relatively high sedimentation rate reflects a nervous and energetic sedimentation, which prevents a cyclic pattern. In addition, Mutterlose et al. (2002) presume the setting of this core on a threshold. The sedimentation rate is also a very important factor to express high frequent cyclicity as the resolution. These sites characterize a starved sedimentation, caused by a rapid subsidence due to rifting. In some cases a low resolution prevents the recognition of high frequency cycles, but precession is also visible in the Type A cycles. Geophysical borehole logs were also used in this study to underline our results of the lightness logs. The resolution of the borehole logs is far below the high resolution of the spectrophotometer and can therefore only be used for long wave signals. This is not the case, if the sedimentation rate is high enough as in core 6814/04-U-02 where the gamma ray log (calculated from the neutron porosity log), the neutron porosity log, and the sonic log contain the obliquity signal.

Type B cycles are characterized by a combination of the obliquity-, the precession-, and the eccentricity signal. There is no visible relation between the L* value and the black shale lithology, except for the siderite concretions at site 6814/04-U-02. Precession and eccentricity are most likely caused by an elevated surface productivity and TOC burial in a sulphate reducing and hence anoxic environment. The Fe-carbonate concretions, mainly siderite, of site 6814/04-U-02 show a very strong cyclic pattern forced by obliquity. Obliquity is often quoted to give a strong signal and control of anoxia. It is therefore a premise for siderite formation. The increased input of labile organic matter is most likely connected with the anoxic conditions, favouring the forming of siderite by sulphate reduction as described by e.g. Berner (1978). In contrast to the other sites of 7430/10-U-01 and 6307/07-U-02, the amount of concretions at site 6814/04-U-02 is very high. This may be related to higher sedimentation rates resulting in more rapid deposition of large quantities of organic matter (Gautier, 1982). Siderite formation is restricted to reducing sediments with microbially iron-reduction under suboxic conditions or by sulphate reduction. A low oxidation rate of organic carbon favours the development of calcite and siderite concretions (Mozley, 1992).

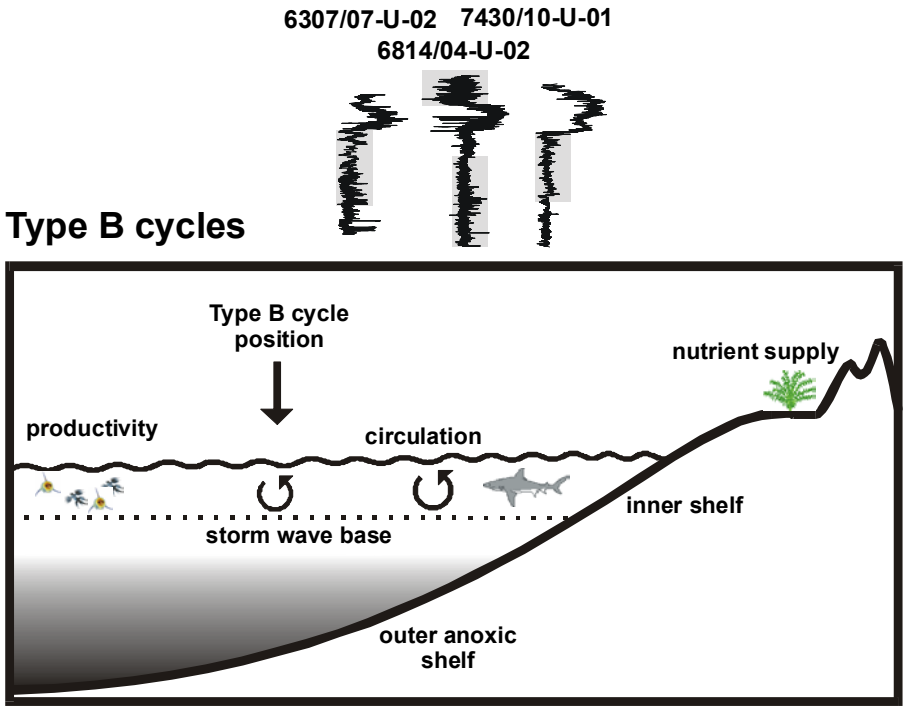

Figure 59 Sketch of the generalized depositional environment of Type B cycle sections

The depositional model represents a deep shelf environment. The Type B redox cycle section of site 6814/04-U-02 reveals the highest C_{org} values of up to 6%. This might confirm the strong obliquity signal as a control for an anoxic environment and preservation. The cyclicity in site 7430/10-U-01 is also characterized by the highest C_{org} content. In this case, obliquity most likely controlled the preservation conditions via anoxic zones. Precession as well as eccentricity seem to control the nutrient supply and, of course, the fresh water run-off. A high fresh water run-off from the hinterland caused by a humid climate leads to a stratification in the water column that in turn favour preservation conditions. This interplay of orbital signals is also visible in the ESA.

Type A cycles are characterized by carbonaceous nannoplankton, which dilute the clayey background sedimentation and are hence mentioned as carbonate productivity cycles. Beneath the well-established eccentricity signals the obliquity, as well as the precession, shares the evolutionary spectra. The southernmost site 6307/07-U-02 illustrates clear signals from 24 m to 27 m. The succeeding section of the Lange Fm. is characterized by dominance of the eccentricity. The dominance of eccentricity is most likely related to the bad preservation of the core which enables high-resolution measurement. Therefore the eccentricity is more pronounced and the precession as well as the obliquity are not expressed. Eccentricity and precession may have controlled weathering, run-off, and nutrient input.

Obliquity prevailed the oceanic features as currents and related preservation conditions. The ESA of site 6307/07-U-02 shows up to 35m, that the obliquity is not expressed but eccentricity controls the carbonate content, which dilutes the dark clayey sediment. This is expressed by a good correlation of the S2 and C_{org} curve as a proxy for preservation in context with a moderate C_{org} content about 3% (Mutterlose et al., 2002). This is most likely a further evidence that obliquity was not established and hence there where no anoxic conditions. Site 7430/10-U-01 shows obliquity and a strong precessional signal, which controls the carbonate content. The fact of a weak obliquity is contradicted in a very low C_{org} content.

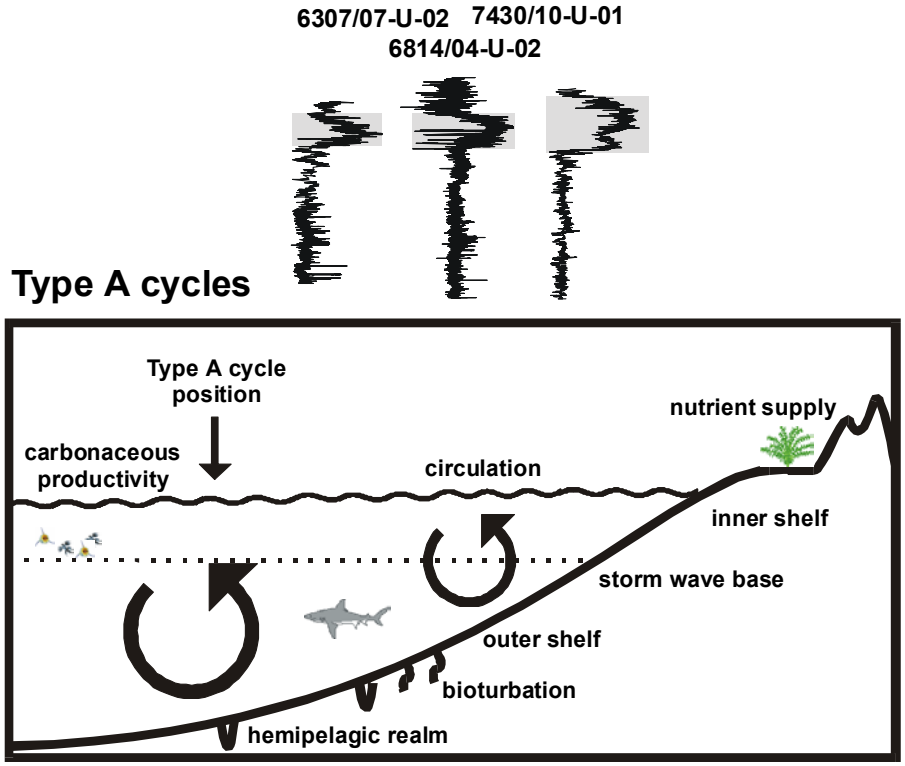

Figure 60 Sketch of the generalized depositional environment of Type A cycle sections

The oceanographic model describes an outer shelf deposition for Type A cycles. Bioturbation and low C_{org} contents at all sites indicate an oxic environment. The clayey sedimentation is diluted by nannoplankton ooze, related to precession as well as to eccentricity. About 38 m at site 7430/10-U-01 exemplify the $\delta^{13}C$ and the C_{min} indicate an elevated primary production (Mutterlose et al., 2002). This zone is also covered by a strong precession signal. Site 6307/07-U-02 demonstrates the highest C_{org} content in a section where obliquity is well established about 25 m. The Type A cycles are thought to represent rather global and typical oceanographic signals than the near shore Type C cycles.

The above mentioned changes of the orbital control are expressed in warmer and colder climates estimated by Swientek and Ricken (2001a) for the Volgian, the Late Berriasian (Ryazanian)/Early Valanginian, the Mid.-Hauterivian, and the Late Barremian. These times are all characterized by significant changes in orbital control and hence various sedimentological factors.

6 Synthesis

Various models describe the sedimentation and preservation of organic matter and they are summarized by Demaison & Moore (1980), Wignall (1994) or Welte et al. (1997). Generally, productivity models contradict preservation models and the different models are still in discussion, as high productivity does not coincide with enhanced preservation conditions (Tyson et al., 1979; Wignall, 1994; Welte et al., 1997). Different models has been proposed to explain organic rich deposits, like oxygen poor zones, caused by phytoplankton blooms (Gallois, 1976), stratified water columns in silled basins (Demaison and Moore, 1980), oceanic upwelling (Parrish and Curtis, 1982) or transgressional expand of oxygen minimum layers (Jenkyns, 1988). The models are mostly related to the depositional environment. For the Late Jurassic/Early Cretaceous some models have been established for the Greenland Norwegian Seaway e.g. Doré (1991), Oschmann (1988), Miller (1990), Wignall (1994), and Abbink et al. (2001).

This study shows that various aspects of the above mentioned models are fulfilled in the here proposed model as tectonic aspects and probably orbitally controlled variations. Obliquity may have triggered the preservation conditions by expanding anoxic “puddles” sensu Wignall (1994), that most likely lead to an oxygen minimum zone on the shelf. Obliquity presumably was also linked to a higher nutrient supply and hence paleoproductivity was controlled by eccentricity and precession. The precession and eccentricity signal seem to modulate the fresh water balance via the terrestrial run-off and hence coincide with obliquity and the preservation of the organic matter. Tectonic most likely was a major factor in controlling subsidence and increase in volume of the basins by rifting. Smelror et al. (2001) described direct links of theses aspects to sedimentation, e.g. by condensed sections. Two above mentioned major temperature increases are related to two major transgressions, which partly caused sediment starvation on the shelf. Black shales characterize the first transgression whereas the second represents a condensed section with carbonaceous sediments of a more hemi-pelagic facies. Some terrestrial signals in this most likely hemi-pelagic facies may originate from some structural heights which developed in the course of tectonic activity.

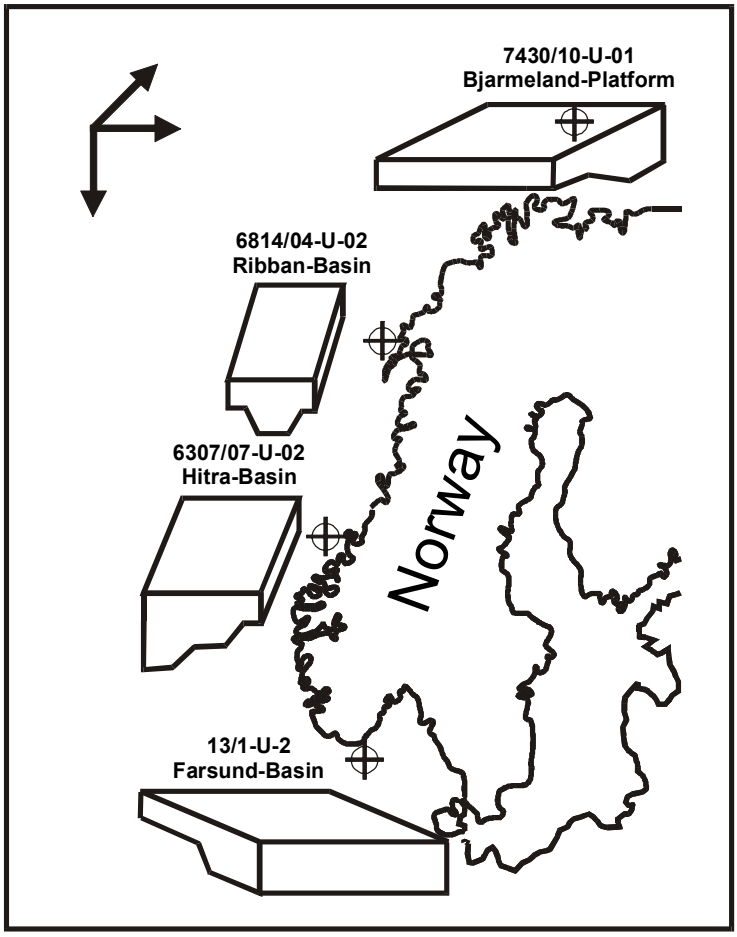

Figure 61 Simplified basin geometry of the investigated sites in the Greenland Norwegian Seaway

Further details are added to the model by the question if humid or arid climate conditions prevailed during the Late Jurassic and Early Cretaceous. The results of clay mineral associations from site 7430/10-U-01 and 6307/07-U-02 indicate a humid climate up to the Berriasian and subsequent arid conditions (Kornpihl, 2001). These humid conditions seem to be related to the Late Cimmerian tectonic activity, which changed the continent configuration and hence climate. The temperature curve, estimated in this study, shows a clear shift in climatic conditions at Late Volgian /Berriasian (Ryazanian) times and has been described by other authors, e.g. Mutterlose et al. (2002), but is in contrast to e.g. Abbink et al. (2001). An extension of the Greenland Norwegian Seaway combined with the climate and a shallow temperature gradient as mentioned above would favour a hypothesis of a circulation system which is characterized by low wind forcing. The basins most likely evolved a stratification of the water column due to fresh water run-off, which in turn provides more nutrient supply. Syn-rift tectonics and/or warmer temperatures presumably caused a sea level

rise and the expansion of the anoxic "puddle" sensu Wignall (1994). Low sedimentation rates, as well as lamination and the lack of bioturbation confirm this theory.

The described circulation model assumes that the seaway was deep enough for currents of both sides and a corresponding driving force. An estuarine circulation model seems most probable to explain the results of this study. The flow of warm and more saline tehyal bottom water to the north and relatively cold arctic surface water currents to the south characterize the Late Kimmeridgian to Late Volgian. The positive freshwater balance results from the continental runoff of this narrow seaway and lead to a stratification of the water column. This model proposes a high productivity and black shale occurrence by introduced nutrients from rivers, upwelling, and internal recycling. The estimated temperature and salinity data from bivalves as bottom water indicators and belemnites as surface current indicators support the thesis of an estuarine circulation. In the carbonaceous Valanginian-Hauterivian section the circulation modus may have changed to a more ventilated model.

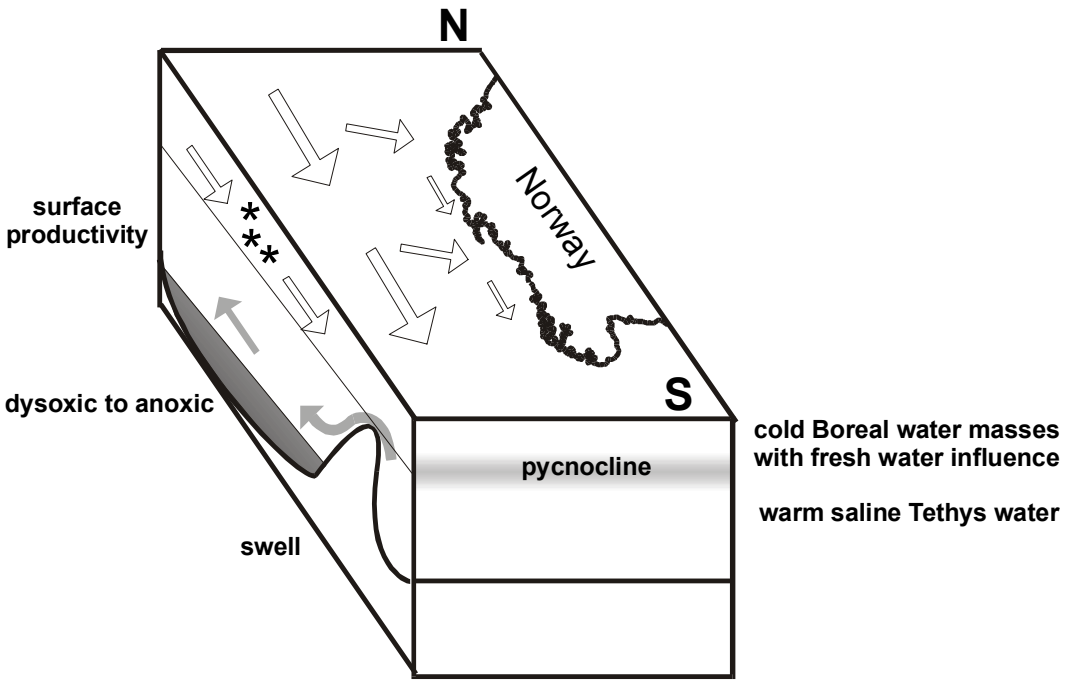

Figure 62 Estuarine circulation model for the Greenland Norwegian Seaway of Late Jurassic/Early Cretaceous times. The model is characterized by a northward flow of warm saline Tethys water and cold Boreal water masses flowing to the south, influenced by fresh water from continental runoff.

Increased tectonic activity of the Late Cimmerian Phase also favours a change in the circulation model caused by new uplift areas, which prevented colder boreal bottom water flow to the south. The Late Jurassic section of the Kimmeridgian to Ryazanian is characterized by a long term high sea level (Fig.63).

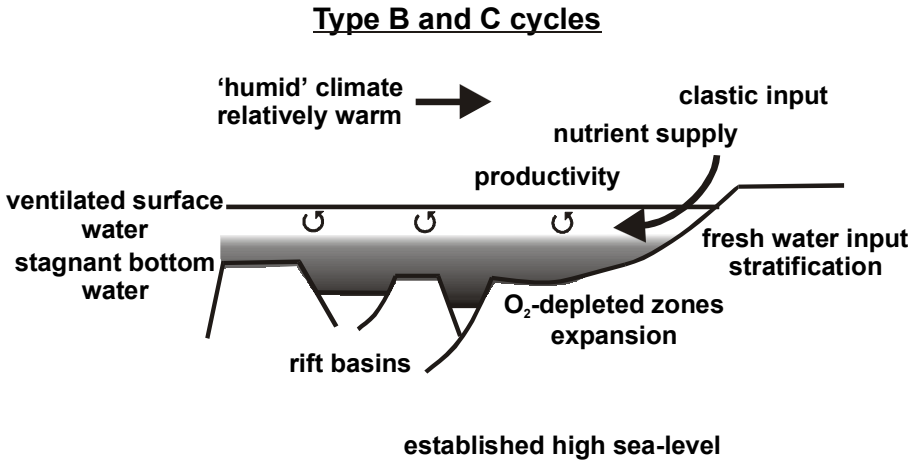

Figure 63 Sketch of the continent-ocean coupling of Kimmeridgian to Ryazanian transgression; Type C & Bs cycle deposition

The humid and relative warm climate caused elevated nutrient supply through weathering and enhance the productivity. These factors may have been driven by eccentricity and precession. The obliquity triggered variations in the preservation conditions of C_{org}. There have been most likely some variations from anoxic to dysoxic or sometimes oxic conditions. The rift basins and the outer shelf generally have been anoxic during all of the time and expansion to the inner shelf took place by different causes. A warm climate seems to induce an expansion of the oxygen depleted zones and an enhanced precipitation. This resulted in an increased fresh water run-off, which presumably caused stratification or an enhanced productivity, leading to O_2-depletion.

The record of the Early Cretaceous Valanginian to Hauterivian sections cannot be explained with the above mentioned model.

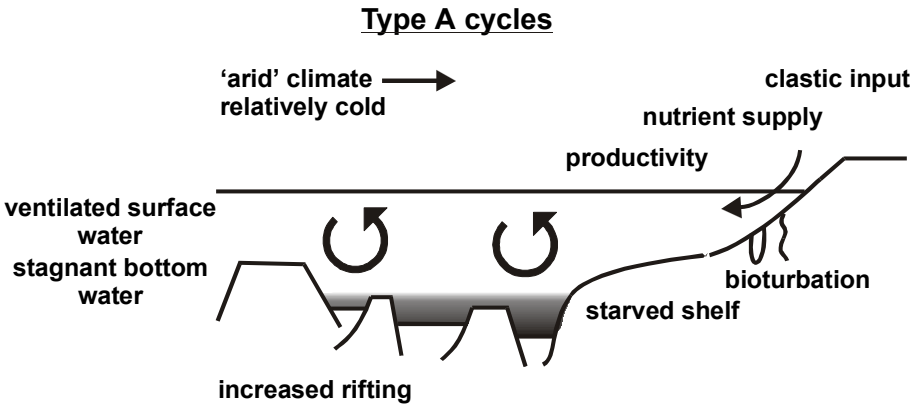

Figure 64 Sketch of the continent-ocean coupling of Valanginian to Hauterivian transgression; Type A cycle deposition

It is charcterized by an increased rifting, disposed to an enhanced subsidence and a restriction of the O_2-depleted zones to the rift basins. The rapid transgression resulted in a starved sedimentation and high oxygen content along the shelf. Bioturbation and related tiering patterns prove a continuous sedimentation and oxic conditions below the storm wave base. Furthermore the arid climate most likely have reduced the nutrient supply and fresh water input. Both models combine the achieved results of complex sedimentological factors and yield the advantage of being consistent to many other authors.

7 Conclusions

1. SEM, CL, and geochemical investigations indicate that most of the belemnite samples from high northern sites preserve their primary stable isotope composition. Bivalves (inoceramids and *Buchia*) in contrast show diagenetic alteration with some exceptions, and are less well preserved than belemnites. Bulk sediment isotopes indicate diagenetic alteration by organic-matter degradation.
2. The temperature increase from the Latest Kimmeridgian to Late Volgian times with a slight decrease in the Mid.-Volgian, succeeded by cooler temperatures of the Early Berriasian (Ryazanian). Relatively warmer temperatures of the Berriasian (Ryazanian) are accompanied by a maximum in the Early Valanginian. The temperature drops in the Valanginian and rises again slightly in the Mid.-Hauterivian to reach a new maximum in the Mid.-Barremian. There is in general a significant warming from Berriasian (Ryazanian) to Barremian times.
3. Assuming an equator to pole temperature gradient of 0.1°C/degree latitude our data fit well to elsewhere published temperature data in higher latitudes and give reason for a more equable climate than today.
4. The Early Berriasian (Ryazanian) and perhaps the Early and Late Hauterivian most likely have had the constitution for sub-freezing temperatures close to the polar latitudes.
5. There is a remarkable correlation of our major temperature data and 3rd order transgressive events of different authors. Minor temperature variations are presumably caused by glacio-eustatic sea-level fluctuations.
6. Milankovitch cycles are documented by silt dilution-, redox-, and carbonate productivity cycles representing a transgressional system.
7. Each cycle type has a very similar hierarchy pattern, which can be traced over the entire transect.
8. Obliquity modulated the marine anoxic conditions, whereas precession and eccentricity forced the terrestrial sediment- and nutrient supply as well as fresh water input. The coexistence of all orbital parameters in the investigated sites through time suggests one superimposing factor that modulated the paleoceanography in the Greenland Norwegian Sea.
9. The deposition of the Late Jurassic black shales is a complex compatibility of tectonics and climate forced by orbital parameters, which leads to an estuarine circulation model of the Greenland Norwegian Seaway.

References

Abbink, O., Targarona, J., Brinkhuis, H. and Visscher, H., 2001. Late Jurassic to earliest Cretaceous paleoclimatic evolution of the southern North Sea. Gobal and Planetary Change, 30: 231-256.

Anderson, T.F. and Arthur, M.A., 1983. Stable isotopes of oxygen and carbon and their application to sedimentologic and environmental problems. In: M.A. Arthur, T.F. Anderson, I.R. Kaplan, J. Veizer and L.S. Land (Editors), Stable isotopes in Sedimentary Geology. SEPM Short Course Notes, pp. 1.1-1.151.

Anderson, T.F., Popp, B.N., Williams, A.C., Ho, L.Z. and Hudson, J.D., 1994. The stable isotopic record of fossils from the Peterborough Member, Oxford Clay Formation (Jurrasic), UK: palaeoenvironmental implications. Journal of the Geological Society, London, 151: 125-138.

Barbin, V., 1999. Cathodoluminescence of carbonate shells: Biochemical vs diagenetic process. In: M. Pagel, V. Barbin, P. Blanc and D. Ohnenstetter (Editors), Cathodoluminescence in Geosciences. Springer-Verlag Heidelberg, pp. 303 -329.

Barron, E.J., Saltzman, E. and Price, D.A., 1980. Occurence of Inoceramus in the South Atlantic and oxygen isotopic paleotemperatures in Hole 530 A. Init. Repts. DSDP, 75: 893-904.

Barron, E.J. and Moore, G.T., 1994. Climate model applications in paleoenvironmental analysis. SEPM Shourt Course Notes, 33, 339 pp.

Berger, A.L., 1977. Support for the astronomical theory of climatic change. Nature, 269: 44 - 445.

Berger, A., 1978. Long-term variations of caloric insolation resulting from Earth's orbital elements. Quaternary Research, 9: 139-167.

Berger, A., Imbrie, J., Hays, J., Kukla, G. and Saltzman, B., 1984. Milankovitch and Climate. C126, I,II. Reidel-Verlag, Dordrecht, 895 pp.

Berger, W.H. and Loutre, M.F., 1989. Pre-Quarternary Milankovitch frequencies. Nature, 342: 133.

Berner, R.A., 1978. Sulphate reduction and the rate of deposition in marine environments. Earth and Planetary Science Letters, 37: 492-498

Braduchan, Y.V., et al., 1986. Bazhenovskii gorizont Zapadnoi Sibiri (stratigraphiya, paleogeographiya, ecosystema, neftenosnost'): Novosibirsk, Nauka, Trudy IGiG, 649: 216.

Brand, U. and Morrison, J.O., 1987. Biogeochemistry of fossil marine invertebrates. Geoscience Canada, 14(2): 85-107.

Bugge, T. et al., 1988. Shallow drilling Barents Sea, Sintef Petroleum Research, Trondheim.

Corfield, R.M., 1995. An introduction to the techniques, limitations and landmarks of carbonate oxygen isotope paleothermometry. In: D.W.J. Bosence and P.A. Allison (Editors), Marine paleoenvironmental analysis from fossils. Geological Society Special Publication, pp. 27-42.

Craig, H., 1965. The measurement of oxygen isotope paleotemperatures. In: E. Tongiori (Editor), Stable isotopes in oceanographic studies and paleotemperatures. Consiglio Nazionale delle Richerche, Laboratorio die Geologia Nucleare, Pisa, pp. 161-182.

Dalland, A., 1981. Mesozoic sedimentary succession at Andøya, northern Norway and relation to structural development of the North Atlantic Area. In: Kerr, J.W. and Ferguson, A.J. (Editors), Geology of the North Atlantic Borderlands. Canadian Society of Petroleum Geologists Memoir, 7: 563-584.

deBoer, P.L. and Smith, D.G., 1994. Orbital forcing and cyclic sequences. Blackwell Scientific Publications, pp. 559.

Demaison, G.J. and Moore, G.T., 1980. Anoxic environments and oil source bed genesis. AAPG Bulletin, 64: 1179-1209.

Ditchfield, P.W., 1997. High northern paleolatitude Jurassic-Cretaceous paleotemperature variation: new data from Kong Karls Land, Svalbard. Paleogeography, Paleoclimatology, Paleoecology, 130: 163-175.

Doré, A.G., 1991. The structural foundation and evolution of Mesozoic seaways between Europe and the Arctic. Palaeogeography, Palaeoclimatology, Palaeoecology, 87: 441-492.

Douglas, R.G. and Savin, S.M., 1975. Oxygen and carbon isotope analyses of Tertiary and Cretaceous microfossils from Shatsky Rise and other sites in the North Pacific Ocean. In: R.L. Larson and R. Moberly (Editors), Initial reports of the Deep Sea Drilling Project. U.S Government Rinting Office, Washington D. C., pp. 509-520.

Einsele, G., Ricken, W. and Seilacher, A., 1991. Cycles and Events in Stratigraphy. Springer-Verlag Heidelberg, 955 pp.

Einsele, G., Ricken, W. and Seilacher, A., 1991b. Cycles and Events in Stratigraphy - Basic concepts and terms. In: G. Einsele, W. Ricken and A. Seilacher (Editors), Cycles and Events in Stratigraphy. Springer-Verlag Heidelberg, pp. 955.

Elorza, J., Garcia-Garmilla, F. & Jagt, J. W.M., 1997. Diagenesis-related differences in isotopic and elemental composition of late Campanian and early Maastrichtian inoceramids and belemnites from NE Belgium: paleoenvironmental implications. Geologie en Mijnbouw, 75: 349-360.

Elorza, J. and Garcia-Garmilla, F., 1996. Petrological and geochemical evidence for diagenesis of inoceramid bivalve shells in the Plentzia Formation (Upper Cretaceous, Basque-Cantabrian Region, northern Spain). Cretaceous Research, 17: 479-503.

Elorza, J. and Garcia-Garmilla, F., 1998. Paleoenvironmental implications and diagenesis of inoceramid shells (Bivalvia) in the mid-Maastrichtian beds of Sopelana, Zumaya and Bidart sections (coast of the Bay of Biscay, Basque Country). Paleogeography, Paleoclimatology, Paleoecology, 141: 303-328.

Embry, A.F., 1992. Mesozoic stratigraphy of Franz Josef Land Archipelago, Arctic Russia-a literature review. In: D.K. Thurston and K. Fujita (Editors), International Conference on Arctic Margins. U. S. Minerals Managnement Service OCS Study MMS 94-0040, Anchorage, Alaska, pp. 15-22.

Epstein, S., Buchsbaum, R., Lowenstamm, H.A. and Urey, H.C., 1953. Revised carbonate-water isotopic temperature scale. Geological Society of America Bulletin, 64: 1315-1326.

Fischer, A.G., de Boer, P.L. and Premoli-Silva, I., 1990. Cyclostratigraphy. In: R.N. Ginsburg and B. Beaudoin (Editors), Cretaceous resources, rhythms and events. NATO ASI, pp. 139-172.

Föllmi, K.B., Garrison, R.E. and Grimm, K.A., 1991. Stratification in phosphatic sediments: Illustrations from the Neogene of California. In: G. Einsele, W. Ricken and A. Seilacher (Editors), Cycles and Events in Sstratigraphy. Springer-Verlag Heidelberg, pp. 493-507.

Frakes, L.A. and Francis, J.E., 1988. A guide to Phanerozoic cold polar climates from high latidude ice-rafting in the Cretaceous. Nature, 333: 547-549.

Frakes, L.A., 1999. Estimating global thermal state from Cretaceous sea surface and continental temperature data. In: E. Barrera and C.C. Johnson (Editors), Evolution of the Cretaceous Ocean-Climate System. The Gological Society of America, pp. 49-57.

Gallois, R.W., 1976. Coccolith blooms in the Kimmeridge Clay and the origin of North Sea oil. Nature, 259: 473-475

Gautier, D.L., 1982. Siderite concretions: Indicators of early diagenesis in the Gammon Shale (Cretaceous). Journal of Sedimentary Petrology, 52: 859-871.

Giraud, F., Beaufort, L. and Cotillon, P., 1995. Periodicities of carbonate cycles in the Valanginian of the Vocontian Trough: A strong obliquity control. In: M.R. House and A.S. Gale (Editors), Orbital Forcing Timescales and Cyclostratigraphy. Geological Society Special Publication, pp. 210.

Golberg, D., 1997. The role of downhole measurements in marine geology and geophysics. Reviews of Geophysics, 35,3: 315-342.

Gradstein, F.M., Kaminski, M.A. and Agterberg, F.P., 1999. Biostratigraphy and paleoceanography of the Cretaceous seaway between Norway and Greenland. Earth-Science Reviews, 46: 27-98.

Gudlaugsson, S.T., Faleide, J.I., Johansen, S.E. and Breivik, A.J., 1998. Late Paleozoic structural development of the South-western Barents Sea. Marine and petroleum Geology, 15: 73-102.

Hallam, A., 1988. A reevaluation of Jurassic eustasy in the light of of new data and the revised Exxon curve. In: T.S.o.E.P.a. Mineralogists (Editor), Sea-Level Changes - An Integrated Approach. SEPM Special Publication, pp. 261-273.

Hallam, A., Grose, J.A. and Ruffell, A.H., 1991. Paleoclimatic significance of changes in clay mineralogy across the Jurassic.Cretaceous boundary in England and France. Paleogeography, Paleoclimatology, Paleoecology, 81: 173-187.

Hansen, J.W. et al., 1991. Shallow drilling Nordland VI and VII, Sintef Petroleum Research, Trondheim.

Haq, B.U., Hardenbol, J. and Vail, P.R., 1988. Mesozoic and Cenozoic chronostratigraphy and cycles of sea-level change, Sea-Level Changes-An Integrated Approach. SEPM Special Publication, pp. 71-108.

Hardenbol, J. et al., 1998. Mesozoic and Cenozoic Sequence Chronostratigraphic Framework of European Basins. In: P.-.C. De Graciansky, J. Hardenbol, T. Jacquin and P.R. Vail (Editors), Mesozoic and Cenozoic Sequence Stratigraphy of European Basins. SEPM Special Publication 60, pp. 3-113.

Hay, W.W. et al., 1999. Alternative global cretaceous paleogeography. In: E. Barrera and C.C. Johnson (Editors), Evolution of the Cretaceous Ocean-Climate System. The Geological Society of America, pp. 1-47.

Hay, W.W., Wold, C.N. and DeConto, R.M., 1998. The role of salinity in circulation of the Cretaceous Ocean. Zbl.Geol.Paläont. Teil 1(11/12): 1445-1454.

Hudson, J.D., 1977. Stable isotopes and limestone lithification. Journal of the Geological Society of London, 133: 311-336.

Imbrie, J., 1985. A theoretical framework for the Pleistocene ice ages. Jounal of the Geological Society of London, 142(3): 417-432.

Jacquin, T., Dardeau, G., Durlet, C., de Graciansky, P.-C. and Hantzpergue, P., 1998. The North Sea Cycle: an overview of 2nd-order transgressive/regressive facies cycles in Western Europe. In: SEPM (Editor), Mesozoic and Cenozoic Sequence Stratigraphy of European Basins. SEPM (Society for Sedimentary Geology), pp. 445-466.

Jenkyns, H.C. and Clayton, C.J., 1997. Lower Jurassic epicontinental carbonates and mudstones from England and Wales: chemostratigraphic signals in the Early Toarcian anoxic event. Sedimentology, 44: 399-416.

Jenkyns, H.C., 1988. The early Toarcian (Jurassic) anoxic event: Stratigraphy, sedimentary, and geochemical evidence. American Journal of Science, 288: 101-151

Kazmin, V.G. and Napatov, L.M., 1998. The Paleographic Atlas of Northern Eurasia; 28 sheets. Russ. Acad. Nat. Scis., Moscow, Russia.

Kemper, E., 1987. Das Klima der Kreide-Zeit. Geol. Jahrbuch, 96: 5-185.

Kerr, R.A., 1981. Milankovitch climate cycles:old and unsteady. Science, 213: 109-1096.

Knott, S.D., Burchell, M.T., Jolley, E.S. and Fraser, A.J., 1993. Mesozoic to Cenozoic plate reconstructions of the North Atlantic and hydrocarbon plays of the Atlantic margin. In: J.R. Parker (Editor), Petroleum Geology of Northwest Europe: Proceedings of the 4th Conference. Geological Society of London, pp. 973-974.

Kornpihl, K., 2001. Der Jura/Kreide-Übergang der Hohen Breiten: Tonmineralassoziationen des Norwegischen Kontinentalschelfs. Diploma Thesis, University of Cologne, 64 pp.

Langrock, U., (in prep.). Mikroskopische und organisch-geochemische Untersuchungen an Schwarzschiefern in der Norwegen-Grönland See und der Barents-See für die Rekonstruktion der Ablagerungsbedingungen zur Jura- Kreide-Grenze. PH.D. Thesis, University of Bremen.

Lomb, N.R., 1976. Least-squares frequency analysis of unequally spaced data. Astrophysics and Space Science, 39: 447-462.

Lipninski, M., (in prep.). Haupt- und Spurenelementsignaturen in Mesozoischen Schwarzschiefern. PH.D. Thesis, University of Oldenburg.

Marshall, D.J., 1988. Cathodoluminescence of Geological Materials. Unwin Hyman LTD., 146 pp.

Marshall, J., D., 1992. Climate and oceanographic isotopic signals from the carbonate rock record and their preservation. Geological Magazine, 129(2): 143-160.

Milankovitch, M., 1920. Théorie mathèmatique des phénoménes termique prodiuts par la radiation solaire. Gauthiers-Villars, Paris.

Milankovitch, M., 1930. Mathematische Klimalehre und astronomische Theorie der Klimaschwankungen, Berlin, 176 pp.

Milankovitch, M., 1941. Kanon der Erdbestrahlung und seine Anwendung auf das Eiszeitproblem, Belgrad, 484 pp.

Miller, R.G., 1990. A paleogeographic approach to the Kimmeridge Clay Formation. In: A.Y. Huc (Editor), Deposition of Organic Facies. Stud. Geol. American Association of Petroleum Geologists, pp. 13-26.

Milliman, J.D., 1974. Marine Carbonates. Springer-Verlag Heidelberg, 375 pp.

Moore, G.T., Hayashida, D.N., Ross, C.A. and Jacobsen, S.R., 1992a. Paleoclimate of the Kimmeridgian/Tithonian (Late Jurassic) world: I. Results using a general circulation model. Paleogeography, Paleoclimatology, Paleoecology, 93: 113-150.

Moore, G.T., Sloan, L.C., Hayashida, D.N. and Umrigar, N.P., 1992b. Paleoclimate of the Kimmeridgian/Tithonian (Late Jurassic) world: II. Sensivity tests comparing three different paleotopographic settings. Paleogeography, Paleoclimatology, Paleoecolgy, 95: 229-252.

Mörner, N.-A., 1994. Internal response to orbital forcing and external cyclic sedimentary sequences. In: P.L. de Boer and D.G. Smith (Editors), Orbital Forcing and Cyclic Sequences. Blackwell Scientific, pp. 25-33.

Morrison, J.O. and Brand, U., 1986. Geochemistry of recent marine invertebrates. Geoscience Canada, 13: 237-254.

Morrison, J.O. and Brand, U., 1988. An evaluation of diagenesis and chemostratigraphy of Upper Cretaceous molluscs from the Canadian Interior Seaway. Chemical Geology (Isotope Geoscience Section), 72: 235-248.

Mozley, P.S. and Wersin, P., 1992. Isotopic composition of siderite as an indicator of depositional environment. Geology, 20: 817-820.

Muller, R.A. and MacDonald, G.J., 1995. Glacial cycles and orbital inclination. Nature, 377: 107-108.

Muller, R.A. and MacDonald, G.J., 1997. Simultaneous presence of orbital inclinationand eccentricity in proxy climate records from Ocean Drilling Programm Site 806. Geology, 25(1): 3-6.

Mutterlose, J. and Kessels, K., 2000. Early Cretaceous calcareous nannofossils from high latitudes: Implications for paleobiogeography and paleoclimate. Paleogeography, Paleoclimatology, Paleoecology, 160: 347-372.

Mutterlose, J., Brumsack, H., Flögel, S., Hay, W., Klein, C., Langrock, U., Lipinski, M., Ricken, W., Söding, E., Stein, R. and Swientek, O., 2002. The Greenland-Norwegian Seaway: a key area for understanding Late Jurassic to Early Cretaceous paleoenvironments. Paleoceanography, submitted.

Nebe, D.W. and Mutterlose, J., 1999. Lower Creatceous pale-dark bedding rhythms, a result of Milankovitch cycles?-A possibility to analyse field data-. Zbl. Geol. Paläont., 1(7-9): 973-988.

Nebe, D.W., 1999. Zyklenuntersuchungen an unterkretazischen Sedimeneten in NW-Deutschland. Ph.D. Thesis, Ruhr-University of Bochum.

Oschmann, W., 1988. Kimmeridge Clay sedimentation-a new cyclic model. Paleogeography, Paleoclimatology, Paleoecology, 65: 217-251.

Oschmann, W., Roessler, J. and Hüssner, H., 1995. Manipulations of insolation data (from Berger & Loutre 1991) for the simulation of "realistic geological situations". Zbl. Geol. Paläont., I(1/2): 317-335.

Pagani, M. and Arthur, M.A., 1998. Stable isotopic studies of Cenoman-Turonian proximal marine fauna from the U. S. Western Interior Seaway. In: SEPM (Editor), Stratigraphy and Paleoenvironment of the Cretaceous Western Interior Seaway, USA. SEPM Concepts in Sedimentology and Paleontology. Society for Sedimentary Geology, pp. 201-225.

Park, J. and Oglesby, R.J., 1990. A comparison of precession and obliquity effects in a Cretaceous paleoclimate situation. Geophysical Research Letters, 17: 1929-1932.

Parrish, J.T. and Curtis, R.L., 1982. Atmospheric circulation, upwelling and organic rich rocks in the Mesozoic and Cenozoic Eras. Paleogeography, Paleoclimatology, Paleoecology, 40: 31-66.

Peper, T. and Cloething, S., 1995. Autocyclic perturbations of orbitally forced signals in the sedimentary record. Geology, 23(10): 937-940.

Pirrie, D. and Marshall, J.D., 1990. Diagenesis of inoceramus and Late Cretaceous paleoenvironmental geochemistry: A case study from James Ross Island, Antarctica. Palaios, 5: 336-345.

Podlaha, O.G., Mutterlose, J. and Veizer, J., 1998. Preservation of $\delta^{18}O$ and $\delta^{13}C$ in belemnite rostra from the Jurassic/Early Cretaceous successions. American Journal of Science, 298: 324-347.

Port, G., 2000. Climatic signals recorded in rock magnetic properties of Pleistocene mediterranean sediments. PH.D. Thesis, University of Cologne.

Price, G.D., 1999. The evidence and implications of polar ice during the Mesozoic. Earth-Science Reviews, 48: 183-210.

Price, G.D., Ruffell, A.H., Jones, C.E., Kalin, R.M. and Mutterlose, J., 2000. Isotopic evidence for temperature variation during the Early Cretaceous (Late Ryazanian-Mid.-Hauterivian). Journal of the Geological Society, London, 157: 335-343.

Railsback, L. B., Anderson, T. F., Ackerly, S. C. and Cisne, J. L., 1989. Paleoceanographic modeling of temperature-salinity profiles from stable isotopic data. Paleoceanography, 4: 585-591.

Rawson, P.F., 1971. The Hauterivian (Lower Cretaceous) biostratigraphy of Speeton Clay of Yorkshire, England. Newsl. Stratigr., Leiden, 1: 61-76.

Rawson, P.F. and Mutterlose, J., 1983. Stratigraphy of the Lower B and basal cement beds of the Speeton Clay, Yorkshire, England. Proc. Geol. Ass., 94(2): 133-146.

Rawson, P.F., 1994. Sea level changes and their influence on ammonite biogeography in the European Early Cretaceous, 3rd Pergola International Symposium. Paleopelagos Spec. Publ., Roma, pp. 317-326.

Rawson, P.F. and Riley, L., 1982. Latest Jurassic-Early Cretaceous Events and the "Late Cimmerian Unconformity" in North Sea area. AAPG Bulletin, 66: 2628-2648.

Richter, D.K. and Zinkernagel,U., 1981. Zur Anwendung der Kathodenlumineszenz in der Karbonatpetrographie. Geologische Rundschau, 70(3): 1,276-1,302.

Ronnevik, H. et al., 1975. The Geology of the Norwegian Continental Shelf. In: A.W. Woodland (Editor), Petroleum and the continental shelf of North West Europe. Applied Science Publishers, pp. 501.

Rose, T., 1999. High resolution paleo- and rock magnetic studies of the cores Kirchrode I and II (Albian, North-West-German Basin). Ph.D. Thesis, University of Cologne, 116 pp.

Ruddiman, W.F. and McIntyre, A., 1984. Ice-age thermal response and climate role of the surface Atlantic Ocean, 40°N to 63°N. Geol. Soc. Am. Bull., 95: 381-396.

Ruffell, A., 1991. Sea-level events during the Early Cretaceous in Western Europe. Cretaceous Research, 12: 527-551.

Saelen, G., 1989. Diagenesis and construction of the belemnite rostrum. Paleontology, 32(4): 765-798.

Saelen, G. and Karstang, T.V., 1989. Chemical signatures of belemnites. N. Jb. Geol. Pläont. Abh., 177(3): 333-346.

Saltzmann, E.S. and Barron, E.J., 1982. Deep circulation in the Late Cretaceous: oxygen isotope paleotemperatures from Inoceramus remains in D.S D.P. cores. Paleogeography, Paleoclimatology, Paleoecology, 40: 167-181.

Sass, E. and Ahuva Almogi-Labin, A.B., 1991. Oxygen-isotope composition of diagentic calcite in organic-rich rocks: Evidence for $\delta^{18}O$ depeletion in marine anaerobic pore water. Geology, 19: 839-842.

Savrda, C.E., Bottjer, D.J. and Seilacher, A., 1991. Redox-related benthic events. In: G. Einsele, W. Ricken and A. Seilacher (Editors), Cycles and Events in Sstratigraphy. Springer-Verlag Heidelberg, pp. 493-507.

Savrda, C.E. and Bottjer, D.J., 1994. Ichnofossils and ichnofabrics in rhytmically bedded pelagic/hemi-pelagic carbonates: Recognition and evaluation of benthic redox and scour cycles. In: P.L. de Boer and D.G. Smith (Editors), Orbital Forcing and Cyclic Sequences. Blackwell Scientific Publications, pp. 195-210.

Scargle, J.D., 1982. Studies in astronomical time series analysis - statistical aspects of spectral analysis of unevenly spaced data. The Astrophysical Journal, 263: 835-853.

Schaaf, M., 1995. Digital Sediment Color Analysis - Development and application to Holocene and Late Pleistocene sediments from East Pacific DSDP/ODP sites. Ph.D. Thesis, Ruhr-University of Bochum, 243 pp.

Schulz, M., 1996. SPECTRUM and ENVELOPE, 65. Berichte Sonderforschungsbereich 313 - University of Kiel, 131 pp.

Schwarzacher, W., 1993. Cyclostratigraphy and the Milankovitch Theory. Developments in Sedimentology, 52. Elsevier.

Skarbø, O. et al., 1988. Shallow drilling of Møre-Trondelag, Sintef Petroleum Research, Trondheim.

Smelror, M., Dypvik, H. and Mørk, A., 1999. Phytoplankton blooms related to the Jurassic-Cretaceous boundary Mjølnir meteorite impact (Barents Sea), Proceedings from Workshop on Geological and Biological Evidence for Global Catastrophes. Lecture Notes in Earth Sciences, Esperaza/Quillan (Aude, France).

Smelror, M. et al., 1989. Shallow drilling Farsund Basin, Sintef Petroleum Research, Trondheim.

Smelror, M., Mørk, A., Monteil, E., Rutledge, D. and Leereveld, H., 1998. The Klippfisk Formation-a new lithostratigraphic unit of Lower Cretaceous platform carbonates on the Western Barents Shelf. Polar Research, 17(2): 181-202.

Smelror, M., Mørk, M.B.E., Mørk, A., Løseth, H. and Weiss, H.M., 2001. Middle Jurassic-Lower Cretaceous transgressive-regressive sequences and facies distribution off northern Nordland and Troms, Norway. In: O.J. Martinsen and T. Dreyer (Editors), Sedimentary environments offshore Norway-Paleozoic to Recent. Norwegian Petroleum Society Special Publication, pp. 21-232.

Sokolov, R.I., 1990. Geologic Map of Russia and Adjacent Countries (1:5,000,000); 4 sheets. All Union Research Geological Institute (VSEGEI), Leningrad.

Spicer, R.A. and Corfield, R.M., 1991. A review ot terrestrial and marine climates in the Cretaceous with implications for modelling the "Greenhouse Earth". Geol. Mag., 129(2): 169-180.

Srivastava, S.P. and Tapscott, C.R., 1986. Plate kinematics of the North Atlantic. In: P.R. Vogt and B.E. Tucholke (Editors), The Western North Atlantic Region. Geology of North America. The Geological Society of America, pp. 379-404.

Stoll, H.M. and Schrag, D.P., 1996. Evidence for glacial control of rapid sea level changes in the Early Cretaceous. Science, 272(21 June): 1771-1774.

Swiecicki, T., Gibbs, P.B., Farrow, G.E. and Coward, M.P., 1998. A tectonostratigraphic framework fot the Mid-Norway region. Marine and Petroleum Geology, 15: 245-276.

Swientek, O and Ricken, W., 2000. Zur Bedeutung von $\delta^{18}O$- und $\delta^{13}C$ Isotopenmessungen als Paläoklimaproxy in der Unterkreide der Norwegen- und der Barents-See. In: Miteilungen der Gesellschaft der Geologie und Bergbaustudenten in Österreich, 43: 132. Sediment 2000, Leoben.

Swientek, O and Ricken, W., 2001a. Paleoclimatic implications from $\delta^{18}O$ and $\delta^{13}C$ stable isotopes of the Lower Cretaceous in high northern latitudes: the Norwegian Seaway. In: Wortmann, U. G. and Funk, H. (Editors), IAS 2001-21st meeting - International Association of Sedimentologists, p. 44- Davos, Switzerland.

Swientek, O and Ricken, W., 2001b. Hochauflösende Klimazyklen in Sedimenten der borealen Unterkreide. In: Gaupp, R. and van der Klauw, S. (Editors), Schriftenreihe der Deutschen Geologischen Gesellschaft,13: 91-92. Sediment 2001, Jena.

Thiede, J., 1979. History of the North Atlantic Ocean: Evolution of an asymmetric zonal paleo-environment in a latitudinal ocean basin. In: M. Talwani, W.W. Hay and W.B. Ryan (Editors), Deep Drilling Results in the Atlantic Ocean, pp. 275-296.

Tucker, M., 1988. Techniques in Sedimentology, 394 pp.

Tyson, R.V., Wilson, R.C. and Downie, C., 1979. A stratified water column environmental model for the Kimmeridge Clay. Nature, 277: 377-380.

Valdes, P.J. and Sellwood, B.W., 1992. A paleoclimate model for the Kimmeridgian. Palogeography, Paleoclimatology, Paleoecology, 95: 47-72.

Valdes, P.J., Sellwood, B.W. and Price, G.D., 1995. Modelling Late Jurassic Milankovitch climate variations. In: M.R. House and A.S. Gale (Editors), Orbital Forcing Timescales and Cyclostratigraphy. Geological Society Special Publication, pp. 210.

van de Schootbrugge, B., Föllmi, K.B., Bulot, L.G. and Burns, S.J., 2000. Paleoceanographic changes during the early Cretaceous (Valanginian-Hauterivian): Evidence from oxygen and carbon stable isotopes. Earth and Planetary Science Letters, 181: 15-31.

Veizer, J., 1974. Chemical diagenesis of belemnite shells and possible consequences for paleotemperature determinations. N. Jahrb. Geol. Paläontol., 147: 91-111.

Veizer, J., 1983. Chemical diagenesis of carbonates: Theory and application of trace element technique. In: M.A. Arthur, T.F. Anderson, I.R. Kaplan, J. Veizer and L.S. Land (Editors), Stable isotopes in Sedimentary Geology. SEPM Short Course Notes, pp. 3.1-3.100.

Walker, G.B., St., 1991. Luminescence petrography and spectroscopic studies of diagenetic minerals. In: C.E. Barker and O.C. Kopp (Editors), Luminescence Microscopy and Spectroscopy. SEPM Short Course Notes 25, pp. 83-96.

Waterhouse, H.K., 1995. High-resolution palynofacies investigation of Kimmeridgian sedimentary cycles. In: M.R. House and A.S. Gale (Editors), Orbital Forcing Timescales and Cyclostratigraphy. Geological Society Special Publication, pp. 210.

Weber, M.E., 1998. Estimation of biogenic carbonate and opal by continuous non-destructive measurements in deep-sea sediments: application to the Eastern Equatorial Pacific. Deep-Sea Research, I(45): 1955-1975.

Wefer, G., 1985. Die Verteilung stabiler isotope in Kalkschalen mariner Organismen. Geologisches Jahrbuch, 82: 111.

Weissert, H. and Lini, A., 1991. Ice age interludes during the time of Cretaceous greenhouse climate? In: D.W. Mueller, J.A. McKenzie and H. Weissert (Editors), Controversies in Modern Geology. Academic Press, London, pp. 173-191.

Weissert, H., Lini, A., Föllmi, K.B. and Kuhn, O., 1998. Correlation of Early Cretaceous carbon isotope stratigraphy and platform drowning events: a possible link? Palaeogeography, Palaeoclimatology, Palaeoecology, 137: 189-203.

Weissert, H. and Mohr, H., 1996. Late Jurassic climate and its impact on carbon cycling. Paleogeography, Paleoclimatology, Paleoecology, 122: 27-43.

Welte, D.H., Horsfield, B and Baker, D.R., 1997. Petroleum and basin Evolution. Springer-Verlag Heidelberg, pp.535

Wignall, P.B., 1994. Black Shales. Oxford Monographs on Geology and Geophysics, 30. Clarendon Press - Oxford, 127 pp.

Wignall, P.B. and Hallam, A., 1991. Biofacies, stratigraphic distribution and depositional models of British onshore Jurassic black shales. In: R.V. Tyson and T.H. Pearson (Editors), Modern and Ancient Continental Shelf Anoxia. Geol. Soc. London Spec. Publ., pp. 291-309.

Ziegler, P.A., 1982. Geological atlas of Western and Central Europe. Shell Int. Petrol. Maats. B.V., Distributed by Elsevier, Amsterdam, 130 pp.

Ziegler, P. A., 1990. Geological Atlas of Western and Central Europe. Geological Society Publishing House, London, U.K., 239 pp.

Zusammenfassung (extended german abstract)

Die Grönland Norwegen See: die klimatische und zyklische Entwicklung von Sedimenten aus dem Späten Jura und der Frühen Kreide

Im Rahmen des DFG-Bündelprogramms "Änderungen im Ozean-Atmosphäresystem und seine Einflüsse auf die Evolution der Biosphäre - ausgewählte Beispiele seit der Atlantiköffnung" wurden vier Kerne der Sintef-Petroleum Research (Trondheim) aus der Norwegen- und der Barents-See untersucht.

Die beprobten Kerne ergeben einen Transsekt, der vom südlichen Norwegen über den norwegischen Kontinentalschelf zur Barents-See reicht. Hierbei handelt es sich um die Kerne 13/1-U-2, 6307/07-U-02, 6814/04-U-02 und 7430/10-U-01.

Stratigraphie

Die Bohrung des Kerns 13/1-U-2 erfolgte im Farsund Becken, 40 km südöstlich von Kristiansand im Raum Skagerrak. Die Kernlänge betrug 90 m, umfasst erdgeschichtlich den Zeitraum des Frühen Volgium und reicht bis in das Berrias. Die Sedimente des Kerns werden dem Børglund-Member der Bream-Formation zugeordnet. Betrachtet man die Schwarzschiefer des A2- Subunits, kann man Fossilien, wie Belemniten, marine Bivalven und Brachiopoden, sowie kleinräumige Bioturbation und authigenen Pyrit nachweisen. Dieser Zustand ändert sich jedoch im dann folgenden sandigen B- Subunit durch zunehmende Bioturbation. Auch im B-Subunit geben Belemniten und Bivalven Hinweise auf ein vollmarines Milieu. Das Subunit-C des Kerns ist lithologisch mit dem Subunit-A2 vergleichbar, wobei man bei ersterem durch erhöhte Bioturbation bessere Sauerstoffbedingungen annehmen kann.

Der Kern 6307/07-U-02 wurde im Hitra Becken nahe der Küste vor Smøla erbohrt und weist eine Länge von ca. 176 m auf. Der Kern deckt den Zeitraum des Späten Kimmeridge bis zum Frühen Valangin ab. Der zu untersuchende Teil des Kernes beginnt mit dem in das Berrias fallende Subunit-2 der Spekk-Formation. Diese Formation besteht aus dunkelgrauen horizontal geschichteten Tonsteinen mit erhöhtem Silt-Gehalt in der unteren Hälfte. Die

horizontalen Laminae zeigen leichte Bioturbation. Die im Hangenden des Kerns enthaltene Lange-Formation des spätesten Berrias - Frühes Valangin ist in zwei Untereinheiten geteilt. Das graue Subunit-1 besteht aus karbonatzementierten Tonsteinen und ist nahezu durchgehend bioturbat. Vereinzelt treten Bivalven auf. Das rote Subunit-2 setzt sich ebenfalls aus karbonatzementierten horizontal geschichteteten rot-braunem Tonstein zusammen, zeichnet sich jedoch durch eine geringere Bioturbation aus.

Der Kern 6814/04-U-02 wurde auf dem Kontinentalschelf vor den Lofoten erbohrt und weist ein Mächtigkeit von ca. 185 m auf. Dieser umfasst den Zeitraum des Unteren Volgium bis in das Frühe Barreme. Die Einteilung des Kerns erfolgt in drei Einheiten. Das Unit-A (Frühes Volgium - Berrias) besteht aus dunkelgrauem, laminiertem pyritischen Tonstein mit geringem Siltanteil. Zwischen 160 m und 125 m befinden sich zahlreiche Siderit- und Ankerit Einschaltungen. Unit-B dagegen beinhaltet grün-graue Kalzit-zementierte Siltsteine mit zahlreichen Kalkknollen und Kalklagen. Datiert wird dieses Unit auf das Frühe Valangin bis Hauterive, wobei die Ablagerungen des Oberen Valangin - Hauterive fehlen können. Das Benthos wird durch zahlreiche Bivalven und Zoophycos-Bauten gebildet, die pelagischen tonigen Karbonate hingegen, sind arm an organischem Material. Das C- Unit (Hauterive - Frühes Barrem) schließlich, besteht aus dunkelgrauen Tonsteinen mit dünnen Karbonat und/oder Silt-Lagen.

Der Kern 7430/10-U-01 entstammt einer Plattform nördlich des Nordkapp Beckens in der Barents-See . Die Kernlänge beträgt ca. 58 m und reicht vom Späten Kimmeridge bis in das Frühe Barreme. Die Hekkingen-Formation des Kernes 7430/10-U-01 (Spätestes Kimmeridge - Berrias) enthält fossilreiche Schwarzschiefer mit einigen Feinsand- und Siltlagen. Unterhalb von 54 m sind zwei coarsening up Sequenzen mit einem zunehmenden Anteil von Laminae zu erkennen. Pyritkonkretionen und Pyrit-Lagen sind in der Formation ebenfalls nachzuweisen. Oberhalb von 54 m treten zunehmend braune Tonsteinlagen hinzu. Die nachfolgende Knurr-Formation (Spätestes Berrias - Frühes Barreme) ist in ein durch Kalk/Mergel-Wechsel und Karbonatkonkretionen geprägtes A-Unit, und ein dunkelolivgraues Tonstein B-Unit unterteilt. Die pelagischen, Nannoplankton enthaltenden Mergel in Unit A, sind gekennzeichnet durch Bioturbation von *Planolites* und *Chondrites*, die im Rahmen von Redox Zyklen in ihrer Intensität und ihrem Tiering-Muste ein variierendes Anordnungsmuster zeigen. Des weiteren weist Unit A eine Vielzahl von Buchien, Inoceramen und einigen Belemniten auf. Das B-Unit ist durchgehend bioturbat.

Im wesentlichen kann die Studie in zwei Bereiche gegliedert werden: Die Bestimmung der Paläowassertemperatur anhand von Sauerstoffisotopen aus Inoceramen, Buchien und Belemniten, sowie die Erfassung orbital gesteuerter Klimazyklizität anhand von Datensätzen, die mit einem Spektrophotometer erzielt wurden.

Paläoklimarekonstruktion

Die Rekonstruktion paläoklimatischer Proxies in Form von $\delta^{18}O$ und $\delta^{13}C$ Isotopen an fossilen Schalen ist in erheblichem Maß an den Grad der Diagenese des untersuchten Materials gekoppelt. Um die Eignung des Materials, und damit der stabilen Isotopen als Paläoklimaproxy zu erfassen, wurden einige Fossilien (Belemniten, Inoceramen und Buchien) mit Hilfe des Raster-Elektronen-Mikroskops, der Kathodenlumineszenz, der OES-MS und der Mikrosonde untersucht.

Raster-Elektronen-Mikroskopie

Das Raster-Elektronenmikroskop erbrachte keine Hinweise auf eine diagenetische Veränderung im karbonatischen Material der untersuchten Organismengruppen. Belemniten und Inoceramen zeigen bei dieser Untersuchung den den typischen Aufbau durch gut definierte polygonale Kalzitprismen und die daraus resultierende Wabenstruktur. Auch zwischen den einzelnen Prismen wurden keine Hinweise auf Neomorphismus oder sekundär gebildeten Kalzit entdeckt. Die Aufnahme von Buchienschalen lässt ebenfalls keine diagenetische Beanspruchung vermuten.

Kathodenlumineszenz

Hier sind zum Teil deutliche diagentische Veränderungen sichtbar. Der Einfluss der Diagenese scheint dabei dem Durchmesser des fossilen Materials und der Struktur zu folgen. Buchienschalen weisen in den KL-Aufnahmen großflächig beeinflusste Bereiche auf, deren orange Farbe auf den Einbau von Mn^{2+} und Fe^{2+} hindeutet. Mn^{2+} und Fe^{2+} rufen als Aktivator-Ionen die Lumineszenz hervor. Inoceramen dagegen zeigen einen weniger starken diagenetischen Stoffaustausch. Diese fallen außerdem durch lumineszierende Bereiche zwischen den Kalzitprismen- und Schalenstrukturgrenzen auf. Hier konnten Porenwässer besonders leicht eindringen und den chemischen Stoffbestand verändern. Die in den Inoceramenschalen lumineszierenden Bereiche innerhalb der Kalzitprismen erscheinen im Durchlichtmikroskop und bei polarisiertem Licht als alterierte und opake Bereiche. Sowohl

der konzentrische Aufbau der Belemniten, als auch das Fehlen von Lumineszenz, erkennbar an einer dunkelroten Farbe zeigt, bis auf äußerst wenige Ausnahmen, keine diagenetische Veränderung. Auch hier ist der diagenetische Stoffaustausch auf Bereiche begrenzt, in die Porenwasser eindringen konnte. Dazu zählen Risse im Rostrum, der Bereich nahe der Apikal-Linie und die äußersten Bereiche des Rostrums.

Anorganische Geochemie

Sowohl die Mikrosonde als auch die OES-MS eigneten sich gut um anorganisch geochemischen Stoffaustausch zu charakterisieren. Die Ergebnisse der Mikrosonde haben gezeigt, dass die meisten Belemniten ihren originären Stoffbestand an Fe (bis zu 700 ppm)und Mn (bis zu 400 ppm) besitzen. Höhere Werte können entsprechend den KL-Aufnahmen, diagentisch veränderten Belemniten zugewiesen werden.
Die Auswertung der OES-MS Ergebnisse der Muscheln (Inoceramen und Buchien) bestätigen die Analyse mit Hilfe der Kathodenlumineszenz. Einige Schalen beider Gruppen beinhalten den ursprünglichen Stoffbestand, wogegen andere Spezies einen Stoffaustausch anzeigen. Ein Vergleich von Belemniten mit Muscheln unter Zuhilfenahme der Sauerstoffisotopendaten, aufgetragen gegen den Mn-Gehalt, zeigt sehr deutlich den guten Erhaltungszustand der Belemniten im Gegensatz zu den zum Teil von der Diagenese erfassten Muscheln.

Stabile $\delta^{18}O$ und $\delta^{13}C$ Isotopen

Die Sauerstoff- und Kohlenstoff-Isotopendaten spiegeln die obigen Ergebnisse wider.
In einem Kreuzplot zwischen $\delta^{18}O$ und $\delta^{13}C$ Isotopen zeigen die Belemniten, mit Ausnahme des Kernes 6814/04-U-02, ursprüngliche Sauerstoffisotopenwerte von ca. 0 bis –1 ‰ PDB. Die Werte der Muscheln dagegen sind, wie aus den oben genannten Untersuchungen zu erwarten, verändert; wenngleich wenige Spezies unveränderte Werte aufweisen. Die Werte der Muscheln sind vor allem durch eine Verschiebung zu leichteren $\delta^{18}O$-Werten hin charakterisiert. Dies könnte durch freigesetztes CO_2, mit leichter Isotopensignatur aus der Oxidation organischen Materials, oder durch einen extremen Süßwassereinfluss bedingt sein. Die $\delta^{13}C$ Werte aller Organismengruppen liegen in einem Bereich zwischen –4 und 4 ‰ PDB. Die $\delta^{13}C$ Werte des Gesamtgesteins, besonders deutlich die des Kerns 13/1-U-2 und des Kerns 6307/07-U-02, weisen diagenetisch veränderte Werte auf. Darauf deuten ebenfalls die leichten $\delta^{18}O$-Werte hin. Die geringe Auflösung der Isotopendaten im Gegensatz zu den Farblogs (L*) erlaubt keine genauere Aussage darüber, ob die Isotopenwerte in einem

direkten Zusammenhang zur Gesteinslithologie stehen. Die Gesamtgestein-Isotopenwerte des Kernes 7430/10-U-01 und des Kernes 6307/07-U-02 scheinen in den organisch reichen Lagen der Hekkingen Fm. bzw. Spekk Fm. leichtere Werte aufzuweisen, als in den karbonatischen Abschnitten der Klippfisk Fm, wogegen dies in Kern 6814/04-U-02 genau umgekehrt zu sein scheint. Im wesentlichen wird in dieser Studie davon ausgegangen, dass der Zerfall und Abbau von organischem Material unter reduzierenden Bedingungen für die Veränderung der Isotopensignale verantwortlich ist. Des weiteren wird der Einfluss von Süßwasser in Betracht gezogen.

Zyklen

Im Laufe der Erdgeschichte überlieferte periodische Klimaschwankungen können auf astronomisch definierte Variationen der Umlaufbahn der Erde um die Sonne, und somit der Verteilung der Sonnenenergie (Insolation) zurückgeführt werden. Die Insolation beeinflusst die Saisonalität des Klimas, und infolgedessen durch verschiedene Rückkopplungsprozesse die Strömungssysteme der Ozeane und Sedimentsysteme. Es werden verschiedenen orbitale Parameter unterschieden, die Einfluss auf das Klima der Erde nehmen. Die Präzession zeigt in der Kreide eine zyklische Schwankung im Bereich von 18.5 und 22.3 ka., die Obliquität von 39 und 51 ka und die Exzentrizität von 95, 123 und 413 ka.

Farblogs

Die Archivhälften der vier Kerne wurden mit einem Spektrophotometer (Minolta, CM-2002) hochauflösend in cm-Intervallen und im Hinblick auf zyklische Sedimentationsmuster untersucht. Der L*-Wert ist eine Funktion der Helligkeit des Sediments. Die Helligkeit ist in karbonatischen Abfolgen proportional zum Karbonatgehalt und in Schwarzschiefern umgekehrt proportional zum TOC-Gehalt.
Die Farblog-Kurven der Kerne 7430/10-U-01, 6814/04-U-02 und 6307/07-U-02 weisen, über eine Paläodistanz von mehr als 1000 km, ein sehr ähnliches Muster auf. Dies deutet auf eine genetische Beziehung der Sedimente entlang dieses Profiles hin.
Bereits makroskopisch konnten in den Kernen verschiedene Zyklen erkannt werden, die sich auch im Farblog deutlich abzeichnen. Diese Zyklen lassen sich ebenfalls über das Profil hinweg korrelieren.

Typ A oder Karbonat Produktivitätszyklen zeichnen sich durch Variationen im Karbonatgehalt bei gleichbleibenden Toneintrag aus. Die karbonatreichen Intervalle des Typ a Zyklus sind reich an Bioturbation, wie beispielsweise *Planolites*. Karbonatärmere Bereiche dadegen sind reicher an organischem Kohlenstoff und beinhalten *Zoophycos* und *Chondrites*. Das in den Zyklen vorhande Tiering-Muster weist auf eine kontinuierliche Sedimentation hin. Die beschriebenen Zyklen sind in Kern 7430/10-U-01 von 34-44 m, in Kern 6814/04-U-02 von 40-67 m und in Kern 6307/07-U-02 von 20-36 m enthalten.

Die Typ B oder Redox Zyklen sind durch organisch reiche Schwarzschiefer gekennzeichnet. Die Zyklizität dieser Schwarzschiefer äußert sich zum Teil nur durch geringe Farbänderungen. Stellenweise sind zusätzlich zyklisch eingeschaltete Fe-Karbonat Konkretionen enthalten. Diese zeigen teilweise eine Bündelung von großen Konkretionen zwischen denen bis zu vier kleinere Konkretionen eingeschaltet sind. Kern 7430/10-U-01 weist diese Zyklen im Bereich von 44-57 m, Kern 6814/04-U-02 im Bereich von 9-40, sowie 96-192 m und Kern 6307/07-U-02 im Bereich von 67-85 m auf.

Typ C oder Silt Verdünnungszyklen treten nur an der Basis von Kern 7430/10-U-01 (bis 57 m) und Kern 6307/07-U-02 (bis 85 m) auf. Diese sind durch aufeinanderfolgende kleinmaßstäbliche Silt-Ereignisse gekennzeichnet, welche die organisch reiche Hintergrundsedimentation verdünnen.

Spektralanalysen

Die Daten der Farblogs dienten als Grundlage für das Programm „Speclab“, mit dessen Anwendung die Steuerung der Zyklen geklärt werden sollte. Es konnten für jeden der oben beschrieben Zyklentypen eindeutig eine orbitale Steuerung im Milankovitch-Bereich nachgewiesen werden. Entscheidend für die Interpretation der Diagramme ist die zugrundeliegende Authentizität der Sedimentationsrate. In dieser Studie stimmten die biostratigraphische Sedimentationsrate mit der Sedimentationsrate, die aus der Spektralanalyse berechnet wurde, überein. Zur Interpretation der Spektrogramme wurden nur Signale mit einer Signifikanz von über 0.2 herangezogen.
Die Spektrogramme der verschiedenen Zyklen sind vergleichbar. So zeigen die Typ C Zyklen der Kerne 7430/10-U-01 und 6307/07-U-02 ein Dominanz der Exzentrizität und Präzession. Die Kerne 7430/10-U-01, 6307/07-U-02 und 6814/04-U-02 weisen als gemeinsames Merkmal die Dominanz der Obliquität in den Typ A Zyklen auf. Typ B Zyklen zeigen zwar

deutlich eine orbitale Steuerung, aber keine eindeutig über die Distanz korrelierbaren Dominanzen.

Evolutionäre Zeitreihenanalysen (ESA)

Die ESA verdeutlichen die Veränderung der Stabilität orbitaler Signale mit der Zeit. Dabei ist zu beobachten, dass in den untersuchten Kernen die Signale bis auf wenige Ausnahmen sehr unruhig verlaufen. Typ A Zyklen besitzen die höchste Stabilität der orbitalen Signale. Dies könnte mit dem niedrigenergetischen hemipleagischen Faziesmilieu zusammenhängen. Im Gegensatz dazu zeigen die Typ C Zyklen die geringsten Stabilitäten und sind durch vor-und zurückspringende Wechsel des Hierarchiemusters gekennzeichnet. Stabile Hierarchiemuster können sowohl durch Wechsel in der Sedimentationsrate, als auch im Einbettungsmilieu verhindert werden. Ein Wechsel in der Sedimentationsrate wird durch ein diagonal verlaufendes Signal angezeigt, wie es z. B. für die Präzession in den Typ C Zyklen des Kernes 6307/07-U-02 der Fall ist. Für den Kern 6814/04-U-02 wurden auch geophysikalische Bohrlochdaten für die ESA verwendet, die aufgrund ihrer geringen Auflösung aber maximal die Obliquität darstellen können.

$\delta^{18}O$ Temperaturbestimmungen

Unter Berücksichtigung aller Ergebnisse zur Diagenese wurden nur solche Spezies verwendet, die einen $\delta^{18}O$-Wert von unter –2 % PDB aufwiesen. Weiterhin wurde zur Temperaturbestimmung ein $\delta_{seawater}$ von –1.2 ‰ PDB für eine eisfreie Kreide gewählt. Auf diesen Annahmen basierend wurden die Temperaturen ermittelt. Unter Zuhilfenahme von Temperaturen anderer Autoren; für den borealen Bereich der Unterkreide, wurde für den Spätesten Jura ein Temperaturgradient von 0,18°C/1° nördlicher Breite und für die Früheste Kreide ein Temperaturgradient von 0.08°C/1° nördlicher Breite errechnet. Nach dem Erstellen einer Matrix mit den zusammengefassten Temperaturen und den entsprechenden Zeitabschnitten, dienten die Temperaturgradienten zur Interpolation. Die Interpolation von Temperaturen vervollständigt damit Zeitabschnitte und Kernpositionen für die keine Sauerstoffisotopen zur Paläotemperaturbestimmung vorhanden waren. Dabei ist herauszustellen, dass sich nur mit Hilfe der in dieser Studie ermittelten Temperaturen schon zwei deutlich Paläoklimatrends rekonstruieren lassen. Es handelt sich um einen Temperaturanstieg vom Späten Kimmeridge bis in das Späte Volgium und einen Anstieg vom Berrias zum Barreme. Dazwischen lässt sich ein Schnitt mit deutlichem Temperaturrückgang

erkennen. Mit Hilfe der interpolierten Temperaturen konnten diese Trends weiter verdeutlicht werden. Demnach kommt es zu einem Temperaturanstieg vom Späten Kimmeridge bis zum Späten Volgium, mit einem geringen Rückgang im Mittleren Volgium. Nach einem Temperaturrückgang im Frühen Berrias folgt der Temperaturanstieg vom Berrias zum Barreme, der durch kühlere Phasen im Valangin und im Frühen-, sowie Späten Hauterive unterbrochen wird. Den Berechnungen dieser Studie zufolge könnten die Temperaturen im Frühem Berrias und in geringerem Maße die des Frühen – und Späten Hauterive am Nordpol zu Vereisungen geführt haben. Ein weiterer Hinweis darauf könnte sein, dass Korrelationen von Temperaturen dieser Studie mit Trans- und Regressionen, die durch andere Autoren beschrieben wurden in Einklang gebracht werden können. Die Steuerung des Meeresspiegels kann, neben einer fraglichen Steuerung durch glazio-eustatische Prozesse, auch durch Tektonik, z.B. in Form von erhöhter Subsidenz im Zuge des Rifting hervorgerufen worden sein.

Zyklizität und orbitale Steuerung

Neben den deutlich ausgeprägten Zyklen der Farblogs zeigen auch einige Isotopenkurven ein zyklisches Verhalten. Leider konnten über die Zyklizität und das dazugehörige ozeanographische Szenario aufgrund der zu geringen Auflösung nur Annahmen gemacht werden. Für die beschriebenen Typ A, B und C Zyklen der Farblogs konnten jedoch Faziesmodelle erstellt werden. Dabei wurde zugrunde gelegt, dass die Exzentrizität und die Präzession vor allem Einfuß auf das terrestrische Klima nehmen. Somit erfolgt eine Steuerung des Klimas über Faktoren wie Vegetation, Erosion und Verwitterung und daraus resultierende Variationen im Nährstoff- und Süßwassereintrag in den Grönländisch Norwegischen Seeweg. Die Obliquität, in dieser Studie verstärkt in Warmzeiten auftretend, hingegen kontrolliert das marine System und die damit verbundenen Faktoren wie Strömungen, Produktivität und vor allem die Erhaltung organischen Materials. Kopplungen zwischen den orbitalen Steuerungen sind zum Teil offensichtlich.

Für die Typ C Zyklen wurde ein Modell ermittelt, welches vor allem durch die Nähe zum Land und die Ablagerung überhalb der Strurmwellenbasis charakterisiert ist. Die terrestrische Komponente der Präzession äußert sich hier besonders durch den eingetragen Silt, wie aus den Spektralanalysen zu entnehmen ist. Die Obliquität steuert die Verteilung der dys- und anoxischen Zonen und der daraus resultierenden Erhaltung von organischem Material von bis zu 10 % in Kern 7430/10-U-01.

Typ B Zyklen entstammen dem äußeren, durch eingeschränkte Sedimentation charakterisierten Schelfbereich und wurden unter der Sturmwellenbasis abgelagert. Das verstärkte Signal der Oliquität in Verbindung mit den Fe-Konkretionen, könnte über erhöhte C_{org}-Ablagerungen in diesen Bereichen und einem daraus resultierenden verbesserten Bildungspotential in Übereinstimmung gebracht werden.

Typ A Zyklen werden einem hemipelagischen, deutlich unter der Sturmwellenbasis liegenden Ablagerungsraum zugeordnet, der gut durchlüftet war, wie eine ausgeprägte Bioturbation bezeugt. Der über die Exzentrizität und Präzession gesteuerte Nährstoffeintrag war höchstwahrscheinlich für die Erhöhung der Karbonatproduktion verantwortlich. Die schwache Ausbildung der Obliquität könnte sich in den geringen TOC-Werten von z.B. max. 3 % in Kern 6814/04-U-02 widerspiegeln.

Synthese

Typ B und Typ C Zyklen des Späten Jura stimmen mit einer langen Transgression überein, die vermutlich ein warmes und humides Klima aufweist, wogegen die kondensierte Abfolge der Typ A Zyklen eher für eine rasche Transgression spricht und wahrscheinlich unter eher kaltem und aridem Klima stattfand. Die wesentlichen Unterschiede in der Entwicklung der Zyklen sind dabei die Ausbildung von anoxischen Bedingungen, die Bereitstellung von Nährstoffen, sowie Süßwassereinfluss und das Maß der tektonischen Aktivität in Form von Rifting.

Die Synthese aller vorliegenden Ergebnisse führt zu einem ästuarinen Zirkulationsmodell. Die Beckengeometrien, ein möglicher Süßwassereintrag, sowie die Bildung von Schwarzschiefern deuten auf ein solches Modell hin. Vermutlich verhinderte eine Schwelle im südlichen Bereich des Seeweges den Wasseraustausch zwischen der Grönland Norwegen See und der Tethys. Dadurch käme es zu einem Eintrag von nordwärts strömendem warmen und salinen Tehthyswasser in den Seeweg. Im Gegenzug könnte kaltes und durch Süßwassereintrag beeinflusstes Wasser aus nördlichern Breiten nach Süden geflossen sein. Dies kann auch aus den $\delta^{18}O$ Werten geeigneter Belemniten und Muscheln abgelesen werden. Zwischen beiden Wassermassen käme es dann zur Ausbildung eines Dichte- und Temperaturkontrastes, der in Form einer Pycnokline ausgebildet ist. Dies fördert die Ausbildung anoxischer Zonen, wodurch die Erhaltung organischen Materials ermöglicht wird. Schließlich weisen die, unter

voll durchlüftenden Bedingungen entstandenen, Typ A Zyklen auf einen eher ozeanischen Charakter hin, und sind somit nicht an eine ästuarine Zirkulation gebunden.

List of Figures

List of Tables

Miszellaneen

Erklärung

Ich versichere, daß ich die von mir vorgelegte Dissertation selbständig angefertigt, die benutzten Quellen und Hilfsmittel vollständig angegeben und die Stellen der Arbeit - einschließlich Tabellen, Karten und Abbildungen -, die anderen Werken im Wortlaut oder dem Sinn nach entnommen sind, in jedem Einzelfall als Entlehnung kenntlich gemacht habe; daß diese Dissertation noch keiner anderen Fakultät oder Universität zur Prüfung vorgelegen hat; daß sie - abgesehen von unten angegebenen Teilpublikationen - noch nicht veröffentlicht worden ist sowie, daß ich eine solche Veröffentlichung vor Abschluß des Promotionsverfahrens nicht vornehmen werde. Die Bestimmungen dieser Promotionsordnung sind mir bekannt. Die von mir vorgelegte Dissertation ist von Prof. Dr. W. Ricken betreut worden.

Oliver Swientek

Lebenslauf (Curriculum Vitae)

Persönliche Daten

Name:	Oliver Swientek
Geburtsdatum:	21.06.1970
Nationalität:	Deutsch

Ausbildung

76-91	Grundschule und Gymnasium in Remscheid
06/91-06/92	Grundwehrdienst
10/92	Beginn des Studiums der Geologie an der Universität zu Köln
11/94	Geologie-Vordiplom
06-08/96	Diplom-Kartierung in Nordspanien
01/97-10/97	Diplom-Arbeit am Alfred-Wegner-Institut für Polar- und Meeresforschung in Bremerhaven
3/99	Geologie-Diplom der Universität zu Köln
4/99-4/02	Promotion and der Universität zu Köln The Greenland Norwegian Seaway: climatic and cyclic evolution of Late Jurassic-Early Cretaceous sediments

Appendix

7430/10-U-01
Stable Isotope Data

Depth (m)	Site	$\delta^{13}C$ ‰ PDB	$\delta^{18}O$ ‰ PDB	$\delta^{13}C$ ‰ PDB	$\delta^{18}O$ ‰ PDB	Material	Stratigraphy
33,82	7430/10-U-01	-1,49	-8,62	-1,94	-8,51	*Buchia*	Klippfisk Fm.
33,98	7430/10-U-01	-2,472	-1,656	-3,548	-8,541	belemnite	Klippfisk Fm.
33,98	7430/10-U-01	-1,352	0,254			belemnite	Klippfisk Fm.
33,98	7430/10-U-01	-1,392	0,254			belemnite	Klippfisk Fm.
33,98	7430/10-U-01	-1,48	0,589			belemnite	Klippfisk Fm.
33,98	7430/10-U-01			-3,97	-8,58	bulk	Klippfisk Fm.
34,16	7430/10-U-01	0,01	0,36	-3,02	-5,52	belemnite	Klippfisk Fm.
34,16	7430/10-U-01	0,78	0,5			belemnite	Klippfisk Fm.
34,16	7430/10-U-01	0,63	0,76			belemnite	Klippfisk Fm.
34,16	7430/10-U-01	0,39	0,62			belemnite	Klippfisk Fm.
34,46	7430/10-U-01			-1,10	-3,23	bulk	Klippfisk Fm.
35,46	7430/10-U-01	0,73	0,13	-2,13	-3,79	inocerame	Klippfisk Fm.
35,66	7430/10-U-01	0,05	-0,74	0,33	-0,65	inocerame	Klippfisk Fm.
36,33	7430/10-U-01			-15,49	-3,56	bulk	Klippfisk Fm.
37,04	7430/10-U-01	-12,22	-13,6	-1,38	-1,58	belemnite	Klippfisk Fm.
37,04	7430/10-U-01	-5,72	-5,35			belemnite	Klippfisk Fm.
37,04	7430/10-U-01	-1,42	-0,1			belemnite	Klippfisk Fm.
37,04	7430/10-U-01	-1,05	0,03			belemnite	Klippfisk Fm.
37,64	7430/10-U-01			-1,38	-2,30	bulk	Klippfisk Fm.
38,73	7430/10-U-01			-1,14	-2,38	bulk	Klippfisk Fm.
38,73	7430/10-U-01			-0,77	-2,61	bulk	Klippfisk Fm.
39,55	7430/10-U-01	-1,27	-1,21	-1,43	-1,92	belemnite	Klippfisk Fm.
39,55	7430/10-U-01	-0,31	-0,43			belemnite	Klippfisk Fm.
39,55	7430/10-U-01	-0,09	-0,03			belemnite	Klippfisk Fm.
39,55	7430/10-U-01	-0,08	0,1			belemnite	Klippfisk Fm.
39,55	7430/10-U-01	-0,37	-0,41			belemnite	Klippfisk Fm.
39,55	7430/10-U-01	-0,19	0,17	-1,21	-1,39	belemnite	Klippfisk Fm.
39,55	7430/10-U-01	-0,08	0,01			belemnite	Klippfisk Fm.
39,55	7430/10-U-01	0,25	0,29			belemnite	Klippfisk Fm.
39,55	7430/10-U-01	-0,04	0,11			belemnite	Klippfisk Fm.
39,55	7430/10-U-01	-0,60	-2,71	-2,34	-2,76	inocerame	Klippfisk Fm.
39,74	7430/10-U-01			-7,83	-7,39	bulk	Klippfisk Fm.
40,62	7430/10-U-01	-0,51	-3,84	-2,75	-2,66	inocerame	Klippfisk Fm.
41,17	7430/10-U-01			-3,46	-4,12	bulk	Klippfisk Fm.
42,62	7430/10-U-01	-0,71	-3,36	-8,66	-6,66	inocerame	Klippfisk Fm.
42,66	7430/10-U-01	-1,38	-0,55	-1,78	-4,75	belemnite	Klippfisk Fm.
42,66	7430/10-U-01	0,08	0,74			belemnite	Klippfisk Fm.
42,66	7430/10-U-01	-0,99	0,88			belemnite	Klippfisk Fm.
42,74	7430/10-U-01	-1,30	-4,65	-5,34	-6,46	inocerame	Klippfisk Fm.
43,78	7430/10-U-01	-2,59	-4,65	-7,21	-6,53	inocerame	Hekkingen Fm.
44,34	7430/10-U-01	0,41	-3,82	-7,01	-6,16	inocerame	Hekkingen Fm.
46,05	7430/10-U-01	-2,22	-5,72	-10,42	-6,16	inocerame	Hekkingen Fm.
46,7	7430/10-U-01	-1,98	-1,85	-7,81	-6,85	inocerame	Hekkingen Fm.
47,26	7430/10-U-01			-9,53	-7,58	bulk	Hekkingen Fm.
48,37	7430/10-U-01	-0,08	-3,34	-4,41	-5,85	inocerame	Hekkingen Fm.
50,25	7430/10-U-01	-0,47	-5,11	-8,92	-6,76	inocerame	Hekkingen Fm.
50,6	7430/10-U-01	-4,51	-5,44	-7,91	-5,96	inocerame	Hekkingen Fm.
51,14	7430/10-U-01			-8,32	-7,08	bulk	Hekkingen Fm.
53,59	7430/10-U-01			-11,19	-8,25	bulk	Hekkingen Fm.
54,23	7430/10-U-01	-1,48	-4,22	-9,12	-7,17	inocerame	Hekkingen Fm.
56,05	7430/10-U-01			-7,20	-6,60	bulk	Hekkingen Fm.
62,35	7430/10-U-01			-10,66	-8,76	bulk	Hekkingen Fm.
62,35	7430/10-U-01			-8,62	-7,37	bulk	Hekkingen Fm.
62,4	7430/10-U-01	4,59	-0,46	-11,43	-9,90	inocerame	Hekkingen Fm.
62,75	7430/10-U-01			-11,38	-9,06	bulk	Hekkingen Fm.
67,20	7430/10-U-01			-15,19	-11,13	bulk	Hekkingen Fm.

6814/04-U-02
Stable Isotope Data

Depth (m)	Site	$\delta^{13}C$ ‰ PDB	$\delta^{18}O$ ‰ PDB	$\delta^{13}C$ ‰ PDB	$\delta^{18}O$ ‰ PDB	Material	Stratigraphy
42,04	6814/04-U-02	-5,25	-2,68	-8,07	-2,55	bulk	Klippfisk Fm.
42,18	6814/04-U-02	-0,68	-3,92	-3,73	-5,47	bulk	Klippfisk Fm.
42,26	6814/04-U-02	-0,66	-4,32	-11,87	-1,85	bulk	Klippfisk Fm.
43,17	6814/04-U-02	1,03	-6,32	-1,22	-5,28	bulk	Klippfisk Fm.
44,27	6814/04-U-02	1,47	-4,88	-4,25	-3,98	*Buchia*	Klippfisk Fm.
44,65	6814/04-U-02	-5,81	-6,27	-12,13	-6,44	*Buchia*	Klippfisk Fm.
45,84	6814/04-U-02	0,93	-5,96	-2,66	-4,35	bulk	Klippfisk Fm.
47,55	6814/04-U-02	0,91	-4,73	-2,85	-4,38	bulk	Klippfisk Fm.
50,34	6814/04-U-02	-1,32	-3,11	-7,03	-6,24	bulk	Klippfisk Fm.
50,93	6814/04-U-02	-0,68	-3,36	-11,01	-5,85	bulk	Klippfisk Fm.
53,1	6814/04-U-02	-2,67	-5,61	-4,01	-6,14	bulk	Klippfisk Fm.
55,05	6814/04-U-02	0,80	-3,26	-4,71	-5,34	*Buchia*	Klippfisk Fm.
55,6	6814/04-U-02	-0,14	-5,52	-4,66	-5,95	bulk	Klippfisk Fm.
56,03	6814/04-U-02	1,44	-4,51	-3,03	-5,70	inocerame	Klippfisk Fm.
60,71	6814/04-U-02	-0,17	-1,19	-5,16	-4,59	bulk	Klippfisk Fm.
62	6814/04-U-02			-9,6	-4,99	bulk	Klippfisk Fm.
62,05	6814/04-U-02	1,60	-2,65			*Buchia*	Klippfisk Fm.
62,06	6814/04-U-02			-5,37	-3,87	bulk	Klippfisk Fm.
62,12	6814/04-U-02			-7,66	-4,08	bulk	Klippfisk Fm.
62,18	6814/04-U-02			-5,51	-4,78	bulk	Klippfisk Fm.
62,28	6814/04-U-02			-12,77	-4,05	bulk	Klippfisk Fm.
62,34	6814/04-U-02			-4,41	-4,2	bulk	Klippfisk Fm.
62,42	6814/04-U-02			-5,08	-3,71	bulk	Klippfisk Fm.
62,48	6814/04-U-02			-5,07	-4,31	bulk	Klippfisk Fm.
62,54	6814/04-U-02			-4,34	-4,66	bulk	Klippfisk Fm.
62,7	6814/04-U-02			-5,25	-4,42	bulk	Klippfisk Fm.
62,74	6814/04-U-02			-3,73	-4,39	bulk	Klippfisk Fm.
62,83	6814/04-U-02			-6,73	-4,05	bulk	Klippfisk Fm.
62,9	6814/04-U-02			-4,44	-4,83	bulk	Klippfisk Fm.
62,96	6814/04-U-02	2,00	-3,64	-3,76	-5,28	bulk	Klippfisk Fm.
63,02	6814/04-U-02			-9,25	-4,13	bulk	Klippfisk Fm.
63,87	6814/04-U-02	0,93	-2,90	-5,21	-5,07	bulk	Klippfisk Fm.
64,14	6814/04-U-02	-3,04	-5,75	-10,43	-4,02	inocerame	Klippfisk Fm.
65,21	6814/04-U-02	0,24	-2,81	-7,00	-5,13	bulk	Klippfisk Fm.
65,28	6814/04-U-02	0,57	-6,40	-4,55	-6	inocerame	Klippfisk Fm.
65,72	6814/04-U-02	-0,82	-4,95	-4,09	-5,57	bulk	Klippfisk Fm.
65,81	6814/04-U-02	1,58	-4,18	-2,89	-5,51	inocerame	Klippfisk Fm.
65,92	6814/04-U-02	-2,58	-5,73	-2,89	-4,73	*Buchia*	Klippfisk Fm.
66,34	6814/04-U-02	0,43	-3,16	-5,02	-2,89	bulk	Klippfisk Fm.
70,11	6814/04-U-02	1,42	-5,53	-9,08	-6,10	inocerame	Hekkingen Fm.
70,76	6814/04-U-02	0,14	-4,53	-3,51	-5,52	*Buchia*	Hekkingen Fm.
70,81	6814/04-U-02	1,07	-4,72			*Buchia*	Hekkingen Fm.
71,46	6814/04-U-02	1,78	-3,87			*Buchia*	Hekkingen Fm.
71,8	6814/04-U-02	1,84	-4,44	-4,64	-5,95	inocerame	Hekkingen Fm.
72,53	6814/04-U-02	-0,99	-2,99	-6,54	-6,07	inocerame	Hekkingen Fm.
73,11	6814/04-U-02	0,26	-3,53	-5,68	-6,40	inocerame	Hekkingen Fm.
74,01	6814/04-U-02	1,84	-4,23	-6,36	-6,25	*Buchia*	Hekkingen Fm.
74,28	6814/04-U-02	1,25	-4,07	-6,24	-6,18	inocerame	Hekkingen Fm.
75,41	6814/04-U-02	0,71	-4,26			inocerame	Hekkingen Fm.
75,65	6814/04-U-02	0,15	-5,28	-5,79	-6,05	inocerame	Hekkingen Fm.
75,81	6814/04-U-02	1,61	-4,09	-7,53	-6,42	inocerame	Hekkingen Fm.
75,9	6814/04-U-02	-0,63	-5,71	-8,71	-6,40	*Buchia*	Hekkingen Fm.
75,95	6814/04-U-02	0,16	-4,41	-5,76	-6,11	inocerame	Hekkingen Fm.
76,01	6814/04-U-02	-2,27	-4,33	-5,53	-5,45	*Buchia*	Hekkingen Fm.
79,12	6814/04-U-02	1,14	-3,35	-8,95	-6,73	inocerame	Hekkingen Fm.

6814/04-U-02
Stable Isotope Data

Depth (m)	Site	δ^{13C} ‰ PDB	$\delta^{18}O$ ‰ PDB	δ^{13C} ‰ PDB	$\delta^{18}O$ ‰ PDB	Material	Stratigraphy
82,88	6814/04-U-02	-1,39	-4,40	-1,66	-5,02	inocerame	Hekkingen Fm.
83,13	6814/04-U-02	0,72	-5,29	-6,97	-6,31	inocerame	Hekkingen Fm.
83,26	6814/04-U-02	-2,30	-5,12	-5,99	-6,14	inocerame	Hekkingen Fm.
83,38	6814/04-U-02	1,35	-3,28	-5,56	-5,74	inocerame	Hekkingen Fm.
83,48	6814/04-U-02	-0,88	-4,25	-9,87	-7,81	inocerame	Hekkingen Fm.
83,48	6814/04-U-02	0,50	-4,57	-7,90	-6,97	inocerame	Hekkingen Fm.
83,73	6814/04-U-02	0,06	-4,72	-2,99	-5,45	inocerame	Hekkingen Fm.
84,06	6814/04-U-02	-1,10	-5,55	-1,73	-4,97	inocerame	Hekkingen Fm.
84,06	6814/04-U-02	-1,08	-5,62			inocerame	Hekkingen Fm.
84,06	6814/04-U-02	-1,12	-5,61			inocerame	Hekkingen Fm.
84,23	6814/04-U-02	1,23	-3,94			inocerame	Hekkingen Fm.
84,23	6814/04-U-02	2,55	-5,66	-4,51	-6,25	inocerame	Hekkingen Fm.
84,53	6814/04-U-02	0,31	-4,53	-5,37	-5,94	inocerame	Hekkingen Fm.
84,55	6814/04-U-02	1,21	-4,17			inocerame	Hekkingen Fm.
84,64	6814/04-U-02	-0,60	-2,75	-4,96	-5,31	inocerame	Hekkingen Fm.
84,71	6814/04-U-02	2,16	-3,20	-2,51	-5,11	inocerame	Hekkingen Fm.
84,92	6814/04-U-02	0,28	-4,33	-6,02	-6,21	inocerame	Hekkingen Fm.
84,92	6814/04-U-02	-1,58	-3,95	-6,30	-6,25	inocerame	Hekkingen Fm.
84,98	6814/04-U-02	1,96	-4,22	-6,03	-6,53	inocerame	Hekkingen Fm.
85,18	6814/04-U-02	-1,45	-5,92	-7,47	-6,55	inocerame	Hekkingen Fm.
85,36	6814/04-U-02	-2,50	-4,20	-9,07	-8,45	inocerame	Hekkingen Fm.
85,58	6814/04-U-02	0,59	-5,13	-7,33	-6,55	inocerame	Hekkingen Fm.
86,49	6814/04-U-02	-1,05	-4,10	-1,15	-5,74	inocerame	Hekkingen Fm.
86,52	6814/04-U-02	1,64	-4,30	-8,06	-6,75	inocerame	Hekkingen Fm.
86,73	6814/04-U-02	-0,98	-4,37	-9,69	-7,14	inocerame	Hekkingen Fm.
86,85	6814/04-U-02	-0,68	-4,78	-10,16	-8,23	inocerame	Hekkingen Fm.
87,01	6814/04-U-02	0,97	-3,03	-4,50	-8,18	inocerame	Hekkingen Fm.
87,23	6814/04-U-02	-1,35	-6,14	-6,13	-6,33	inocerame	Hekkingen Fm.
87,55	6814/04-U-02	1,95	-4,32	-5,38	-6,44	inocerame	Hekkingen Fm.
87,62	6814/04-U-02	-0,64	-3,55	-3,95	-5,44	inocerame	Hekkingen Fm.
87,77	6814/04-U-02	2,34	-3,65	-6,45	-6,34	inocerame	Hekkingen Fm.
87,91	6814/04-U-02	0,08	-4,34	-4,23	-7,81	inocerame	Hekkingen Fm.
87,96	6814/04-U-02	-1,39	-4,87	-6,21	-6,49	inocerame	Hekkingen Fm.
87,96	6814/04-U-02	-0,48	-3,87			inocerame	Hekkingen Fm.
88,42	6814/04-U-02	2,81	-5,17			inocerame	Hekkingen Fm.
88,65	6814/04-U-02	0,47	-5,47	-2,24	-5,70	inocerame	Hekkingen Fm.
88,73	6814/04-U-02	-0,43	-4,71			inocerame	Hekkingen Fm.
88,9	6814/04-U-02	-0,09	-4,01	-5,59	-5,43	inocerame	Hekkingen Fm.
89,26	6814/04-U-02	-2,94	-4,77	-5,40	-5,40	inocerame	Hekkingen Fm.
89,42	6814/04-U-02	0,43	-4,17			inocerame	Hekkingen Fm.
89,52	6814/04-U-02	0,91	-4,42			inocerame	Hekkingen Fm.
89,63	6814/04-U-02	1,30	-4,74	-0,24	-5,45	inocerame	Hekkingen Fm.
89,84	6814/04-U-02	0,51	-4,29	-8,98	-6,89	inocerame	Hekkingen Fm.
89,9	6814/04-U-02	-2,61	-4,17			inocerame	Hekkingen Fm.
90,02	6814/04-U-02	3,02	-4,15			inocerame?	Hekkingen Fm.
90,15	6814/04-U-02	-1,88	-5,52			inocerame	Hekkingen Fm.
90,3	6814/04-U-02	-1,26	-4,02			inocerame	Hekkingen Fm.
90,4	6814/04-U-02	0,77	-4,77	-6,65	-5,85	inocerame	Hekkingen Fm.
90,84	6814/04-U-02	-0,43	-3,72	-4,07	-4,54	inocerame	Hekkingen Fm.
90,86	6814/04-U-02	0,96	-5,07	-0,54	-5,40	inocerame	Hekkingen Fm.
91,73	6814/04-U-02	2,16	-6,29	-8,32	-12,76	inocerame?	Hekkingen Fm.
95,03	6814/04-U-02	1,388	-2,306	-5,848	-5,452	belemnite	Hekkingen Fm.
95,03	6814/04-U-02	1,578	-2,816			belemnite	Hekkingen Fm.
95,03	6814/04-U-02	0,688	-2,996			belemnite	Hekkingen Fm.
95,03	6814/04-U-02			-5,848	-5,452	bulk	Hekkingen Fm.

6814/04-U-02
Stable Isotope Data

Depth (m)	Site	δ^{13C} ‰ PDB	$\delta^{18}O$ ‰ PDB	δ^{13C} ‰ PDB	$\delta^{18}O$ ‰ PDB	Material	Stratigraphy
95,26	6814/04-U-02	1,412	-2,621	-10,63	-8,341	belemnite	Hekkingen Fm.
95,26	6814/04-U-02	0,228	-3,126			belemnite	Hekkingen Fm.
95,26	6814/04-U-02	-0,172	-2,756			belemnite	Hekkingen Fm.
95,26	6814/04-U-02	0,638	-3,136			belemnite	Hekkingen Fm.
95,26	6814/04-U-02	0,598	-3,186			belemnite	Hekkingen Fm.
95,26	6814/04-U-02			-10,67	-8,41	bulk	Hekkingen Fm.
95,9	6814/04-U-02	-2,04	-4,59	-3,69	-5,37	inocerame	Hekkingen Fm.
96,11	6814/04-U-02	0,37	-3,15	-3,57	-5,55	inocerame	Hekkingen Fm.
96,58	6814/04-U-02	2,03	-5,12			*Buchia*	Hekkingen Fm.
96,95	6814/04-U-02	2,96	-2,02			*Buchia*	Hekkingen Fm.
96,99	6814/04-U-02	2,94	-2,75	-0,67	-4,85	inocerame	Hekkingen Fm.
97,15	6814/04-U-02	0,40	-4,79			inocerame	Hekkingen Fm.
97,48	6814/04-U-02	0,858	-1,426	-4,728	-6,282	belemnite	Hekkingen Fm.
97,48	6814/04-U-02	0,358	-1,446			belemnite	Hekkingen Fm.
97,48	6814/04-U-02	0,178	-0,796			belemnite	Hekkingen Fm.
97,48	6814/04-U-02	0,978	-1,406			belemnite	Hekkingen Fm.
97,48	6814/04-U-02			-6,77	-7,07	bulk	Hekkingen Fm.
97,73	6814/04-U-02	0,90	-3,77	-1,13	-4,95	inocerame	Hekkingen Fm.
98,29	6814/04-U-02	2,08	-4,11	-7,34	-5,77	inocerame	Hekkingen Fm.
101,24	6814/04-U-02	1,27	-3,02	-6,44	-6,54	*Buchia*	Hekkingen Fm.
101,5	6814/04-U-02	2,57	-3,67	-4,62	-5,36	inocerame	Hekkingen Fm.
101,83	6814/04-U-02	1,82	-4,33	-10,54	-7,69	inocerame	Hekkingen Fm.
102,05	6814/04-U-02	0,50	-2,45			inocerame	Hekkingen Fm.
102,45	6814/04-U-02			-4,89	-5,06	inocerame	Hekkingen Fm.
103,63	6814/04-U-02	2,39	-2,44	-6,70	-6,04	inocerame	Hekkingen Fm.
104,27	6814/04-U-02	2,53	-1,99	-11,38	-7,89	inocerame	Hekkingen Fm.
104,56	6814/04-U-02	2,65	-2,77	-12,59	-8,56	*Buchia*	Hekkingen Fm.
106,24	6814/04-U-02	2,29	-4,04	-8,99	-6,75	inocerame	Hekkingen Fm.
108,38	6814/04-U-02	-14,45	-6,25	-11,29	-7,80	inocerame	Hekkingen Fm.
108,81	6814/04-U-02	2,40	-3,12	-11,82	-8,08	inocerame	Hekkingen Fm.
109,71	6814/04-U-02	2,53	-2,68	-8,65	-6,57	*Buchia*	Hekkingen Fm.
110,23	6814/04-U-02	2,43	-3,74	-5,31	-4,96	*Buchia*	Hekkingen Fm.
110,93	6814/04-U-02	0,54	-2,12	-6,35	-6,71	inocerame	Hekkingen Fm.
111,56	6814/04-U-02	3,29	-3,02	-10,72	-6,69	inocerame	Hekkingen Fm.
112,4	6814/04-U-02	2,48	-2,93	-10,44	-7,26	*Buchia*	Hekkingen Fm.
112,71	6814/04-U-02	2,47	-2,50	-6,78	-6,62	inocerame	Hekkingen Fm.
113,86	6814/04-U-02	3,07	-3,82			inocerame	Hekkingen Fm.
114,6	6814/04-U-02	0,79	-1,94	-5,51	-4,66	inocerame	Hekkingen Fm.
114,6	6814/04-U-02	0,89	-1,95			inocerame	Hekkingen Fm.
114,6	6814/04-U-02	1,03	-1,87			inocerame	Hekkingen Fm.
114,79	6814/04-U-02	0,55	-4,92	-7,60	-6,06	*Buchia*	Hekkingen Fm.
116,83	6814/04-U-02	3,12	-4,03	-7,87	-4,74	inocerame	Hekkingen Fm.
118,27	6814/04-U-02	1,93	-1,91			*Buchia*	Hekkingen Fm.
119,86	6814/04-U-02	1,07	-2,83			*Buchia*	Hekkingen Fm.
120,01	6814/04-U-02	0,96	-3,40	-6,44	-6,54	inocerame	Hekkingen Fm.
121,31	6814/04-U-02	1,80	-2,12	-11,24	-7,97	bulk	Hekkingen Fm.
121,91	6814/04-U-02	3,99	-5,43	-6,19	-5,97	inocerame	Hekkingen Fm.
122,78	6814/04-U-02	3,08	-1,54	-5,91	-5,22	inocerame	Hekkingen Fm.
122,94	6814/04-U-02	2,06	-3,59			*Buchia*	Hekkingen Fm.
123,81	6814/04-U-02	1,57	-3,35	-8,12	-7,07	inocerame	Hekkingen Fm.
124,5	6814/04-U-02	1,25	-3,04	-10,61	-7,70	inocerame	Hekkingen Fm.
125,06	6814/04-U-02	1,01	-4,18	-3,68	-3,23	inocerame	Hekkingen Fm.
125,72	6814/04-U-02	1,82	-2,02	-3,98	-4,00	inocerame	Hekkingen Fm.
126,54	6814/04-U-02	3,14	-4,40			*Buchia*	Hekkingen Fm.
126,64	6814/04-U-02	2,97	-4,30	-6,98	-5,90	inocerame	Hekkingen Fm.

6814/04-U-02
Stable Isotope Data

Depth (m)	Site	δ^{13C} ‰ PDB	$\delta^{18}O$ ‰ PDB	δ^{13C} ‰ PDB	$\delta^{18}O$ ‰ PDB	Material	Stratigraphy
127,62	6814/04-U-02	2,81	-2,20	-4,91	-4,85	inocerame	Hekkingen Fm.
128,92	6814/04-U-02	2,60	-2,33	-4,66	-2,93	inocerame	Hekkingen Fm.
130,54	6814/04-U-02	1,06	-3,09	-1,73	-2,74	inocerame	Hekkingen Fm.
131,21	6814/04-U-02	1,88	-2,65	-7,18	-5,85	bulk	Hekkingen Fm.
133,82	6814/04-U-02	4,01	-3,48	-4,46	-3,99	inocerame	Hekkingen Fm.
136,32	6814/04-U-02	1,93	-3,36	-5,73	-6,16	inocerame	Hekkingen Fm.
136,74	6814/04-U-02	2,35	-3,58	-2,69	-4,52	inocerame	Hekkingen Fm.
137,53	6814/04-U-02	-0,27	-3,74	-4,19	-3,77	inocerame	Hekkingen Fm.
138,28	6814/04-U-02			-0,33	-3,79	inocerame	Hekkingen Fm.
140,09	6814/04-U-02	0,76	-0,91	-2,86	-2,73	inocerame	Hekkingen Fm.
144,69	6814/04-U-02	1,93	-0,27	-3,60	-3,15	inocerame	Hekkingen Fm.
149,27	6814/04-U-02	0,53	-3,51	-0,64	-1,68	inocerame	Hekkingen Fm.
152,36	6814/04-U-02	2,49	-2,11	-2,71	-3,43	inocerame	Hekkingen Fm.
152,73	6814/04-U-02	1,53	-2,01	-2,78	-3,75	inocerame	Hekkingen Fm.
153	6814/04-U-02	-1,74	-3,73	-1,88	-2,82	inocerame	Hekkingen Fm.
153,1	6814/04-U-02	3,58	-3,20	-2,88	-3,16	inocerame	Hekkingen Fm.
154	6814/04-U-02	1,51	-3,57	-8,97	-6,44	inocerame	Hekkingen Fm.
155,07	6814/04-U-02	3,24	-1,92			*Buchia*	Hekkingen Fm.
156,2	6814/04-U-02	3,49	-2,54			bulk	Hekkingen Fm.
156,8	6814/04-U-02	2,98	-3,15	-1,79	-3,42	inocerame	Hekkingen Fm.
156,91	6814/04-U-02	3,60	-1,88	-9,82	-7,7	*Buchia*	Hekkingen Fm.
157,15	6814/04-U-02	2,01	-3,02			bulk	Hekkingen Fm.
157,36	6814/04-U-02	-0,23	-3,53	-2,60	-3,27	inocerame	Hekkingen Fm.
159,36	6814/04-U-02	3,40	-2,76	-2,73	-4,63	inocerame	Hekkingen Fm.
160,62	6814/04-U-02	2,32	-3,07			*Buchia*	Hekkingen Fm.
161,19	6814/04-U-02	2,66	-1,58	0,08	-3,42	inocerame	Hekkingen Fm.
161,42	6814/04-U-02	3,19	-1,41			*Buchia*	Hekkingen Fm.
162,32	6814/04-U-02	2,76	-3,45			*Buchia*	Hekkingen Fm.
162,66	6814/04-U-02	2,14	-4,01	-1,84	-8,67	*Buchia*	Hekkingen Fm.
163,76	6814/04-U-02	1,13	-3,30	-6,15	-9,4	*Buchia*	Hekkingen Fm.
164,23	6814/04-U-02	-1,06	-5,13	-10,69	-6,85	inocerame	Hekkingen Fm.
164,73	6814/04-U-02	3,41	-2,57			*Buchia*	Hekkingen Fm.
164,73	6814/04-U-02	2,06	-3,29			*Buchia*	Hekkingen Fm.
165,51	6814/04-U-02	1,55	-3,56	-6,93	-7,29	inocerame	Hekkingen Fm.
166,32	6814/04-U-02	2,48	-2,77	1,86	-1,74	inocerame	Hekkingen Fm.
166,62	6814/04-U-02	3,12	-4,09	-4,28	-6,09	Buchia	Hekkingen Fm.
168,73	6814/04-U-02	1,79	-4,21	-0,43	-5,00	inocerame	Hekkingen Fm.

6307/07-U-02
Stable Isotope Data

Depth (m)	Site	$\delta^{13}C$ ‰ PDB	$\delta^{18}O$ ‰ PDB	$\delta^{13}C$ ‰ PDB	$\delta^{18}O$ ‰ PDB	Material	Startigraphy
15,93	6307/07-U-02	1,28	-5,25	-0,94	-2,74	inocerame	Lange Fm.
17,55	6307/07-U-02	0,63	-2,86	-0,49	-1,75	inocerame	Lange Fm.
18,00	6307/07-U-02	0,82	-4,48	-0,60	-2,10	inocerame	Lange Fm.
18,79	6307/07-U-02	0,55	-3,04	-1,04	-2,27	inocerame	Lange Fm.
19,00	6307/07-U-02	-0,16	-4,06	-0,55	-1,97	inocerame	Lange Fm.
19,63	6307/07-U-02	0,84	-4,68	-1,06	-2,55	inocerame	Lange Fm.
20,17	6307/07-U-02			-0,89	-2,46	bulk	Lange Fm.
20,46	6307/07-U-02	-0,27	-4,48	-1,72	-3,87	inocerame	Lange Fm.
21,11	6307/07-U-02	-0,67	-3,54	-1,09	-2,47	inocerame	Lange Fm.
21,76	6307/07-U-02	0,74	-2,98	-1,05	-1,80	inocerame	Lange Fm.
21,85	6307/07-U-02			-2,02	-4,94	bulk	Lange Fm.
22,71	6307/07-U-02	0,16	-1,98	-1,43	-2,22	inocerame	Lange Fm.
22,79	6307/07-U-02			-1,76	-2,37	bulk	Lange Fm.
22,84	6307/07-U-02	0,17	-4,02	-1,52	-2,30	inocerame	Lange Fm.
22,84	6307/07-U-02	-0,37	-2,47	-2,01	-2,64	inocerame	Lange Fm.
23,50	6307/07-U-02	0,73	-2,21	-1,54	-1,99	inocerame	Lange Fm.
23,75	6307/07-U-02	-3,748	-0,072			belemnite	Lange Fm.
23,75	6307/07-U-02	-2,43	0,079			belemnite	Lange Fm.
23,75	6307/07-U-02	-0,28	-3,52	-2,23	-2,49	*Buchia*	Lange Fm.
23,96	6307/07-U-02			-2,23	-3,34	inocerame	Lange Fm.
24,03	6307/07-U-02	-1,24	-3,13	-2,77	-3,00	inocerame	Lange Fm.
25	6307/07-U-02			-0,42	-2,14	bulk	Lange Fm.
25,08	6307/07-U-02			-0,52	-1,74	bulk	Lange Fm.
25,14	6307/07-U-02			-1,65	-4	bulk	Lange Fm.
25,2	6307/07-U-02			-2	-2,72	bulk	Lange Fm.
25,3	6307/07-U-02			-2,73	-3,74	bulk	Lange Fm.
25,38	6307/07-U-02			-2,11	-3,05	bulk	Lange Fm.
25,45	6307/07-U-02			-1,32	-2,58	bulk	Lange Fm.
25,54	6307/07-U-02			-10,86	-1,23	bulk	Lange Fm.
25,63	6307/07-U-02			-2,25	-5,02	bulk	Lange Fm.
25,68	6307/07-U-02			-9,45	-1,59	bulk	Lange Fm.
25,73	6307/07-U-02			-5,99	-2,99	bulk	Lange Fm.
25,78	6307/07-U-02			-5,52	-4,06	bulk	Lange Fm.
25,85	6307/07-U-02			-2,88	-4,88	bulk	Lange Fm.
25,89	6307/07-U-02			-2,94	-5,27	bulk	Lange Fm.
26,47	6307/07-U-02	-0,08	-6,60	0,10	-3,63	inocerame	Lange Fm.
26,57	6307/07-U-02	1,36	-3,34			inocerame	Lange Fm.
26,65	6307/07-U-02			-1,08	-3,94	bulk	Lange Fm.
27,18	6307/07-U-02	0,27	-4,85			inocerame	Lange Fm.
27,20	6307/07-U-02	0,14	-4,14	-0,08	-3,68	inocerame	Lange Fm.
27,20	6307/07-U-02			-0,34	-3,96	bulk	Lange Fm.
27,26	6307/07-U-02	0,50	-5,01	-3,21	-3,88	inocerame	Lange Fm.
27,26	6307/07-U-02			-4,74	-4,47	bulk	Lange Fm.
27,93	6307/07-U-02			1,21	-3,00	bulk	Lange Fm.
28,93	6307/07-U-02	-2,85	-4,80	-3,17	-5,63	inocerame	Lange Fm.
28,93	6307/07-U-02			-3,21	-5,60	bulk	Lange Fm.
29,96	6307/07-U-02	-2,04	-3,45	-2,26	-4,01	*Buchia*	Lange Fm.
30,38	6307/07-U-02	-1,35	-5,44	-2,37	-5,52	inocerame	Lange Fm.
30,38	6307/07-U-02			-2,64	-5,87	bulk	Lange Fm.
31,32	6307/07-U-02			-2,75	-6,12	bulk	Lange Fm.
31,43	6307/07-U-02			-3,51	-6,97	bulk	Lange Fm.
31,57	6307/07-U-02			-2,00	-5,22	bulk	Lange Fm.
31,72	6307/07-U-02			-3,35	-6,53	bulk	Lange Fm.
31,88	6307/07-U-02			-2,22	-5,48	bulk	Lange Fm.
35,66	6307/07-U-02			-0,32	-0,65	bulk	Lange Fm.

6307/07-U-02
Stable Isotope Data

Depth (m)	Site	δ^{13C} ‰ PDB	$\delta^{18}O$ ‰ PDB	δ^{13C} ‰ PDB	$\delta^{18}O$ ‰ PDB	Material	Startigraphy
42,22	6307/07-U-02			-3,47	-7,72	bulk	Spekk Fm.
45,63	6307/07-U-02	3,42	0,94	-0,18	-1,45	inocerame	Spekk Fm.
47,31	6307/07-U-02			-10,49	-12,50	bulk	Spekk Fm.
51,67	6307/07-U-02	-7,60	-10,74	-9,15	-12,14	inocerame	Spekk Fm.
51,71	6307/07-U-02			-10,43	-13,10	bulk	Spekk Fm.
53,60	6307/07-U-02			-7,58	-11,51	bulk	Spekk Fm.
59,16	6307/07-U-02			-10,33	-12,26	bulk	Spekk Fm.
61,06	6307/07-U-02			-13,75	-20,42	bulk	Spekk Fm.
64,70	6307/07-U-02			-9,27	-13,45	bulk	Spekk Fm.
69,54	6307/07-U-02			-14,48	-14,82	bulk	Spekk Fm.
73,24	6307/07-U-02			-1,73	-7,67	bulk	Spekk Fm.
75,10	6307/07-U-02			0,20	-6,97	bulk	Spekk Fm.
77,57	6307/07-U-02			0,29	-7,28	bulk	Spekk Fm.
77,77	6307/07-U-02			0,99	-6,70	bulk	Spekk Fm.
77,84	6307/07-U-02			1,29	-6,86	bulk	Spekk Fm.
79,21	6307/07-U-02			1,88	-6,57	bulk	Spekk Fm.
80,87	6307/07-U-02			-17,78	-14,37	bulk	Spekk Fm.
94,34	6307/07-U-02			-11,28	-21,34	bulk	Spekk Fm.
103,91	6307/07-U-02			0,45	-6,90	bulk	Spekk Fm.
106,46	6307/07-U-02			-1,97	-7,94	bulk	Rogn Fm.

13/1-U-2
Stable Isotope Data

Depth (m)	Site	$\delta^{13}C$ ‰ PDB (belemnite)	$\delta^{18}O$ ‰ PDB (belemnite)	$\delta^{13}C$ ‰ PDB (bulk)	$\delta^{18}O$ ‰ PDB (bulk)	Stratigraphy
141,7	13/1-U-2	-0,98	-1,02	0,10	-0,47	Bream Fm.
142	13/1-U-2	-0,01	-1,12			Bream Fm.
142	13/1-U-2	0,61	-1,18			Bream Fm.
142	13/1-U-2	0,47	-1,35			Bream Fm.
142	13/1-U-2	0,39	-1,22			Bream Fm.
142	13/1-U-2	-0,55	-1,43			Bream Fm.
142,2	13/1-U-2			-0,02	-1,09	Bream Fm.
142,48	13/1-U-2			-0,14	-1,02	Bream Fm.
145	13/1-U-2	0,68	-1,29	-0,11	-1,42	Bream Fm.
145,03	13/1-U-2	0,77	-0,89	-0,09	-0,88	Bream Fm.
145,05	13/1-U-2	1,3	-0,95	0,01	-0,66	Bream Fm.
145,05	13/1-U-2	1,39	-1,2			Bream Fm.
145,05	13/1-U-2	1,29	-1,11			Bream Fm.
145,1	13/1-U-2	1,06	-1,25	-0,06	-0,69	Bream Fm.
145,12	13/1-U-2	-1,72	-2,29	0,12	-0,53	Bream Fm.
145,2	13/1-U-2	0,8	-1,23	0,12	-0,45	Bream Fm.
145,28	13/1-U-2	-0,77	-1,28	0,02	-0,50	Bream Fm.
145,28	13/1-U-2	-0,54	-1,16			Bream Fm.
145,28	13/1-U-2	0,9	-1,07			Bream Fm.
145,28	13/1-U-2	1,04	-1,19			Bream Fm.
145,33	13/1-U-2	0,09	-0,92	0,1	-0,8	Bream Fm.
145,33	13/1-U-2	0,88	-1,36			Bream Fm.
145,33	13/1-U-2	1,44	-0,88			Bream Fm.
145,33	13/1-U-2	0,27	-1,02			Bream Fm.
145,38	13/1-U-2	0,9	-1,2			Bream Fm.
145,38	13/1-U-2	0,99	-1,16			Bream Fm.
145,38	13/1-U-2	0,54	-1,18			Bream Fm.
145,38	13/1-U-2	0,97	-1,13			Bream Fm.
145,46	13/1-U-2	-0,19	-1,01	0,03	-0,71	Bream Fm.
145,46	13/1-U-2	0,69	-1,23			Bream Fm.
145,6	13/1-U-2			-0,24	-0,41	Bream Fm.
150,18	13/1-U-2	-0,01	-0,73	-6,18	-5,98	Bream Fm.
150,18	13/1-U-2	0,59	-0,76			Bream Fm.
150,18	13/1-U-2	0,3	-0,72			Bream Fm.
150,18	13/1-U-2	0,04	-0,84			Bream Fm.
150,22	13/1-U-2	-0,01	-1,4	-5,95	-5,37	Bream Fm.
150,22	13/1-U-2	0,25	-0,79			Bream Fm.
150,22	13/1-U-2	-0,38	-0,69			Bream Fm.
150,31	13/1-U-2	-0,53	-1,87	-6,64	-5,89	Bream Fm.
150,34	13/1-U-2	-0,98	-1,42	-3,03	-3,30	Bream Fm.
150,34	13/1-U-2	0,23	-1,45			Bream Fm.
150,65	13/1-U-2	0,43	-1,61	-0,55	-1,23	Bream Fm.
150,65	13/1-U-2	0,59	-1,74			Bream Fm.
150,65	13/1-U-2	0,04	-1,48			Bream Fm.
150,65	13/1-U-2	-0,84	-1,74			Bream Fm.
150,68	13/1-U-2	0,38	-0,74	-3,89	-4,71	Bream Fm.
150,77	13/1-U-2	0,73	-0,92	-0,63	-1,36	Bream Fm.
150,77	13/1-U-2	0,54	-1,35			Bream Fm.
150,92	13/1-U-2	-1,02	-2,49	-0,53	-1,13	Bream Fm.
151,06	13/1-U-2	0,47	-1,67	-0,87	-2,19	Bream Fm.
151,06	13/1-U-2	0,8	-1,97			Bream Fm.
151,06	13/1-U-2	0,35	-1,9			Bream Fm.
151,06	13/1-U-2	0,51	-1,74			Bream Fm.
151,06	13/1-U-2	0,11	-1,97			Bream Fm.

13/1-U-2
Stable Isotope Data

Depth (m)	Site	δ^{13C} ‰ PDB	$\delta^{18}O$ ‰ PDB	δ^{13C} ‰ PDB	$\delta^{18}O$ ‰ PDB	Stratigraphy
		(belemnite)	(belemnite)	(bulk)	(bulk)	Bream Fm.
151,06	13/1-U-2	0,76	-1,71			Bream Fm.
151,09	13/1-U-2	-0,18	-1,25			Bream Fm.
151,09	13/1-U-2	-0,27	-0,54			Bream Fm.
151,12	13/1-U-2	0,43	-0,65			Bream Fm.
151,12	13/1-U-2	0,85	-0,81	-3,97	-5,20	Bream Fm.
151,13	13/1-U-2	0,54	-0,74			Bream Fm.
151,13	13/1-U-2	0,57	-0,26			Bream Fm.
151,32	13/1-U-2	-0,43	-0,83	-1,07	-2,19	Bream Fm.
151,32	13/1-U-2	-0,07	-0,28			Bream Fm.
151,32	13/1-U-2	0,11	-0,04			Bream Fm.
151,4	13/1-U-2	0,42	-1,25	-1,06	-1,58	Bream Fm.
151,49	13/1-U-2			-1,47	-2,44	Bream Fm.
151,51	13/1-U-2	0,57	-0,91	-0,83	-1,25	Bream Fm.
151,54	13/1-U-2	0,52	-1,68	-0,44	-0,88	Bream Fm.
151,66	13/1-U-2	0,43	-1,03	-0,76	-1,11	Bream Fm.
151,72	13/1-U-2	0,58	-0,94	-0,40	-0,84	Bream Fm.
151,72	13/1-U-2	0,17	-1,18			Bream Fm.
151,92	13/1-U-2			-0,14	-0,95	Bream Fm.
152,11	13/1-U-2	0,85	-1	-0,35	-1,19	Bream Fm.
152,29	13/1-U-2	0,36	-1,15	-1,11	-1,86	Bream Fm.
152,29	13/1-U-2	0,13	-1,24			Bream Fm.
152,29	13/1-U-2	-1,25	-3,08			Bream Fm.
152,29	13/1-U-2	0,82	-1,64			Bream Fm.
152,29	13/1-U-2	0,24	-1,6			Bream Fm.
152,29	13/1-U-2	0,31	-1,49			Bream Fm.
152,3	13/1-U-2	0,97	-1,19	-2,32	-2,91	Bream Fm.
152,3	13/1-U-2	1,38	-1,06			Bream Fm.
152,3	13/1-U-2	1,43	-1,03			Bream Fm.
152,3	13/1-U-2	0,55	-1,12			Bream Fm.
152,37	13/1-U-2	0,42	0,3	-3,48	-3,73	Bream Fm.
152,37	13/1-U-2	1,12	-0,16			Bream Fm.
152,37	13/1-U-2	-0,04	-0,52			Bream Fm.
152,37	13/1-U-2	0,38	-0,44			Bream Fm.
152,41	13/1-U-2	0,63	-0,77	-2,34	-3,02	Bream Fm.
152,41	13/1-U-2	0,18	-0,95			Bream Fm.
152,41	13/1-U-2	0,23	-1,01			Bream Fm.
152,41	13/1-U-2	-0,14	-0,75			Bream Fm.
152,41	13/1-U-2	-0,31	-1,39			Bream Fm.
152,41	13/1-U-2	-0,15	-0,87			Bream Fm.
152,44	13/1-U-2	0,6	-0,82	-4,11	-4,33	Bream Fm.
152,44	13/1-U-2	0,06	-0,98			Bream Fm.
152,44	13/1-U-2	0	-1,11			Bream Fm.
152,44	13/1-U-2	0,07	-0,88			Bream Fm.
152,6	13/1-U-2	-0,94	-1,3	-3,49	-5,18	Bream Fm.
152,6	13/1-U-2	-0,6	-1,34			Bream Fm.
152,79	13/1-U-2	-1,23	-1,65	-4,63	-4,63	Bream Fm.
152,81	13/1-U-2			-5,55	-5,24	Bream Fm.
152,83	13/1-U-2	-0,5	-1,74	-2,69	-4,07	Bream Fm.
152,83	13/1-U-2	-0,32	-0,85			Bream Fm.
152,83	13/1-U-2	0,19	-1,04			Bream Fm.
152,83	13/1-U-2	0,02	-1,06			Bream Fm.
152,83	13/1-U-2	0,45	-1,12			Bream Fm.
152,83	13/1-U-2	0,54	-0,5			Bream Fm.
152,9	13/1-U-2	0,37	-1,12	-5,33	-5,63	Bream Fm.

13/1-U-2
Stable Isotope Data

Depth (m)	Site	δ^{13C} ‰ PDB	$\delta^{18}O$ ‰ PDB	δ^{13C} ‰ PDB	$\delta^{18}O$ ‰ PDB	Stratigraphy
		(belemnite)	(belemnite)	(bulk)	(bulk)	Bream Fm.
152,9	13/1-U-2	-0,23	-1,54			Bream Fm.
152,9	13/1-U-2	-1,43	-1,4			Bream Fm.
152,9	13/1-U-2	-1,57	-1,37			Bream Fm.
153,2	13/1-U-2	0,35	-0,95	-5,02	-4,98	Bream Fm.
153,2	13/1-U-2	0,3	-0,87			Bream Fm.
153,2	13/1-U-2	-0,23	-1,13			Bream Fm.
153,2	13/1-U-2	-0,33	-1,18			Bream Fm.
153,2	13/1-U-2	-1	-0,1			Bream Fm.
153,23	13/1-U-2	0,59	-0,64	-5,06	-4,8	Bream Fm.
153,23	13/1-U-2	0,95	-0,29			Bream Fm.
153,23	13/1-U-2	-1,34	-1,11			Bream Fm.
153,23	13/1-U-2	1,07	-0,87			Bream Fm.
153,24	13/1-U-2	0,37	-1,12	-7,16	-5,37	Bream Fm.
153,24	13/1-U-2	0,1	-1,39			Bream Fm.
153,28	13/1-U-2	-0,33	-2,53	-5,41	-4,77	Bream Fm.
153,28	13/1-U-2	0,04	-2,76			Bream Fm.
153,28	13/1-U-2	-0,4	-2,14			Bream Fm.
153,34	13/1-U-2	0,65	-1,17	-6,39	-4,68	Bream Fm.
153,34	13/1-U-2	0,04	-1,3			Bream Fm.
153,34	13/1-U-2	-0,38	-1,72			Bream Fm.
153,35	13/1-U-2	1,18	-1,42	-5,95	-5,11	Bream Fm.
153,35	13/1-U-2	1,23	-1,19			Bream Fm.
153,52	13/1-U-2	0,61	-1,7	-6	-4,92	Bream Fm.
153,52	13/1-U-2	-1,07	-1,71			Bream Fm.
153,52	13/1-U-2	0,51	-1,1			Bream Fm.
154,22	13/1-U-2	0,51	-0,98	-5,33	-6,16	Bream Fm.
154,22	13/1-U-2	0,56	-1,25			Bream Fm.
154,22	13/1-U-2	-0,03	-1,22			Bream Fm.
154,22	13/1-U-2	-0,98	-0,7			Bream Fm.
154,53	13/1-U-2	0,11	-1,14	-2,96	-4,29	Bream Fm.
154,53	13/1-U-2	-0,03	-1,14			Bream Fm.
154,53	13/1-U-2	-1,6	-1,22			Bream Fm.
154,53	13/1-U-2	-0,99	-1,1			Bream Fm.
154,72	13/1-U-2	0,7	-0,53			Bream Fm.
154,72	13/1-U-2	-0,59	-1,07			Bream Fm.
154,72	13/1-U-2	0,34	-0,8			Bream Fm.
155,8	13/1-U-2	0,31	-1,13	-2,23	-3,44	Bream Fm.
155,8	13/1-U-2	0,68	-0,89			Bream Fm.
155,8	13/1-U-2	0,35	-1,11			Bream Fm.
155,8	13/1-U-2	-1,47	-1,78			Bream Fm.
155,87	13/1-U-2	-0,04	-1,14			Bream Fm.
156,87	13/1-U-2	-0,47	-0,89			Bream Fm.
157,41	13/1-U-2	-0,37	-1,34	-2,87	-5,08	Bream Fm.
157,41	13/1-U-2	-0,43	-1,58			Bream Fm.
157,41	13/1-U-2	-0,41	-1,34			Bream Fm.
157,41	13/1-U-2	-1,07	-1,71			Bream Fm.
157,87	13/1-U-2	-0,81	-0,96			Bream Fm.
158,87	13/1-U-2	-0,91	-1,26			Bream Fm.
159,72	13/1-U-2	0,5	-1,37	-1,74	-3,33	Bream Fm.
159,72	13/1-U-2	0,44	-1,37			Bream Fm.
159,87	13/1-U-2	0,32	-1,32			Bream Fm.
160	13/1-U-2	0,37	-0,92	-1,12	-1,90	Bream Fm.
171,75	13/1-U-2	0,54	-0,891	-0,702	-0,926	Bream Fm.
171,75	13/1-U-2	0,752	-1,022			Bream Fm.

13/1-U-2
Stable Isotope Data

Depth (m)	Site	δ^{13C} ‰ PDB	$\delta^{18}O$ ‰ PDB	δ^{13C} ‰ PDB	$\delta^{18}O$ ‰ PDB	Bream Fm.
		(belemnite)	(belemnite)	(bulk)	(bulk)	Bream Fm.
171,75	13/1-U-2	0,25	-1,011			Bream Fm.
171,75	13/1-U-2	-0,15	-0,721			Bream Fm.
178,89	13/1-U-2	-0,48	-0,83	-1,67	-1,84	Bream Fm.
188,84	13/1-U-2	-1,382	-0,806	-0,062	-1,556	Bream Fm.
188,84	13/1-U-2	-0,862	-0,916			Bream Fm.
188,84	13/1-U-2	-0,612	-1,096			Bream Fm.
193,51	13/1-U-2	-0,118	-2,242			Bream Fm.
193,51	13/1-U-2	-0,27	-1,531			Bream Fm.
193,51	13/1-U-2	-0,658	-1,702			Bream Fm.
194,95	13/1-U-2	0,872	-1,172	-5,14	-2,221	Bream Fm.
194,95	13/1-U-2	0,602	-1,322			Bream Fm.
194,95	13/1-U-2	-0,48	-1,521			Bream Fm.
194,95	13/1-U-2	-1	-1,891			Bream Fm.
195,38	13/1-U-2	0,89	-1,281	-3,69	-3,63	Bream Fm.
195,38	13/1-U-2	-0,118	-1,202			Bream Fm.
195,84	13/1-U-2	0,272	-1,161	-1,84	-3,36	Bream Fm.
195,84	13/1-U-2	-1,932	-1,706			Bream Fm.
195,96	13/1-U-2	0,828	-1,096	-0,53	-1,78	Bream Fm.
195,96	13/1-U-2	0,312	-1,331			Bream Fm.
195,96	13/1-U-2	-0,748	-1,201			Bream Fm.
198,36	13/1-U-2	1,22	-1,351	-3,582	-3,976	Bream Fm.
198,36	13/1-U-2	0,582	-1,402			Bream Fm.
198,36	13/1-U-2	-0,268	-1,562			Bream Fm.
199,45	13/1-U-2	1,302	-1,171			Bream Fm.
199,45	13/1-U-2	0,448	-1,246	-1,392	-3,086	Bream Fm.
202,12	13/1-U-2			-1,52	-3,92	Bream Fm.
203,12	13/1-U-2	0,93	-0,96			Bream Fm.
203,12	13/1-U-2	0,24	-0,99			Bream Fm.
203,54	13/1-U-2	1,218	-1,606	-1,282	-0,996	Bream Fm.
203,54	13/1-U-2	1,052	-1,351			Bream Fm.
207,9	13/1-U-2	0,788	-1,316	-3,232	-1,056	Bream Fm.

Microprobe Data

7430/10-U-01							
34,16m	Na_2O (wt%)	K_2O (wt%)	MgO (wt%)	FeO (wt%)	MnO (wt%)	CaO (wt%)	Total (wt%)
No.							
1	0.060	0.008	0.624	0.001	0.001	53.879	54.713
2	0.079	0.011	0.837	0.000	0.001	53.007	54.189
3	0.185	0.006	0.893	0.000	0.010	56.584	57.763
5	0.225	0.009	0.835	0.000	0.000	55.541	57.067
6	0.122	0.000	0.301	0.000	0.006	54.741	55.481
7	0.232	0.015	0.494	0.016	0.000	55.062	56.164
8	0.189	0.000	0.383	0.021	0.006	54.927	55.760
9	0.154	0.003	0.482	0.031	0.000	53.266	54.137
11	0.183	0.000	0.521	0.007	0.000	54.179	55.154
12	0.125	0.000	0.221	0.000	0.000	53.897	54.432
13	0.190	0.007	0.354	0.000	0.000	53.688	54.484
14	0.192	0.000	0.394	0.000	0.009	53.042	53.875
15	0.242	0.000	0.541	0.002	0.000	54.995	56.084
16	0.146	0.000	0.269	0.000	0.000	55.925	56.560
17	0.182	0.008	0.508	0.020	0.012	55.761	56.765
18	0.147	0.004	0.404	0.015	0.000	53.733	54.538
19	0.134	0.000	0.261	0.000	0.000	55.385	56.231
20	0.151	0.000	0.285	0.000	0.003	54.873	55.631
21	0.121	0.000	0.179	0.009	0.000	54.506	55.016
22	0.155	0.000	0.218	0.002	0.000	56.487	57.189
24	0.101	0.007	0.217	0.000	0.001	54.129	54.786
25	0.143	0.000	0.254	0.017	0.015	53.898	54.598
26	0.156	0.002	0.389	0.032	0.008	53.908	54.759
27	0.138	0.000	0.336	0.008	0.000	53.907	54.655
28	0.142	0.000	0.283	0.006	0.008	53.409	54.004
29	0.189	0.000	0.515	0.011	0.005	52.171	53.125
30	0.161	0.000	0.389	0.029	0.008	54.652	55.514
32	0.187	0.000	0.319	0.000	0.000	53.761	54.572
33	0.246	0.011	0.812	0.000	0.008	52.893	54.221
34	0.218	0.000	0.441	0.022	0.000	52.709	53.652
35	0.154	0.002	0.314	0.000	0.000	54.579	55.273
36	0.154	0.005	0.357	0.012	0.000	55.773	56.604
37	0.170	0.000	0.372	0.003	0.000	55.114	55.741
38	0.161	0.000	0.613	0.000	0.000	54.421	55.429
39	0.187	0.006	0.344	0.027	0.000	55.236	56.055
40	0.196	0.009	0.649	0.000	0.032	53.591	54.770
41	0.209	0.015	0.851	0.010	0.000	53.437	54.763
42	0.142	0.000	0.314	0.007	0.000	55.990	56.724
43	0.169	0.011	0.426	0.006	0.023	54.854	55.723
44	0.138	0.000	0.355	0.025	0.020	53.104	53.985
45	0.221	0.004	0.807	0.007	0.000	54.343	55.716
46	0.154	0.003	0.246	0.000	0.000	54.893	55.611
47	0.187	0.000	0.687	0.016	0.000	54.806	55.942
50	0.168	0.001	0.384	0.012	0.000	55.106	55.911
51	0.162	0.004	0.417	0.009	0.000	54.807	55.714
52	0.136	0.000	0.342	0.000	0.009	53.059	53.862
53	0.161	0.006	0.800	0.000	0.020	52.653	53.960
54	0.144	0.003	0.245	0.003	0.013	53.775	54.413
55	0.248	0.004	0.680	0.015	0.005	53.538	54.792
56	0.162	0.010	0.370	0.006	0.000	54.451	55.411
58	0.117	0.018	0.341	0.031	0.016	54.450	55.249
59	0.198	0.000	0.534	0.021	0.000	52.021	53.075
60	0.193	0.005	0.787	0.000	0.002	54.355	55.634

61	0.223	0.006	0.565	0.014	0.004	53.030	54.190
62	0.173	0.000	0.520	0.006	0.007	53.766	54.751
63	0.165	0.002	0.389	0.015	0.000	55.564	56.446
64	0.162	0.000	0.300	0.000	0.000	52.417	53.172
65	0.198	0.001	0.506	0.000	0.002	52.464	53.403
66	0.108	0.000	0.227	0.018	0.000	54.255	54.928
67	0.193	0.003	0.517	0.024	0.000	52.968	53.972
7430/10-U-01							
39,55m	Na_2O (wt%)	K_2O (wt%)	MgO (wt%)	FeO (wt%)	MnO (wt%)	CaO (wt%)	Total (wt%)
No.							
1	0.036	0.001	0.460	0.016	0.026	55.613	56.152
2	0.040	0.003	0.364	0.039	0.110	52.824	53.380
3	0.246	0.000	0.566	0.032	0.004	54.226	55.074
4	0.209	0.004	0.434	0.009	0.000	54.876	55.532
5	0.187	0.002	0.393	0.016	0.000	59.536	60.134
6	0.135	0.003	0.300	0.000	0.000	54.935	55.373
7	0.168	0.005	0.282	0.000	0.007	56.108	56.570
8	0.213	0.000	0.550	0.009	0.000	53.019	53.791
9	0.043	0.000	0.472	0.014	0.000	54.631	55.160
10	0.042	0.000	0.507	0.023	0.171	55.098	55.841
11	0.051	0.005	0.604	0.046	0.070	55.614	56.390
12	0.047	0.010	0.719	0.039	0.007	52.718	53.540
13	0.042	0.003	0.531	0.012	0.000	55.643	56.231
14	0.080	0.000	0.558	0.034	0.000	55.273	55.945
15	0.075	0.000	0.580	0.007	0.008	53.625	54.295
16	0.082	0.006	0.488	0.000	0.000	55.240	55.816
17	0.065	0.007	0.475	0.025	0.000	54.942	55.514
18	0.060	0.005	0.430	0.000	0.005	53.748	54.248
19	0.096	0.006	0.461	0.007	0.000	55.339	55.909
20	0.099	0.005	0.665	0.034	0.000	55.388	56.191
21	0.198	0.012	0.439	0.044	0.017	54.052	54.762
23	0.263	0.000	0.467	0.000	0.006	52.439	53.175
24	0.141	0.000	0.417	0.007	0.011	54.975	55.551
25	0.100	0.000	0.390	0.159	0.346	54.075	55.070
27	0.109	0.031	0.441	0.206	0.602	54.323	55.712
7430/10-U-01							
37,4m	Na_2O (wt%)	K_2O (wt%)	MgO (wt%)	FeO (wt%)	MnO (wt%)	CaO (wt%)	Total (wt%)
No.							
57	0.017	0.003	0.273	0.008	0.000	55.308	55.609
58	0.038	0.000	0.445	0.051	0.119	54.141	54.794
59	0.015	0.000	0.431	0.011	0.013	55.266	55.736
60	0.139	0.000	0.679	0.073	0.007	54.185	55.083
61	0.030	0.000	0.332	0.013	0.000	52.196	52.571
62	0.235	0.000	0.465	0.016	0.000	55.661	56.377
63	0.202	0.008	0.462	0.023	0.000	53.519	54.214
64	0.309	0.000	0.648	0.026	0.000	55.047	56.030
65	0.199	0.000	0.453	0.047	0.000	56.257	56.956
66	0.213	0.000	0.365	0.008	0.011	54.744	55.341
67	0.243	0.001	0.777	0.005	0.010	55.077	56.113
68	0.194	0.000	0.368	0.012	0.004	54.171	54.749
69	0.038	0.004	0.337	0.023	0.217	54.254	54.873
70	0.012	0.000	0.344	0.072	0.358	56.019	56.805
71	0.028	0.000	0.441	0.106	0.318	53.394	54.287
72	0.039	0.004	0.376	0.115	0.303	55.392	56.229

73	0.021	0.001	0.500	0.066	0.142	58.016	58.746
74	0.025	0.004	0.459	0.065	0.231	55.913	56.697
75	0.029	0.000	0.475	0.129	0.463	55.770	56.866
76	0.016	0.007	0.531	0.086	0.377	55.805	56.822
77	0.014	0.000	0.476	0.065	0.355	55.725	56.635
78	0.015	0.001	0.475	0.020	0.138	50.786	51.435
79	0.017	0.008	0.424	0.096	0.285	53.833	54.663
80	0.061	0.000	0.484	0.102	0.278	52.238	53.163
81	0.014	0.000	0.505	0.064	0.175	52.783	53.541
82	0.043	0.000	0.493	0.051	0.137	55.695	56.419
83	0.024	0.000	0.640	0.062	0.171	53.975	54.872
84	0.027	0.008	0.518	0.116	0.382	56.144	57.195
85	0.032	0.005	0.535	0.177	0.417	50.906	52.072
86	0.156	0.265	0.472	0.076	0.108	50.953	52.030
87	0.244	0.000	0.580	0.009	0.000	51.414	52.247
88	0.000	0.013	0.304	0.031	0.000	56.166	56.514
89	0.020	0.062	0.459	0.087	0.025	52.716	53.369
90	0.014	0.005	0.422	0.024	0.006	53.772	54.243
91	0.002	0.004	0.513	0.000	0.000	57.308	57.827
92	0.008	0.002	0.446	0.035	0.000	55.406	55.897
93	0.057	0.006	0.409	0.103	0.000	57.585	58.160
94	0.000	0.002	0.300	0.022	0.000	59.603	59.927
95	0.037	0.016	0.465	0.094	0.000	56.890	57.502
96	0.033	0.016	0.406	0.016	0.000	56.698	57.169
99	0.000	0.047	0.288	0.785	0.416	50.604	52.140
100	0.036	0.034	0.328	0.047	0.000	56.603	57.048
101	0.056	0.005	0.456	0.000	0.050	54.430	54.997
102	0.098	0.012	0.477	0.017	0.003	47.709	48.316
103	0.007	0.068	0.322	0.857	0.253	48.194	49.701
104	0.000	0.000	0.203	0.006	0.011	54.948	55.168
105	0.103	0.015	0.467	0.046	0.000	42.424	43.055
106	0.002	0.010	0.422	0.191	0.000	41.710	42.335
107	0.131	0.006	0.500	0.000	0.000	45.457	46.094
109	0.032	0.012	0.364	0.343	0.484	43.910	45.145
110	0.094	0.018	0.439	0.036	0.123	47.824	48.534
111	0.063	0.000	0.000	0.043	0.005	0.276	0.426
7430/10-U-01							
42,66m	Na_2O (wt%)	K_2O (wt%)	MgO (wt%)	FeO (wt%)	MnO (wt%)	CaO (wt%)	Total (wt%)
No.							
1	0.112	0.010	0.231	0.023	52.096	0.021	52.493
2	0.169	0.000	0.321	0.011	53.796	0.015	54.312
3	0.155	0.000	0.157	0.033	51.395	0.000	51.740
4	0.096	0.002	0.074	0.013	54.141	0.000	54.326
5	0.107	0.000	0.112	0.023	50.755	0.002	50.999
6	0.146	0.014	0.158	0.008	51.834	0.000	52.160
8	0.099	0.000	0.121	0.035	52.623	0.016	52.894
9	0.072	0.000	0.039	0.012	53.391	0.021	53.535
10	0.070	0.005	0.163	0.067	51.119	0.095	51.519
11	0.083	0.000	0.063	0.002	52.406	0.000	52.554
12	0.059	0.000	0.067	0.016	51.739	0.000	51.881
13	0.097	0.008	0.069	0.030	53.277	0.016	53.497
14	0.076	0.000	0.120	0.040	50.396	0.000	50.632
15	0.032	0.002	0.064	0.024	50.461	0.000	50.583
16	0.083	0.000	0.312	0.000	52.085	0.025	52.505
17	0.025	0.000	0.070	0.000	52.395	0.000	52.490

18	0.049	0.005	0.074	0.011	53.090	0.000	53.229
19	0.074	0.005	0.240	0.034	53.207	0.000	53.560
20	0.059	0.000	0.042	0.000	51.760	0.002	51.863
21	0.068	0.000	0.076	0.027	50.424	0.019	50.614
22	0.065	0.000	0.077	0.021	52.569	0.000	52.732
23	0.112	0.004	0.319	0.000	51.696	0.000	52.131
24	0.118	0.013	0.149	0.000	52.570	0.006	52.856
25	0.111	0.004	0.097	0.008	51.650	0.000	51.870
26	0.121	0.003	0.427	0.005	55.092	0.003	55.651
27	0.048	0.000	0.678	0.494	50.340	0.267	51.827
28	0.108	0.011	0.191	0.029	49.891	0.017	50.247
29	0.055	0.010	0.221	0.080	50.915	0.011	51.292
30	0.100	8.151	1.178	0.990	0.700	0.002	11.121
7430/10-U-01							
33,98m	Na_2O (wt%)	K_2O (wt%)	MgO (wt%)	FeO (wt%)	MnO (wt%)	CaO (wt%)	Total (wt%)
No.							
1	0.202	0.017	0.816	0.077	0.024	53.432	54.568
2	0.200	0.006	0.458	0.026	0.010	58.277	58.977
3	0.223	0.014	0.954	0.019	0.003	54.603	55.816
4	0.232	0.000	0.845	0.003	0.001	53.303	54.384
5	0.152	0.000	0.281	0.000	0.017	54.054	54.504
6	0.138	0.002	0.247	0.022	0.000	54.215	54.624
7	0.133	0.006	0.287	0.029	0.005	54.533	54.993
8	0.166	0.000	0.732	0.000	0.000	57.042	57.940
9	0.141	0.002	0.311	0.054	0.000	54.013	54.521
6814/04-U-02							
96,03m	Na_2O (wt%)	K_2O (wt%)	MgO (wt%)	FeO (wt%)	MnO (wt%)	CaO (wt%)	Total (wt%)
No.							
1	0.252	0.000	0.212	0.000	0.017	55.239	55.720
2	0.187	0.005	0.074	0.007	0.003	58.304	58.580
3	0.210	0.002	0.056	0.000	0.000	55.667	55.935
4	0.250	0.009	0.094	0.000	0.000	57.937	58.290
5	0.198	0.000	0.105	0.000	0.000	55.845	56.148
6	0.201	0.004	0.165	0.014	0.000	59.987	60.371
7	0.136	0.000	0.098	0.016	0.010	60.280	60.540
8	0.129	0.000	0.107	0.000	0.000	58.681	58.917
9	0.180	0.000	0.227	0.000	0.000	56.865	57.272
10	0.179	0.000	0.215	0.006	0.008	54.484	54.892
11	0.188	0.006	0.301	0.017	0.000	54.086	54.598
6814/04-U-02							
97,48m	Na_2O (wt%)	K_2O (wt%)	MgO (wt%)	FeO (wt%)	MnO (wt%)	CaO (wt%)	Total (wt%)
No.							
42	0.138	0.000	0.061	0.010	53.103	0.000	53.312
43	0.151	0.000	0.079	0.000	51.293	0.000	51.523
44	0.118	0.000	0.078	0.020	55.884	0.000	56.100
45	0.183	0.014	0.098	0.050	52.303	0.000	52.648
46	0.174	0.012	0.108	0.015	52.827	0.003	53.139
47	0.162	0.005	0.109	0.000	56.217	0.008	56.501
48	0.135	0.000	0.064	0.009	54.962	0.002	55.172
49	0.116	0.000	0.159	0.000	57.419	0.012	57.706
50	0.094	0.006	0.049	0.000	53.464	0.026	53.639
51	0.106	0.010	0.096	0.000	53.427	0.000	53.639

52	0.112	0.000	0.087	0.000	54.208	0.000	54.407
53	0.082	0.000	0.083	0.000	53.425	0.016	53.606
54	0.126	0.001	0.111	0.033	56.492	0.032	56.795
55	0.110	0.005	0.161	0.000	54.360	0.006	54.642
56	0.118	0.000	0.367	0.000	55.962	0.000	56.447
57	0.131	0.000	0.220	0.025	54.044	0.003	54.423
58	0.111	0.003	0.123	0.002	54.277	0.006	54.522
59	0.052	0.000	0.096	0.000	54.432	0.000	54.580
60	0.098	0.000	0.140	0.000	53.198	0.000	53.436
61	0.118	0.007	0.196	0.000	53.437	0.023	53.781
62	0.120	0.005	0.206	0.006	51.443	0.000	51.780
63	0.074	0.000	0.247	0.031	58.868	0.000	59.220
6814/04-U-02							
95,26m	Na_2O (wt%)	K_2O (wt%)	MgO (wt%)	FeO (wt%)	MnO (wt%)	CaO (wt%)	Total (wt%)
No.							
10	0.237	0.002	0.174	0.001	0.002	57.154	57.570
11	0.141	0.000	0.148	0.022	0.000	55.196	55.507
12	0.124	0.000	0.318	0.002	0.000	55.775	56.219
13	0.158	0.004	0.391	0.000	0.000	55.337	55.890
14	0.123	0.007	0.208	0.030	0.014	55.210	55.592
15	0.135	0.000	0.256	0.000	0.000	53.538	53.929
16	0.062	0.004	0.383	0.071	0.000	55.268	55.788
17	0.121	0.005	0.137	0.019	0.001	53.603	53.886
18	0.113	0.019	0.152	0.020	0.000	50.470	50.774
6307/07-U-02							
23,75m	Na_2O (wt%)	K_2O (wt%)	MgO (wt%)	FeO (wt%)	MnO (wt%)	CaO (wt%)	Total (wt%)
No.							
12	0.018	0.000	0.529	1.336	0.995	57.874	60.752
13	0.060	0.000	1.195	0.949	0.936	57.376	60.516
14	0.060	0.000	1.713	0.120	0.179	54.857	56.929
15	0.065	0.002	1.552	0.105	0.158	57.006	58.888
16	0.207	0.005	0.528	0.008	0.000	59.930	60.678
17	0.237	0.000	0.669	0.000	0.000	55.147	56.053
18	0.220	0.000	0.591	0.019	0.000	56.932	57.762
19	0.338	0.005	0.745	0.006	0.000	57.181	58.275
20	0.168	0.007	0.316	0.000	0.000	54.091	54.582
21	0.160	0.011	0.303	0.000	0.000	54.947	55.421
13/1-U-2							
171,75m	Na_2O (wt%)	K_2O (wt%)	MgO (wt%)	FeO (wt%)	MnO (wt%)	CaO (wt%)	Total (wt%)
No.							
28	0.125	0.000	0.203	0.000	0.008	59.014	59.350
29	0.171	0.008	0.446	0.000	0.000	53.723	54.348
30	0.209	0.010	0.594	0.000	0.000	54.359	55.172
31	0.146	0.009	0.182	0.000	0.000	60.593	60.930
32	0.170	0.000	0.402	0.001	0.004	58.879	59.456
33	0.143	0.000	0.200	0.002	0.004	53.160	53.509
34	0.114	0.000	0.148	0.006	0.000	58.672	58.940
35	0.155	0.000	0.209	0.009	0.003	58.238	58.614
36	0.167	0.000	0.238	0.004	0.000	60.157	60.566
37	0.137	0.000	0.153	0.012	0.000	59.214	59.516
38	0.165	0.000	0.226	0.000	0.000	60.319	60.710
39	0.167	0.010	0.246	0.001	0.003	57.974	58.401

40	0.194	0.000	0.395	0.000	0.003	58.172	58.764
41	0.139	0.005	0.184	0.000	0.019	59.474	59.821
42	0.124	0.002	0.135	0.007	0.000	59.421	59.689
43	0.106	0.004	0.246	0.000	0.000	59.174	59.530
44	0.093	0.004	0.133	0.017	0.000	53.214	53.461
45	0.120	0.000	0.119	0.000	0.001	58.565	58.805
46	0.145	0.002	0.201	0.035	0.000	57.227	57.610
47	0.122	0.003	0.139	0.012	0.000	58.834	59.110
48	0.228	0.001	0.513	0.003	0.001	55.486	56.232
49	0.155	0.007	0.150	0.010	0.014	58.006	58.342
50	0.162	0.000	0.181	0.023	0.004	58.765	59.135
51	0.149	0.003	0.256	0.005	0.000	54.497	54.910
52	0.147	0.004	0.146	0.000	0.003	58.161	58.461
53	0.145	0.002	0.169	0.000	0.000	54.810	55.126
54	0.205	0.003	0.283	0.002	0.000	54.284	54.777
55	0.211	0.004	0.460	0.009	0.013	60.144	60.841
13/1-U-2							
199,45m	Na_2O (wt%)	K_2O (wt%)	MgO (wt%)	FeO (wt%)	MnO (wt%)	CaO (wt%)	Total (wt%)
No.							
31	0.092	0.005	0.100	0.004	24.484	0.012	24.697
32	0.317	0.000	0.466	0.015	51.148	0.011	51.957
33	0.293	0.014	0.327	0.000	55.543	0.004	56.181
34	0.293	0.000	0.289	0.024	56.582	0.000	57.188
35	0.259	0.000	0.261	0.013	55.146	0.000	55.679
36	0.181	0.000	0.164	0.009	58.539	0.027	58.920
37	0.129	0.000	0.195	0.011	58.421	0.011	58.767
38	0.122	0.001	0.370	0.014	57.801	0.029	58.337
39	0.162	0.000	0.315	0.005	53.930	0.013	54.425
40	0.166	0.004	0.775	0.006	55.546	0.038	56.535
41	0.242	0.014	0.994	0.039	48.166	0.004	49.459
13/1-U-2							
203,94m	Na_2O (wt%)	K_2O (wt%)	MgO (wt%)	FeO (wt%)	MnO (wt%)	CaO (wt%)	Total (wt%)
No.							
1	0.187	0.004	0.332	0.000	0.000	57.889	58.412
2	0.169	0.010	0.416	0.000	0.008	58.270	58.873
3	0.199	0.000	0.626	0.036	0.004	57.063	57.928
4	0.249	0.013	0.599	0.003	0.000	57.291	58.155
5	0.278	0.003	0.422	0.000	0.000	56.938	57.641
6	0.269	0.000	0.377	0.017	0.007	56.967	57.637
7	0.221	0.017	0.389	0.027	0.013	56.938	57.605
8	0.225	0.000	0.328	0.000	0.000	57.326	57.879
9	0.199	0.000	0.309	0.018	0.003	57.899	58.428
10	0.206	0.000	0.689	0.000	0.000	55.479	56.374
11	0.123	0.003	0.378	0.009	0.000	56.956	57.469
12	0.131	0.004	0.274	0.013	0.000	54.334	54.756
13	0.218	1.184	3.362	5.896	0.059	0.226	10.945
13/1-U-2							
98,36m	Na_2O (wt%)	K_2O (wt%)	MgO (wt%)	FeO (wt%)	MnO (wt%)	CaO (wt%)	Total (wt%)
No.							
14	0.002	0.008	0.557	2.175	0.757	49.797	53.296
15	0.017	0.000	0.619	2.558	0.850	58.422	62.466
16	0.006	0.007	0.718	2.873	0.899	53.050	57.553

17	0.299	0.016	0.902	0.017	0.003	56.302	57.539
18	0.220	0.015	0.627	0.000	0.001	57.984	58.847
19	0.176	0.008	0.447	0.000	0.003	57.324	57.958
20	0.164	0.000	0.208	0.000	0.000	57.753	58.125
21	0.190	0.003	0.211	0.000	0.027	58.054	58.485
22	0.143	0.000	0.166	0.000	0.006	58.630	58.945
23	0.151	0.001	0.243	0.003	0.000	55.604	56.002
24	0.074	0.003	0.130	0.000	0.000	57.581	57.788
25	0.125	0.000	0.147	0.012	0.002	55.439	55.725
26	0.138	0.001	0.322	0.000	0.004	54.444	54.909
27	0.127	0.006	0.217	0.013	0.000	54.313	54.676
28	0.140	0.000	0.278	0.006	0.000	55.093	55.517
29	0.139	0.005	0.200	0.013	0.000	54.190	54.547
30	0.144	0.001	0.384	0.000	0.001	56.705	57.235
31	0.186	0.010	0.595	0.000	0.000	56.540	57.331
32	0.153	0.004	0.258	0.000	0.001	56.476	56.892
33	0.182	0.008	0.329	0.002	0.000	56.550	57.071
34	0.147	0.000	0.312	0.000	0.011	55.293	55.763
35	0.149	0.000	0.337	0.023	0.000	55.636	56.145
36	0.131	0.006	0.235	0.000	0.010	54.821	55.203
37	0.159	0.009	0.332	0.000	0.001	56.603	57.104
38	0.171	0.000	0.381	0.010	0.019	56.633	57.214
39	0.173	0.000	0.484	0.015	0.012	52.239	52.923
40	0.063	0.808	0.626	2.329	0.024	0.747	4.597
13/1-U-2							
193,51m	Na_2O (wt%)	K_2O (wt%)	MgO (wt%)	FeO (wt%)	MnO (wt%)	CaO (wt%)	Total (wt%)
No.							
41	0.274	0.030	0.634	0.038	0.000	47.069	48.045
42	0.283	0.016	0.560	0.000	0.007	53.373	54.239
43	0.273	0.008	0.644	0.000	0.000	53.901	54.826
44	0.236	0.019	0.571	0.000	0.000	55.577	56.403
45	0.281	0.013	1.233	0.000	0.005	54.860	56.392
46	0.234	0.006	1.035	0.005	0.008	54.222	55.510
47	0.277	0.016	1.030	0.003	0.000	54.097	55.423
48	0.227	0.000	0.753	0.030	0.000	52.083	53.093
49	0.202	0.000	0.620	0.000	0.018	55.845	56.685
50	0.216	0.013	0.757	0.013	0.004	54.134	55.137
51	0.233	0.032	0.727	0.093	0.000	46.991	48.076
13/1-U-2							
198,36m	Na_2O (wt%)	K_2O (wt%)	MgO (wt%)	FeO (wt%)	MnO (wt%)	CaO (wt%)	Total (wt%)
No.	Na2O	K2O	MgO	FeO	MnO	CaO	Total
52	0.000	0.000	0.610	2.551	0.856	56.901	60.918
53	0.223	0.005	0.383	0.059	0.056	58.114	58.840
54	0.180	0.008	0.396	0.002	0.030	58.645	59.261
55	0.190	0.010	0.279	0.004	0.008	57.316	57.807
56	0.172	0.009	0.305	0.000	0.015	57.668	58.169
57	0.147	0.011	0.153	0.015	0.015	55.777	56.118
58	0.137	0.000	0.168	0.000	0.000	54.154	54.459
59	0.152	0.007	0.499	0.000	0.000	58.382	59.040
60	0.141	0.004	0.363	0.000	0.000	58.475	58.983
61	0.162	0.002	0.538	0.000	0.000	59.092	59.794
62	0.000	0.000	0.682	2.870	0.934	54.761	59.247
63	0.000	0.000	0.703	3.631	1.111	57.119	62.564

OES-MS Data

Site	Mg	Ca	Na	Mn	Sr	Material
Depth (m)	ppm	ppm	ppm	ppm	ppm	
6814/04-U-02						
50,93	2243,54	242809,83	2069,81	1464,12	587,22	*Buchia*
71,80	571,37	106512,39	1347,30	152,07	416,15	*Buchia*
73,11	932,16	259521,05	2160,33	190,83	725,57	*Buchia*
75,41	1102,67	261623,36	2108,65	562,72	659,82	*Buchia*
75,95	923,00	216692,72	2081,44	257,78	580,43	*Buchia*
84,55	1334,64	259062,38	3425,49	72,06	626,65	inocerame
86,49	2939,07	246025,50	3461,70	87,87	651,22	inocerame
90,40	1142,35	224408,23	2586,40	109,36	427,38	inocerame
90,86	1321,87	220923,73	2967,92	132,07	486,27	inocerame
96,11	1714,90	244408,11	2748,15	133,65	507,50	inocerame
97,73	584,58	224231,92	2782,68	45,60	456,55	*Buchia*
102,45	431,24	260408,12	2096,85	60,08	719,02	*Buchia*
114,60	497,68	266916,68	2681,69	195,54	740,25	*Buchia*
120,01	578,37	217204,52	2111,00	79,47	653,74	*Buchia*
121,31	390,42	264420,57	2735,82	131,49	690,50	*Buchia*
128,92	846,70	264821,89	2345,77	244,04	741,90	*Buchia*
7430/10-U-01						
33,82	2539,82	234805,99	2844,26	1335,22	877,26	inocerame
35,46	1745,14	282441,73	1367,15	160,60	236,53	inocerame
39,55	3008,75	244498,14	1494,94	1113,52	408,53	*Buchia*
43,78	700,48	266676,82	2135,00	381,05	695,34	*Buchia*
44,34	638,60	267217,28	1812,12	230,74	682,44	*Buchia*
55,23	812,16	256159,02	2620,08	305,47	743,61	*Buchia*
6307/07-U-02						
15,93	274,01	42,96	158,62	914,08	853,94	*Buchia*
17,55	2763,21	232593,99	1964,11	1257,20	472,93	*Buchia*
19,00	2331,73	248957,86	2318,28	1377,37	532,75	*Buchia*
19,63	3245,79	195137,85	2161,14	1873,76	351,85	*Buchia*
20,46	3382,59	212298,78	1740,90	2238,65	374,06	*Buchia*
22,71	1954,33	250712,35	1903,25	1211,93	510,87	*Buchia*
22,84	1919,83	261816,61	1973,61	885,52	544,89	*Buchia*
22,84	2224,13	257647,79	2057,60	1181,41	495,01	*Buchia*
23,96	2476,19	391898,37	1309,14	5277,36	631,48	*Buchia*
26,57	872,98	263540,32	2208,13	848,28	578,88	*Buchia*
51,67	4486,30	3029,67	128,32	44,56	3,40	inocerame

Acknowledgments

Thanks to

- Prof. Dr. Werner Ricken for the initiation of this study and the support
- Prof. Dr. Klaus Krumsiek
- the German Science Council for financial support (RI 525/11)
- all participants of the project, especially Markus Lipinski, Uwe Langrock and Christian Klein
- Øystein How, Dr. Hermann Weiss, Dr. Atle Mørk, and Dr. Ute Mann (all SINTEF Petroleum Research-Trondheim/Norway)
- Dr. Helmut Erlenkeuser, Leibniz-Laboratory - Kiel
- all colleagues at the Department of Geology at the University of Cologne for numerous discussions and help especially to Heiko Freitag, Markus Hirschfeld, Guido Lüniger, Alexander Neber, Dr. Thomas Pletsch, Anette Regier, Markus Seidel, Dr. Jutta Weber
- Dipl.-Geol. Kristijan Kornpihl the loyal varlet
- my family and friends for numerous support and favours

My special expression of thanks is dedicated to Daniela - for all.